R-13-21

Calculation of open repository inflows for Forsmark

Steven Joyce, David Swan, Lee Hartley
AMEC

July 2013

Svensk Kärnbränslehantering AB
Swedish Nuclear Fuel
and Waste Management Co

Box 250, SE-101 24 Stockholm
Phone +46 8 459 84 00

ISSN 1402-3091
SKB R-13-21
ID 1392828

Calculation of open repository inflows for Forsmark

Steven Joyce, David Swan, Lee Hartley
AMEC

July 2013

Abstract

The work reported here describes the application of the SR-Site modelling methodology to the calculation of inflows to deposition holes, deposition tunnels and pilot holes under open repository conditions and hydraulic injection tests to selected pilot holes drilled in advance of deposition holes.

In the first part of the study, the likely distributions of inflows to deposition holes and deposition tunnels are presented. Also investigated is the impact of excluding deposition locations based on inflow criteria for an open repository on the performance measure distributions of equivalent Darcy flux, U_r, and flow-related transport resistance, F_r, for a closed, saturated repository. Five cases of the SR-Site Hydrogeological model, including one case with no EDZ are considered.

For the SR-Site modelling, the repository layout was divided into three distinct areas, or blocks, each representing a group of deposition tunnels and deposition holes associated with one or two main tunnels. In the second part of the study, inflows to pilot holes are calculated for a single block under open repository conditions and compared with the corresponding inflows to deposition holes in the same block, calculated in the first part of the study. In contrast to the case when all deposition tunnels in a block are open, a more likely scenario is one where only a limited number of tunnels in a block are open at any one time. For this scenario, inflows to pilot holes are also calculated for a selected area of the repository which is partially open and where some tunnels are already closed and backfilled and new tunnels are opened, two at a time, in six phases.

In the third part of the study, injection tests in pilot holes are simulated for part of the repository-scale model under open conditions to determine if these are correlated with inflow measurements or performance measures, and hence if they can be used as deposition hole rejection criteria. Using the same repository block as for the second part of the study, up to three pilot holes in each deposition tunnel are selected to illustrate injection into pilot holes to which an overpressure of 5 bar is applied. The steady-state flow from the injection pilot hole and the pressure responses in neighbouring pilot holes in the same tunnel are calculated. An effective transmissivity for each injection pilot hole is also calculated as total outflow divided by the head change in the pilot hole (an injected specific capacity) and compared with the total transmissivity of the natural fractures intersecting that hole.

Contents

1 Introduction

SKB have submitted a license application for a spent nuclear fuel repository at Forsmark. Part of this license application includes the SR-Site safety assessment to demonstrate the long-term safety of the proposed repository. SR-Site included groundwater flow and transport modelling of a KBS-3 repository during operational and post-closure phases under different climate conditions. During construction of the repository, decisions on the placement of deposition holes will be partly determined by inflows measured in deposition tunnels and the pilot holes for the deposition tunnels and deposition holes.

In the first part of this study, four cases are considered based on alternative realisations of the SR-Site Hydrogeological base case model (see Joyce et al. 2010a, Chapter 4) plus one case where the excavated damaged zone (EDZ) is not included.

The statistical distributions of inflows to deposition holes and tunnels under open repository conditions are calculated for each case together. The impact on performance measure distributions for a closed, saturated repository is also assessed of excluding deposition hole locations based on inflows above 0.1 L/min, Full Perimeter Criteria (FPC) and Extended Full Perimeter Criteria (EFPC). The performance measures considered are the equivalent Darcy flux, U_r, and the flow-related transport resistance along groundwater pathways, F_r (a measure of the potential for retention and retardation of radionuclides in the rock). These performance measures, along with FPC and EFPC are described fully in Joyce et al. (2010a, Section 3.2.6). The results from this work are compared to the inflow calculations to deposition holes reported in Svensson and Follin (2010, Section 5.2.1), where the models are based on an equivalent continuous porous medium (ECPM) concept and where grouting has been included, in contrast to the discrete fracture network model (DFN) concept used in this work and with no grouting. The results from this part of the study are presented in Section 3.

For the SR-Site modelling, the repository layout was divided into three distinct areas, or blocks, each representing a group of deposition tunnels and deposition holes. In the second part of this study, inflows to pilot holes for deposition holes are calculated for a single block under fully open repository conditions and compared with the inflows to deposition holes in the same block, as calculated in the first part of the study. In contrast to the case when all deposition tunnels in a block are open, a more likely scenario is where only a limited number of tunnels in a block are open at any one time. For this scenario, inflows to pilot holes are also calculated for a selected area of the repository which is partially open and where some tunnels are already closed and backfilled and new tunnels are opened, two at a time, in six phases. The results from this part of the study are presented in Section 4.

In the third part of this study, the merit of performing injection tests in pilot holes for deformation holes during construction is considered. Simulations of injection tests are carried out for part of the repository-scale model under open conditions to determine if these are correlated with inflow measurements or performance measures for deposition holes, and hence if they can be used as rejection criteria for deposition hole locations. With the same repository block as used for the second part of this study, up to three pilot holes in each deposition tunnel are selected to illustrate injection into pilot holes to which an overpressure of 5 bar is applied. The steady-state flow from the injection pilot hole and the pressure responses in neighbouring pilot holes in the same tunnel are calculated. An effective transmissivity for each injection pilot hole is also calculated as total outflow divided by the head change in the pilot hole (an injected specific capacity) and compared with the total transmissivity of the natural (non-EDZ) fractures intersecting that hole. The results from this part of the study are presented in Section 5.

2 Model description

2.1 Conceptual model

The Forsmark site consists of fractured crystalline rock overlain with Quaternary deposits. Based on the characteristics of the geology, the rock was sub-divided into rock domains (SKB 2008, Section 5.4), as shown in Figure 2-1. The repository itself is located in a tectonic lens in which the bedrock is less affected by ductile deformation within surrounding belts of high ductile strain. The upper 200 m of the bedrock is characterised by an increased intensity of sub-horizontal to gently dipping fractures and sheet-joints forming a shallow bedrock aquifer. Below this is sparsely fractured bedrock of low permeability.

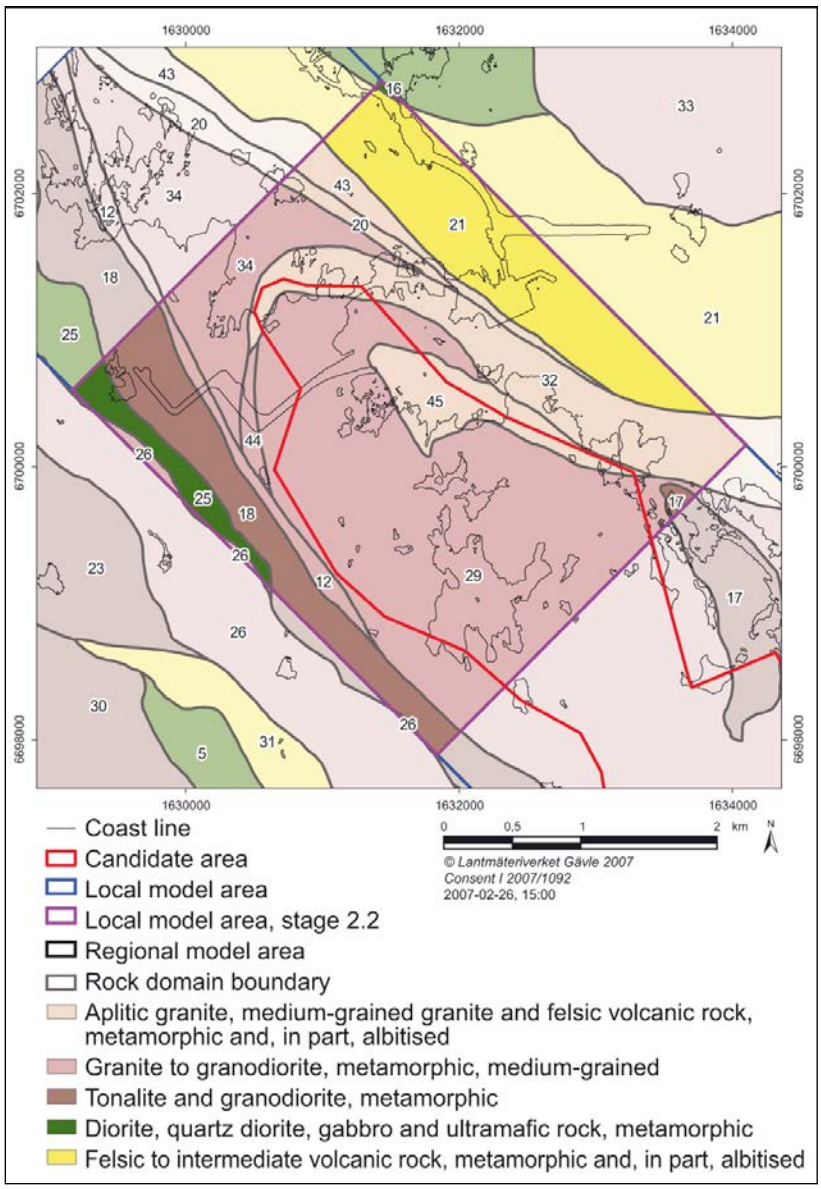

Figure 2-1. *Illustrations of the rock domains at the surface of the local model areas for Forsmark (SKB 2008, Figure 5-24b).*

A conceptual model of the site hydrogeology was developed during the site-descriptive modelling (SDM), culminating in SDM-Site (SKB 2008), serving as a basis for the SR-Site safety assessment (SKB 2011). The conceptual model describes three hydraulic domains:

- HCD (Hydraulic Conductor Domain) representing deformation zones.
- HRD (Hydraulic Rock mass Domain) representing the less fractured bedrock in between the deformation zones.
- HSD (Hydraulic Soil Domain) representing the regolith (Quaternary deposits).

These domains are illustrated in Figure 2-2. The HSD is not included in this study.

The deformation zones forming the HCD are defined as structures along which there is a concentration of brittle, ductile or combined brittle and ductile deformation. They are envisaged as being composed of swarms of smaller fractures. Each deformation zone structure is characterised by a transmissivity and thickness. Analysis of the site data identified a depth trend for the deformation zone transmissivities, which decrease with depth. An initial deterministic model of the HCD was devised with a uniform horizontal transmissivity (Figure 2-3: top). However, variants were also produced that introduced stochastic horizontal variability, conditioned on borehole measurements to provide both statistical properties (mean, standard deviation, depth trend) and deterministic values at the borehole intercepts with deformation zones (Figure 2-3: bottom).

The fractured bedrock between the deformation zones was divided into a number of fracture domains, characterised by fracture properties and location. These fracture domains were denoted FFM01 to FFM06 and are shown schematically in Figure 2-4 to Figure 2-6. Fracture domain FFM06 had a similar structural context to FFM01 and so these two fracture domains were merged. There was insufficient data to fully describe FFM04 and FFM05 and so their properties were characterised by analogy to FFM03.

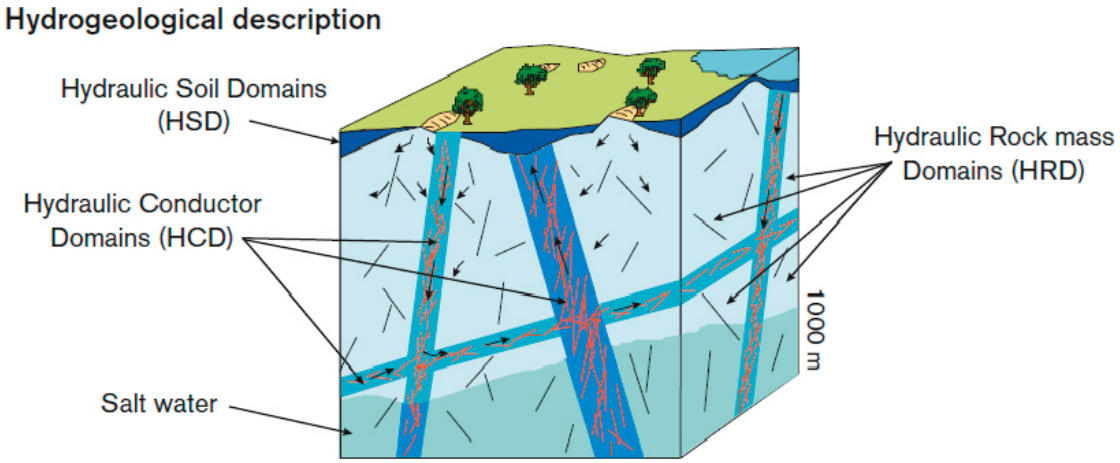

Figure 2-2. *Schematic diagram showing the division of the crystalline bedrock and the regolith (Quaternary deposits) into three hydraulic domains, HCD, HRD and HSD (Rhén et al. 2003, Figure 3-2).*

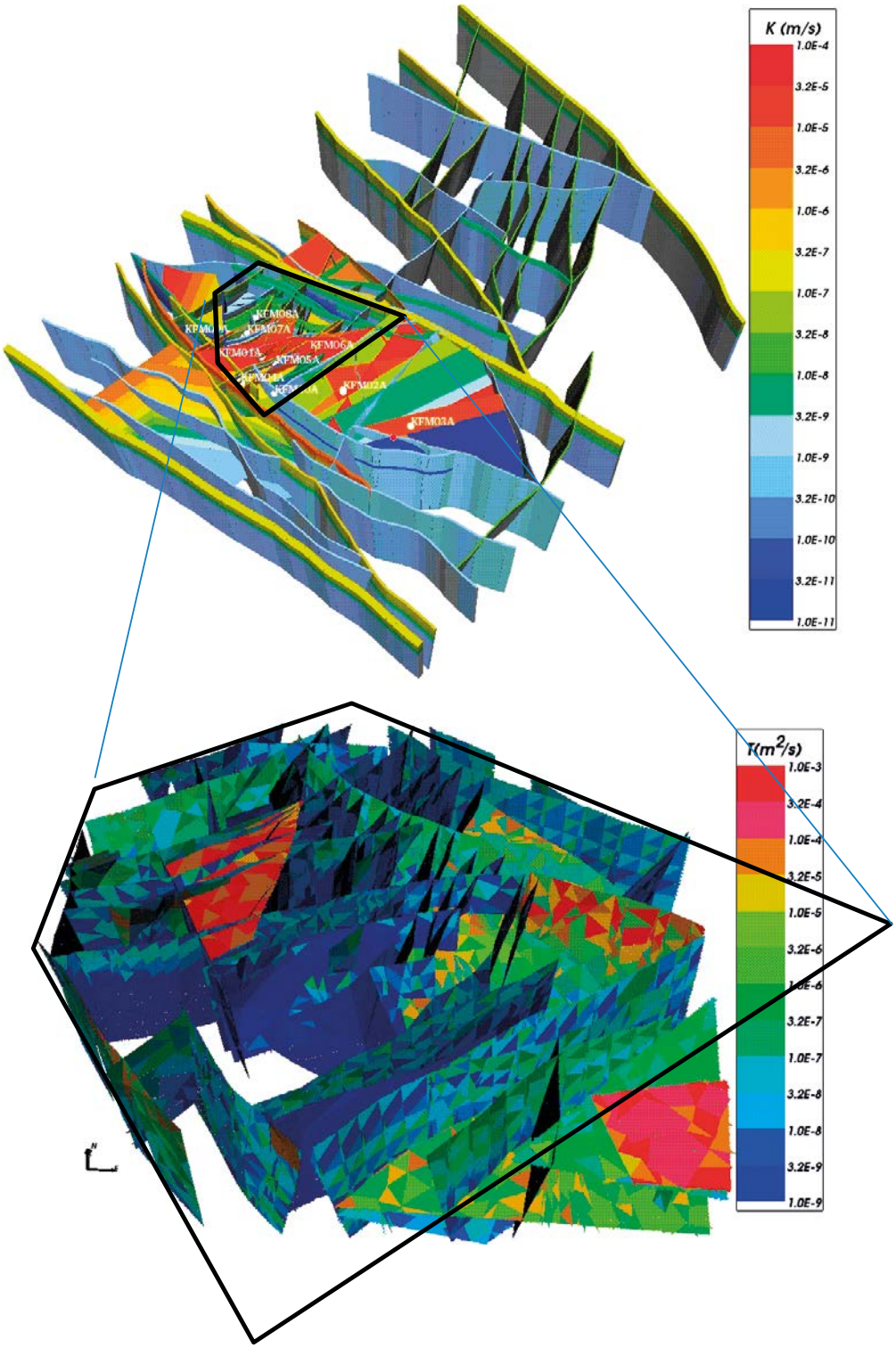

Figure 2-3. *Property model of the deformation zones. Top: Regional scale deformation zones with deterministic properties, represented as volumes to show their assigned width and coloured by hydraulic conductivity. Bottom: Visualisation of one stochastic realisation of the deformation zones that occur inside the local model domain, represented as surfaces and coloured by transmissivity. Adapted from Follin (2008, Figures 6-1 and 6-2).*

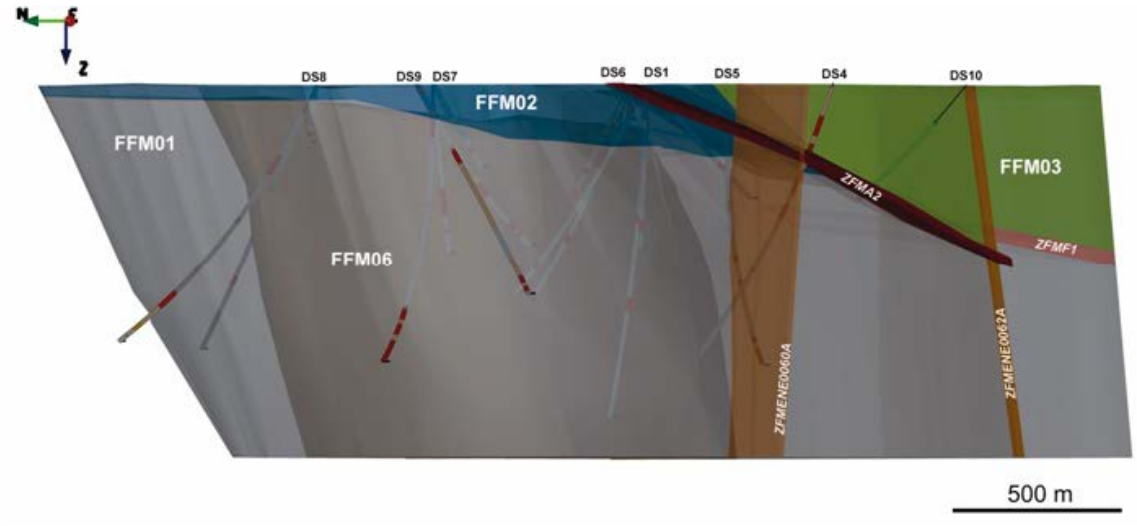

Figure 2-4. *Three-dimensional representation of the fracture domain model, viewed towards ENE. Fracture domains FFM01, FFM02, FFM03 and FFM06 are coloured grey, dark grey, blue and green, respectively. The gently dipping and sub-horizontal zones A2 and F1 as well as the steeply dipping deformation zones ENE0060A and ENE0062A are also shown. (Follin 2008, Figure 3-10).*

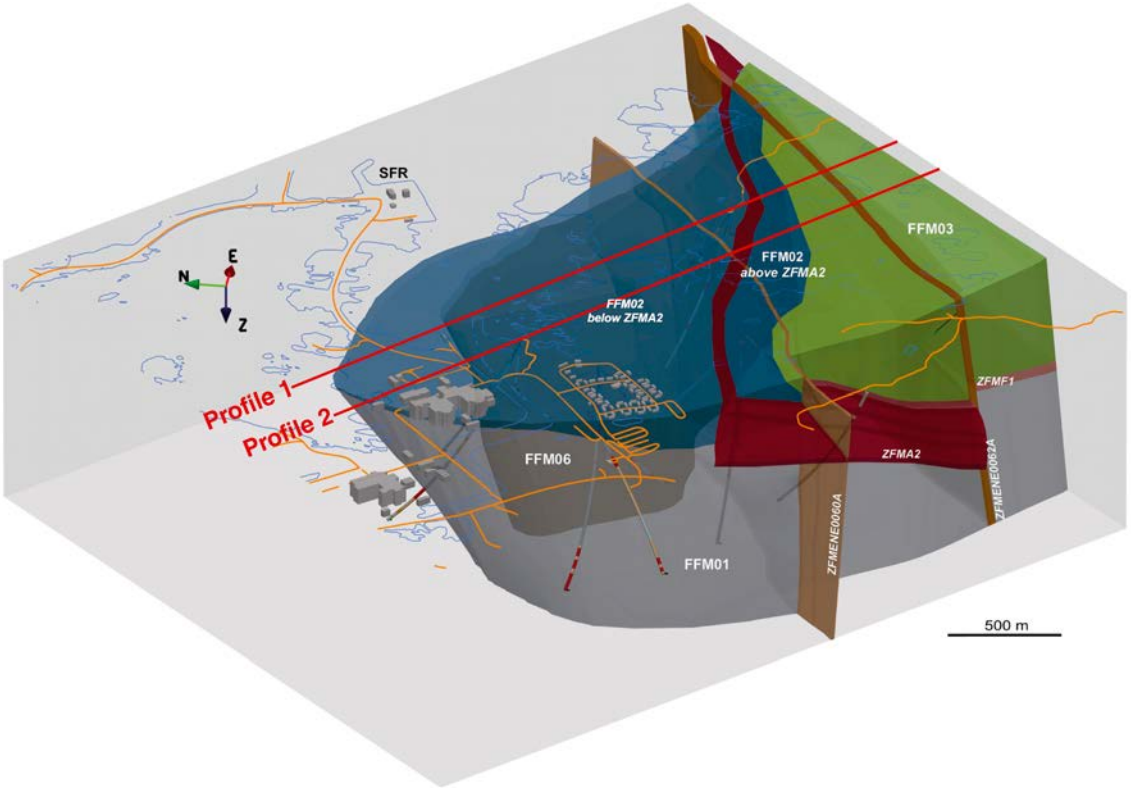

Figure 2-5. *Three-dimensional view towards ENE showing the relationship between deformation zone A2 (red) and fracture domain FFM02 (blue). Profile 1 and 2 are shown as cross-sections in Figure 2-6. (Follin 2008, Figure 3-11).*

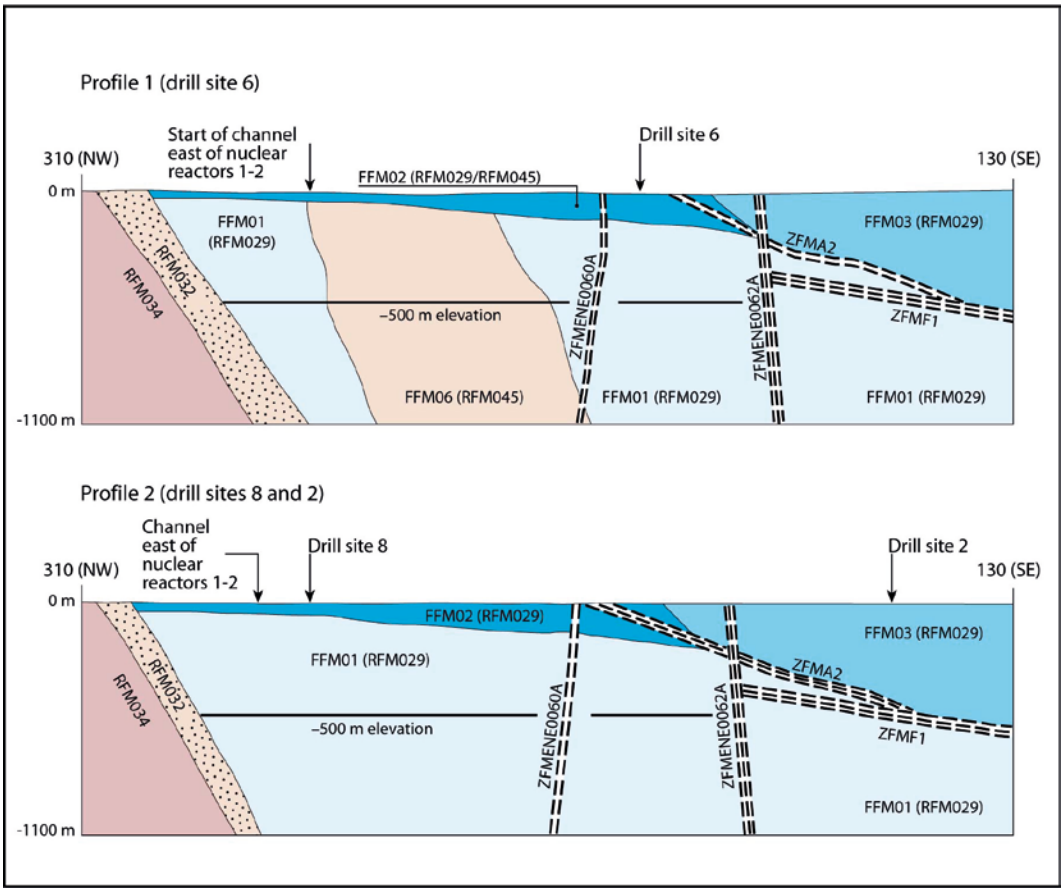

Figure 2-6. *Simplified profiles in a NW-SE direction that pass through the target volume. The locations of the profiles are shown in Figure 2-5. The key fracture domains, FFM01, -02 and -06, for a final repository at Forsmark occur in the footwall of zones A2 (gently dipping) and F1 (sub-horizontal). The major steeply dipping zones ENE0060A and ENE0062A are also included in the profiles. (Olofsson et al. 2007, Figure 5-1).*

Due to the depth trend in fracture intensity in Forsmark, the FFM01/06 domain was divided into three depth zones (above –200 m, –200 m to –400 m and below –400 m elevation). The FFM03, FFM04 and FFM05 domains were divided into two depth zones (above and below –400 m elevation). Additionally, fractures were divided by orientation into four sub-vertical fracture sets (NS, NE, NW, EW) and one sub-horizontal fracture set (HZ). A process of analysis and calibration allowed a parameterisation of a hydrogeological discrete fracture network (Hydro-DFN) to be produced. This assumed a power-law relationship between intensity and fracture size:

$$f(r) = \frac{k_r r_0^{k_r}}{r^{k_r+1}} \qquad (2\text{-}1)$$

where r_0 and k_r are the location parameter and the shape parameter, respectively. Additionally, a semi-correlated relationship between fracture size and transmissivity was used for the hydrogeological base case:

$$\log(T) = \log(a\, r^b) + \sigma_{\log(T)}\, N[0,1] \qquad (2\text{-}2)$$

where T is the fracture transmissivity, r is the fracture radius, a and b are constants and $N[0,1]$ denotes a normally distributed random deviate with a mean equal to zero and a standard deviation of 1. The parameters defining the Hydro-DFN for each fracture domain are given in Table 2-1.

Table 2-1. Hydrogeological DFN parameters for the semi-correlated transmissivity model of each fracture domain with depth dependency (taken from the "alternative" parameters in Follin (2008, Tables C-1 to C-3)).

Fracture domain (m RHB 70)	Fracture set name	Orientation set pole: (trend, plunge), conc.	Size model, power-law (r_0, k_r) (m, –)	Intensity, (P_{32}), valid size interval: (r_0, 564 m) (m^2/m^3)	Parameter values for the transmissivity model shown in Eq. (2-2) T (m^2s^{-1})
FFM01	NS	(292, 1) 17.8	(0.038, 2.50)	0.073	
FFM06 > –200	NE	(326, 2) 14.3	(0.038, 2.70)	0.319	
	NW	(60, 6) 12.9	(0.038, 3.10)	0.107	$(a,b,\sigma) = (6.3 \times 10^{-9}, 1.3, 1.0)$
	EW	(15, 2) 14.0	(0.038, 3.10)	0.088	
	HZ	(5, 86) 15.2	(0.038, 2.38)	0.543	
FFM01	NS	As above	As above	0.142	
FFM06 –200 to –400	NE	As above	As above	0.345	
	NW	As above	As above	0.133	$(a,b,\sigma) = (1.3 \times 10^{-9}, 0.5, 1.0)$
	EW	As above	As above	0.081	
	HZ	As above	As above	0.316	
FFM01	NS	As above	As above	0.094	
FFM06 < –400	NE	As above	As above	0.163	
	NW	As above	As above	0.098	$(a,b,\sigma) = (5.3 \times 10^{-11}, 0.5, 1.0)$
	EW	As above	As above	0.039	
	HZ	As above	As above	0.141	
FFM02 > –200	NS	(83, 10) 16.9	(0.038, 2.75)	0.342	
	NE	(143, 9) 11.7	(0.038, 2.62)	0.752	
	NW	(51, 15) 12.1	(0.038, 3.20)	0.335	$(a,b,\sigma) = (9.0 \times 10^{-9}, 0.7, 1.0)$
	EW	(12, 0) 13.3	(0.038, 3.40)	0.156	
	HZ	(71, 87) 20.4	(0.038, 2.58)	1.582	
FFM03	NS	(292, 1) 17.8	(0.038, 2.60)	0.091	
FFM04	NE	(326, 2) 14.3	(0.038, 2.50)	0.253	
FFM05 > –400	NW	(60, 6) 12.9	(0.038, 2.55)	0.258	$(a,b,\sigma) = (1.3 \times 10^{-8}, 0.4, 0.8)$
	EW	(15, 2) 14.0	(0.038, 2.40)	0.097	
	HZ	(5, 86) 15.2	(0.038, 2.55)	0.397	
FFM03	NS	As above	As above	0.102	
FFM04	NE	As above	As above	0.247	
FFM05 < –400	NW	As above	As above	0.103	$(a,b,\sigma) = (1.8\times 10^{-8}, 0.3, 0.5)$
	EW	As above	As above	0.068	
	HZ	As above	As above	0.250	

2.2 Methods and tools

The modelling was carried out using ConnectFlow version 10.4.1 (AMEC 2012a, b, c). ConnectFlow is a suite of groundwater flow and transport software that is able to represent rock using continuous porous medium (CPM), discrete fracture network (DFN), or combined CPM/DFN concepts. This study uses a DFN concept to represent the bedrock, where flow in fractured rock is assumed to be predominantly through an inter-connected network of flow-conductive fractures with groundwater moving from one fracture to another at the intersections between them. The DFN concept is very

useful since it naturally reflects the individual flow conduits in fractured rock, and the available field data. The equations used are specified in AMEC (2012c). The properties of the network are usually characterised in terms of:

- Spatial distribution (e.g. Poisson, fractal, clustered around points or lineaments).
- Fracture intensity (and its spatial variation).
- Fracture sets distinguished by orientation.
- Fracture size (e.g. log-normal, power-law distributions).
- Transmissivity-size relationships.

The properties of each fracture are primarily:

- Size.
- Orientation (strike and dip).
- Transmissivity (and possibly spatial variability within the fracture).
- Transport aperture.
- Storativity.

In ConnectFlow, fractures are usually rectangular, but may be right-angled triangles where a complex surface has been triangulated into many pieces (e.g. for a deformation zone). For stochastic fractures, the properties are sampled from probability distribution functions (PDFs) specified for each fracture set. The properties may be sampled independently or correlated with other properties.

The main tunnels, deposition tunnels and deposition holes are represented as a CPM embedded within the DFN representation of the bedrock. Internal boundary conditions between the CPM and DFN domains ensure continuity of pressure and conservation of mass. On the DFN side of the interface, these boundary conditions are defined at nodes that lie along the lines (traces) that make up the intersections between fractures and the interface surface. On the CPM side, the boundary conditions are applied to nodes in finite-elements that abut the interface surface. Thus, extra equations are added to the discrete system matrix to link nodes in the DFN model to nodes in the finite-element CPM model, as shown in Figure 3-5. By using equations to ensure both continuity of pressure and continuity of mass, a more rigorous approach to embedding is obtained than by simply interpolating pressures between separate DFN and CPM models. The equations used are specified in AMEC (2012a).

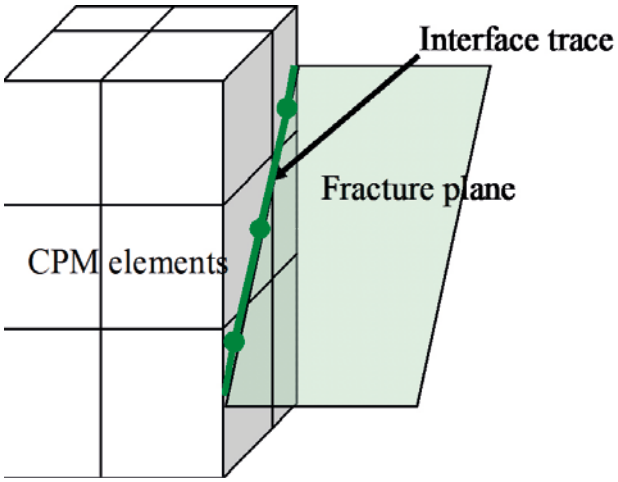

Figure 2-7. *Illustration of embedding between DFN and CPM sub-models. A finite-element CPM mesh is shown on the left. The right hand surface is intersected by a single fracture plane. Extra equations are used to link the DFN to the CPM. (Joyce et al. 2010a, Figure 3-5).*

2.3 Numerical models

The models used in this work are based on the repository-scale SR-Site Hydrogeological DFN model as described in Joyce et al. (2010a, Section 4.3), incorporating the same depth dependent hydraulic conductor domain (HCD) properties and the same hydraulic rock mass domains (HRD) as SR-Site. The deformation zones are modelled as surfaces that are composed of many rectangular or triangular planes that discretise the geometry and hydraulic properties. The HRD fractures are generated according to the parameters in Table 2-1. The fractures are square planes ranging in length from 0.7 m to 1,000 m close to the repository structures and from 10 m to 1,000 m elsewhere. An excavation damaged zone (EDZ) was represented in the repository-scale model as a set of horizontal fractures with appropriate hydraulic and transport properties below each tunnel, with a vertical cross fracture present to provide an intersection with the tunnel. Figure 2-8 shows a close-up view of the repository structures in part of the repository-scale model, including the EDZ.

All models have a constant transmissivity within each individual HRD fracture. Essentially, the modelled transmissivity is the effective transmissivity for flow over the area of the fracture. In reality, there is likely to be heterogeneity over each fracture, which may lead to greater variability in inflows between deposition holes. This variability would be quantified by Posiva Flow Log (PFL) test data under pumping conditions in deep boreholes. However, at Forsmark, hydraulic conditions at depth are such that there are very few flowing features above the PFL detection limit at repository depth between deformation zones with which to assess alternative concepts for heterogeneity using only the available surface acquired data.

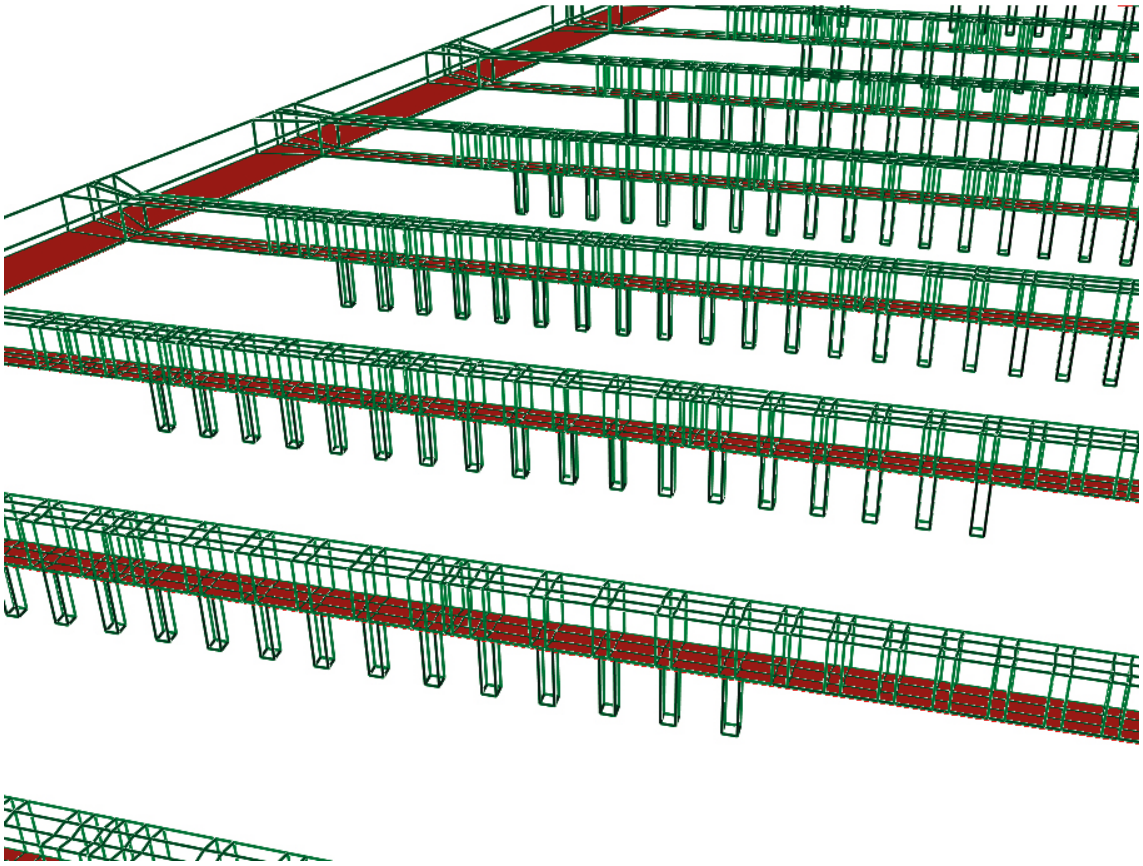

Figure 2-8. *Repository-scale model. Close-up view of deposition holes, deposition tunnels and part of a main tunnel. Tunnels are shown in green wireframe and the EDZ is coloured red. (Joyce et al. 2010a, Figure 4-14).*

The SR-Site repository-scale model uses a continuous porous medium (CPM) to represent the main tunnels, deposition tunnels and deposition holes in the repository. The CPM repository structures are then embedded within a DFN representation of the HRD surrounding the repository.

A total of five cases of the repository-scale model are considered:

- the SR-Site Hydrogeological base case model (r0) with one realisation of the stochastic fractures, but with deterministic properties for the deformation zones with a depth trend.
- the SR-Site Hydrogeological base case with no excavation damaged zone (EDZ) using one realisation of the stochastic fractures, but with deterministic properties for the deformation zones with a depth trend.
- three additional realisations of the SR-Site Hydrogeological base case model (r2, r3 and r5) including stochastic horizontal variation in deformation zone properties with a depth trend.

The cases considered in this work are summarised in Table 2-2. Case r0 is selected as the base case and cases r2 and r3 are selected with alternative stochastic HCD and HRD representations (r1 has the same stochastic DFN as r0 and so is not used for this study). Case r5 has been shown to have anomalous performance measures, influenced by a large sub-vertical stochastic fracture intersecting the boundary (Joyce et al. 2010a, Section 6.2.7) and so has been selected instead of r4 to examine the effect on inflows where such fractures occur. In all cases, grouting is not included.

For each case in Table 2-2, three separate simulations are performed to model the phased construction of the repository, based on the SR-Site models developed by Joyce et al. (2010a). The SR-Site models are based on three sub-models, each representing a single block (DA-A, DA-B and DA-C), corresponding to the three main repository areas containing the deposition tunnels and deposition holes and are equivalent to the blocks described in Svensson and Follin (2010, Figure 1-2). The repository layout used for this work is shown in Figure 2-9, with the three blocks shown: DA-A (in blue), DA-B (in green) and DA-C (in red). The repository layout and design is described in SKB (2010).

The three simulations are used to depict the following situations:

- tunnels in area DA-A open, with DA-B and DA-C yet to be opened.
- tunnels in area DA-B open with DA-A closed and backfilled and DA-C yet to be opened.
- tunnels in area DA-C open, with DA-A and DA-B closed and backfilled.

Each block extends from –800 m elevation to a top surface mapped to the topography of the bedrock below the overburden. No overburden is present for the repository-scale model.

When the tunnels and deposition holes are open prior to backfilling, these volumes could have been represented as voids in the model with atmospheric pressure boundary conditions on the faces. Instead, a CPM representation of the tunnels and deposition holes was maintained through the phased opening of tunnels (described in Section 4.2), but properties and internal boundary conditions of these volumes were modified according to whether they were open or closed at each particular phase considered.

Table 2-2. Summary of the cases considered in this work.

Case	HCD realisation	HRD realisation	EDZ
r0	Deterministic	Realisation 1	Yes
r2	Stochastic realisation 2	Realisation 2	Yes
r3	Stochastic realisation 3	Realisation 3	Yes
r5	Stochastic realisation 5	Realisation 5	Yes
r0 no EDZ	Deterministic	Realisation 1	No

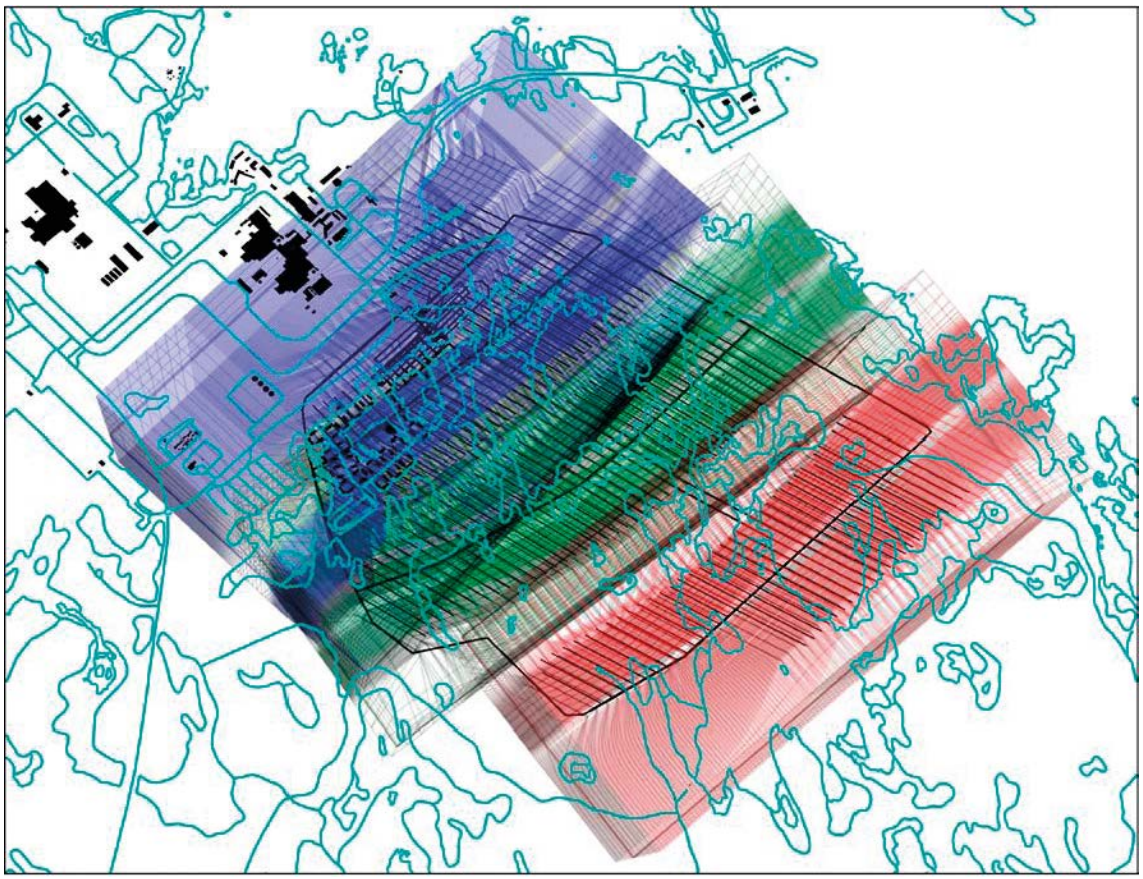

Figure 2-9. *Repository-scale blocks: DA-A is coloured blue; DA-B is coloured green and DA-C is coloured red. The repository structures and buildings are shown in black. The shoreline at 2000 AD is shown in blue. (Joyce et al. 2010a, Figure 4-12).*

Under open or partially open conditions, the areas of the repository that are open have atmospheric pressure boundary conditions applied at nodes inside the open tunnels and have a hydraulic conductivity set to 0.1 m/s, which represents a high conductivity and is consistent with the value for the open repository calculations used for Laxemar (Joyce et al. 2010b, Appendix G). A value of 1.0 is set for the porosity of the open areas of the repository. The high hydraulic conductivity ensures that any flow in the open structures is delivered directly to the boundary condition nodes at atmospheric pressure. Thus, the CPM parts represented in this way become a sink for groundwater inflows in the same way as the void representation, but with the flexibility to conveniently switch structures between open and closed states. For areas that are closed and backfilled, the hydraulic conductivity and porosity values are unchanged from the backfill values, as described for SR-Site (see Joyce et al. 2010a, Table 4.2).

This study uses existing models from SR-Site developed by Joyce et al. (2010a) which are based on three sub-models, each representing a single block (equivalent to DA-A, DA-B and DA-C). Because the repository is split into the three sub-models, some of the repository features (i.e. the central area, main tunnels and transport tunnels) would intersect the model boundaries of the sub-models. Due to the boundary conditions applied, artificially large inflows into these repository features could result that would obscure the inflows from natural fractures, potentially leading to a significant distortion of the calculated tunnel and deposition hole inflows. As a result, parts of the repository outside of the deposition holes, deposition tunnels and main tunnels have not been included in the models. The removal of these structures may cause a minor increase in flows to the deposition tunnels, since flow may be diverted to them that would otherwise have gone to these structures. Of course, large stochastic fractures may also intersect the model boundary leading to high inflows, but these are not removed.

Figure 2-10 shows a slice through the repository model at an elevation of –470 m, showing the repository layout (in blue, green and red) together with the main deformation zones. As previously indicated, the model includes the same depth-dependent hydraulic conductor domain (HCD) as used in SR-Site (see Joyce et al. 2010a, Chapter 4). Figure 2-11 gives a slice through the regional-scale model described in Joyce et al. (2010a, Section 4.1) showing the distribution of the HRD fracture domains. Figure 2-12 shows a corresponding slice for the repository-scale model described in Joyce et al. (2010a, Section 4.3). Note that the FFM04 and FFM05 domains are close to the perimeter of the repository. These domains were associated with higher fracture intensity and flows in the SDM, although their parameterisation was based on limited data (see Follin et al. 2007, Section 11.7).

The groundwater flow simulations are carried out as described in Joyce et al. (2010a, Section 4.3.3), where the steady-state groundwater flow field in the repository-scale model is calculated using pressures and densities imported from the SR-Site regional-scale model using the hydrogeological conditions for 2000 AD, but with an atmospheric pressure boundary condition applied to main tunnels, deposition tunnels and deposition holes to simulate an open repository.

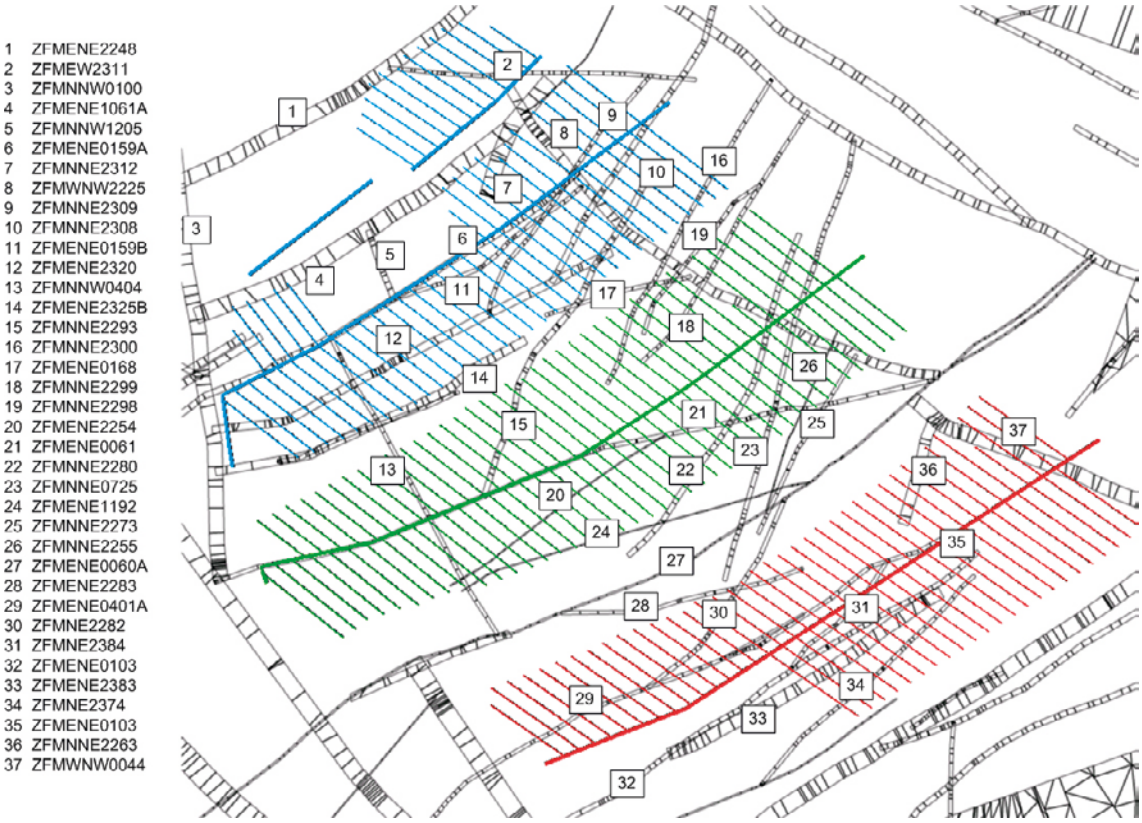

Figure 2-10. *Repository tunnel layout, showing the three blocks: DA-A (in blue), DA-B (in green) and DA-C (in red), and the deformation zones in black.*

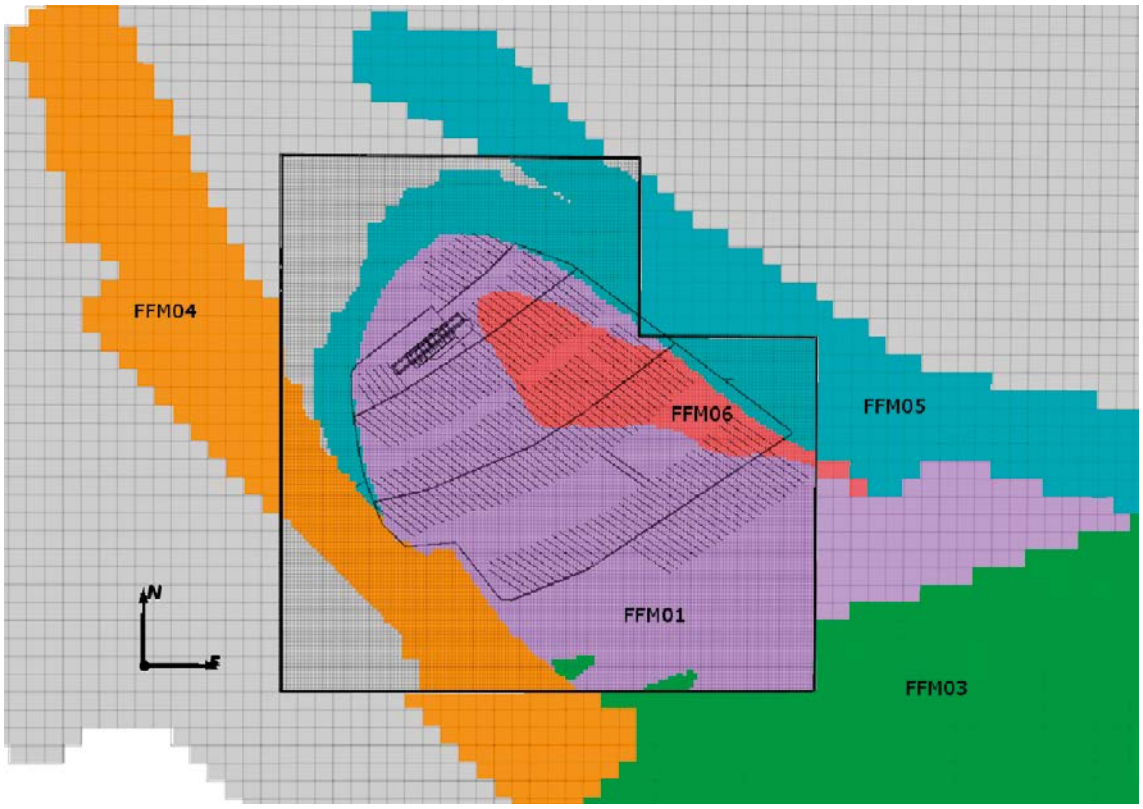

Figure 2-11. *Distribution of fracture domains at repository elevation (–470 m) as implemented in the regional-scale hydrogeological base case model. FFM02 (not shown) lies above FFM01 and FFM06. The black outline shows the boundary of the local area. The repository layout is superimposed in grey for context.*

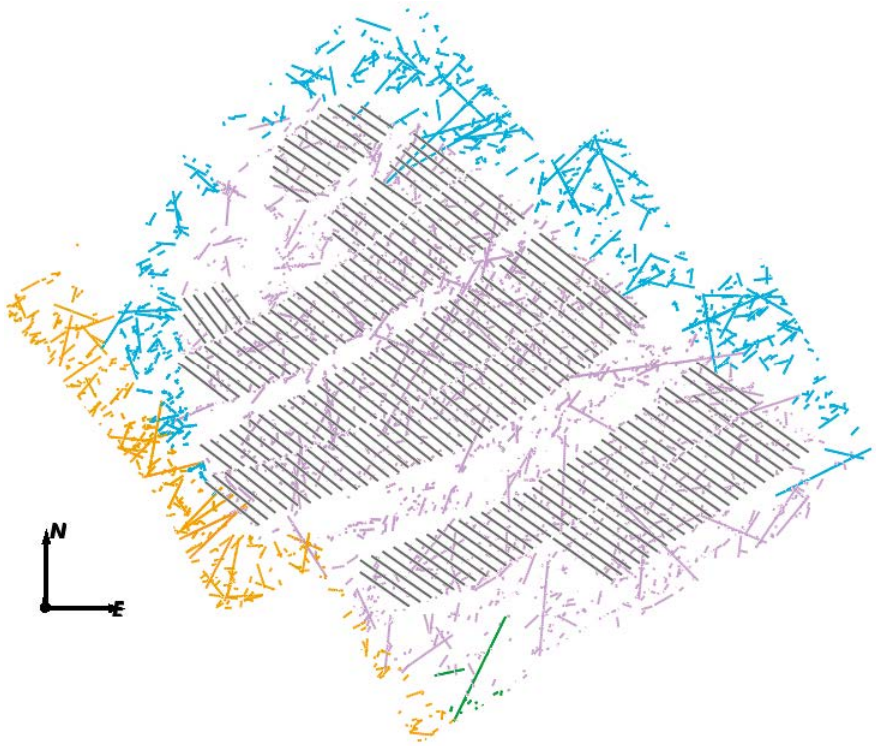

Figure 2-12. *A slice through the fractures in the repository-scale hydrogeological base case model at repository elevation (–470 m) and coloured by fracture domain. FFM01/06 is purple, FFM03 is green, FFM04 is orange and FFM05 is blue. FFM02 (not shown) lies above FFM01/06. The deposition tunnels are superimposed in grey for context.*

3 Inflows to deposition holes and tunnels

This section presents statistics and analyses of the inflows to deposition holes and tunnels calculated under open repository conditions, where the deposition holes and tunnels are at atmospheric pressure. The statistics presented are based on the simulated inflows from ungrouted fractures intersecting underground openings where only inflows greater than $1 \cdot 10^{-11}$ m^3/s ($6 \cdot 10^{-7}$ L/min) are included due to potential numerical issues with inflows below this level.

As well as the statistical analysis, the spatial distribution of inflows to both deposition holes and tunnels is presented. Where practical, results are presented comparing the results for all five cases described in Table 2-2, otherwise, results are presented for the base case (r0) and results for the other cases are presented in Appendix A.

Table 3-1 shows the total inflows to each block for the various cases. The total inflows are the sum of the inflows to deposition holes and deposition tunnels in each block. It can be seen from the table that there is a large variability in the inflows between the five cases, with the greatest differences in the inflows found in cases r3 and r5 for block DA-B compared to the other cases. For the r3 and r5 cases, a large stochastic fracture intersects both the model boundary and some of the tunnels and deposition holes in block DA-B (see Figure 3-1), giving rise to localised high inflows to some deposition holes and tunnels and hence the larger inflows to the block. For comparison, block inflows presented in Svensson and Follin (2010, Section 5.2.1) are also shown. The inflows presented by Svensson and Follin are calculated using an equivalent continuous porous medium (ECPM) model based on case r0, but with grouting included. The inflows reported in Table 3-1 are for their grouting levels I or II, in which the conductivity of all cells in contact with the repository has a maximum value of $1 \cdot 10^{-7}$ m/s or $1 \cdot 10^{-8}$ m/s, respectively. In contrast, grouting has not been included for the DFN cases reported here. The inclusion of grouting would be expected to reduce inflows very significantly for blocks DA-B and DA-C, which have the highest inflows.

Table 3-1. Total inflows to deposition tunnels and holes in each block [L/min] for each case.

Case	Block DA-A	Block DA-B	Block DA-C	Total
r0	138	767	746	1,651
r2	228	1,203	996	2,426
r3	151	5,335	829	6,315
r5	99	74,907	802	75,808
r0 no EDZ	138	765	747	1,650
Svensson and Follin (1)	360	480	540	1,380
Svensson and Follin (2)	240	360	480	1,080

(1) Block inflows from Svensson and Follin (2010, Table 5.1) for grouting level I.

(2) Block inflows from Svensson and Follin (2010, Table 5.1) for grouting level II.

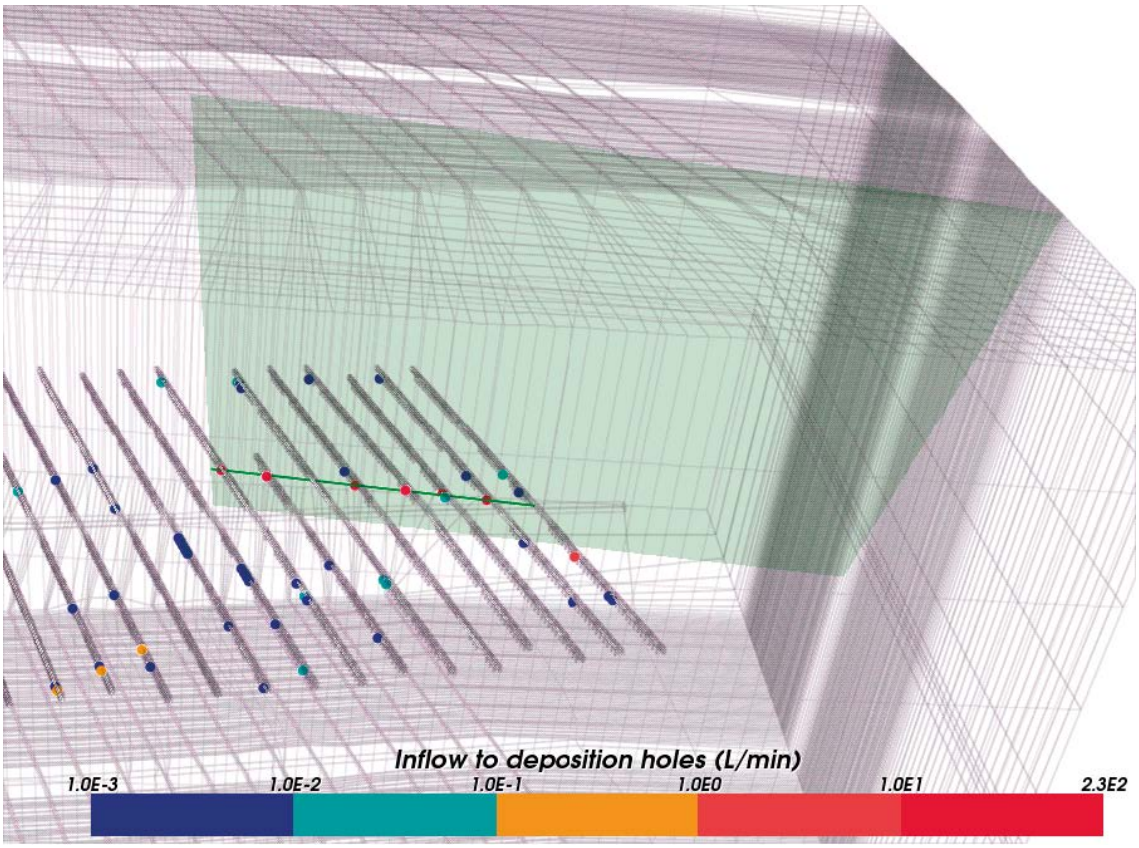

Figure 3-1. *Large stochastic fracture (light green) for case r3 in block DA-B. The green line shows where the fracture intersects the deposition tunnels. The deposition tunnels are shown in dark grey and the model boundary in light grey. Inflows to deposition holes are shown as filled circles, coloured by inflow. The large fracture can clearly be seen to intersect with both the model boundary as well as some of the deposition holes in block DA-B, resulting in large inflows to those deposition holes intersected by the fracture.*

3.1 Inflows to deposition holes

The total inflow to a deposition hole depends on the total transmissivity of flowing fractures (both natural and those representing the EDZ) that intersect the hole and the flow in the surrounding fracture network. Table 3-2 shows the total inflows to all deposition holes for each of the five cases considered, together with the number of intersections with natural fractures attributed to each fracture type, sub-divided into deformation zone fractures, EDZ (inflows only), sub-vertical (fracture sets NS, NE, NW and EW) and sub-horizontal (fracture set HZ) stochastic fractures. The small differences between cases r0 and "r0 no EDZ" are due to differences in flow causing some intersections to fall below the $6 \cdot 10^{-7}$ L/min cut-off limit. The high inflows for cases r3 and r5 are due to a single large fracture generated for each of these two cases, as explained previously. This is shown more clearly when the inflows from sub-vertical fractures are broken down by fracture domain and depth in Table 3-3. For cases r3 and r5, it is evident that the large inflows are due to a small number of intersections, from one or two large fractures centred in the top 200 m of the model. It should also be noted that Table 3-3 shows that, apart from the large inflows in r3 and r5 from single large fractures, the majority of the flows to deposition holes from sub-vertical fractures are from hydraulic rock domains FFM04 and FFM05 (see Figure 2-11 and Figure 2-12).

Table 3-2 also indicates relatively high inflows to deposition holes from intersections with deformation zones for all cases. It is intended that deposition hole locations will avoid deformation zones and deposition hole gaps have been incorporated into the repository layout to allow this. However, in a few locations, the gaps in the repository layout are not consistent with the positions of the deformation zones at repository depth and so a small number of deposition holes are intersected. The number of intersections of deposition holes with the deformation zones is the same across all

cases, as would be expected, although the inflows do vary from one case to another. Average inflows from deformation zones are also generally higher than those from natural fractures. It is also interesting to note that although there are a large number of sub-horizontal fracture intersections, the inflows from these fractures are much less, on average, compared to the inflows from sub-vertical fractures. As an example, Figure 3-2 illustrates the inflows to deposition holes along the deformation zones ZFMENE0401 and ZFMENE2374 in block DA-C.

Table 3-2. Total flow into all deposition holes (6916) [L/min] / Count of intersections with natural fractures by fracture type and case.

Case	Deformation Zone	EDZ	Sub-horizontal	Sub-vertical	Total
r0	18.1 / 9	0.7	3.3 / 1,001	27.0 / 537	49.1 / 1,547
r2	26.3 / 9	0.9	6.5 / 844	56.0 / 528	89.7 / 1,381
r3	5.8 / 9	1.6	2.0 / 912	906.4 / 580	915.7 / 1,501
r5	12.1 / 9	0.6	1.7 / 770	5,757.8 / 528	5,772.1 / 1,307
r0 no EDZ	18.4 / 9	0.00	3.3 / 987	26.7 / 516	48.4 / 1,512

Table 3-3. Total flow into deposition holes from sub-vertical fractures [L/min] / Count of intersections with natural fractures by fracture domain and depth of fracture centre.

Case	FFM01/6 0–200 m	FFM01/6 200–400 m	FFM01/6 >400 m	FFM04/5 0–800 m
r0	0.0 / 0	5.3 / 13	0.3 / 514	21.4 / 10
r2	0.0 / 0	3.8 / 27	0.6 / 484	51.6 / 17
r3	867.0 / 6	8.8 / 25	0.7 / 539	30.6 / 10
r5	5,752.2 / 2	1.0 / 8	0.8 / 512	3.7 / 6
r0 no EDZ	0.0 / 0	5.1 / 13	0.3 / 493	21.2 / 10

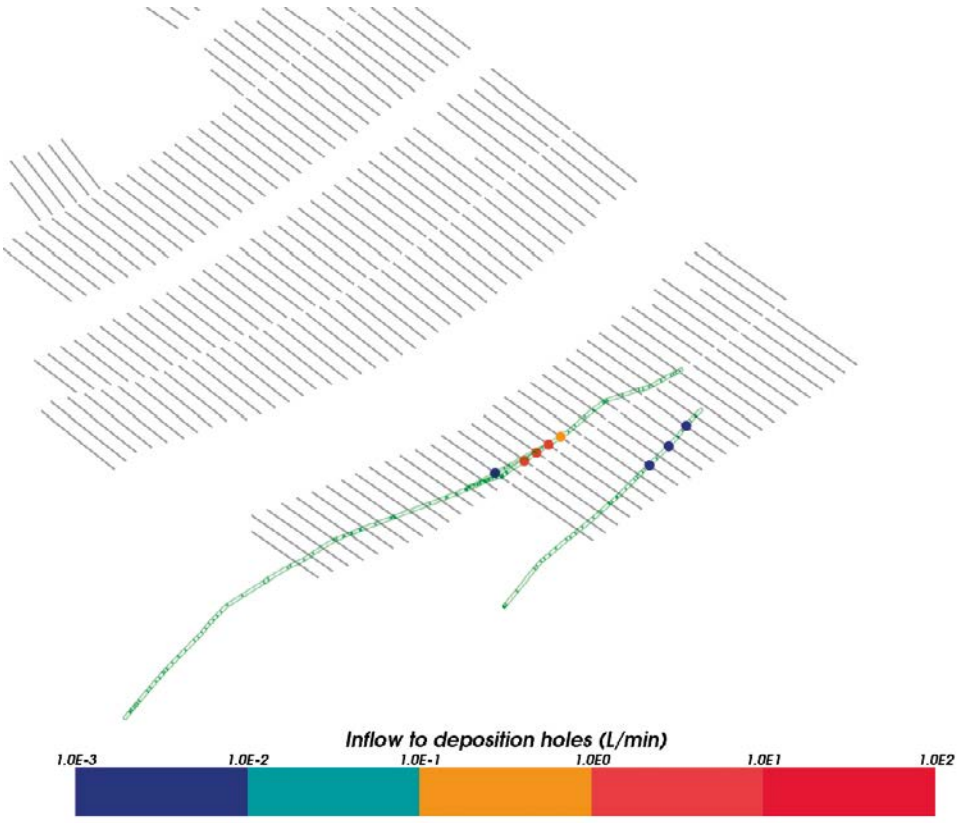

Figure 3-2. *Inflows to deposition holes from deformation zones, coloured by inflow in block DA-C.*

Figure 3-3 shows the complementary cumulative distribution of the transmissivity of individual natural fractures with an inflow intersecting each deposition hole for all five cases. It is seen from this figure that there is little difference between each of the cases, and that the percentage of fractures that intersect deposition holes having transmissivities with log values above –8.5, varies between 22% and 32% of all intersecting fractures.

The comparison of the complementary cumulative distribution of inflows to deposition holes for each case is shown in Figure 3-4. The inflows to deposition holes across different cases where the EDZ is included (i.e. r0, r2, r3 and r5) are all relatively consistent for all inflow ranges. When the EDZ is excluded, the additional inflows to deposition holes provided by the EDZ are then absent leading to a reduction in inflows below $1 \cdot 10^{-3}$ L/min for the no EDZ case compared to the other cases. Above $1 \cdot 10^{-3}$ L/min, little difference is seen between the cases.

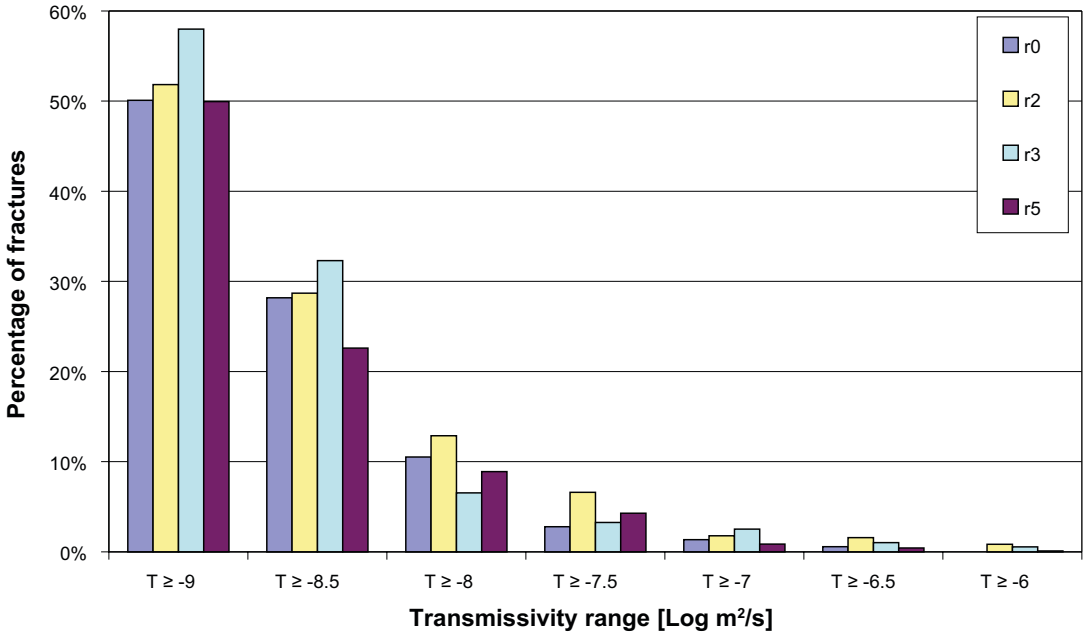

Figure 3-3. *Complementary cumulative distributions of the transmissivity of fractures with inflows intersecting the deposition holes. The transmissivities of the EDZ fractures are not included.*

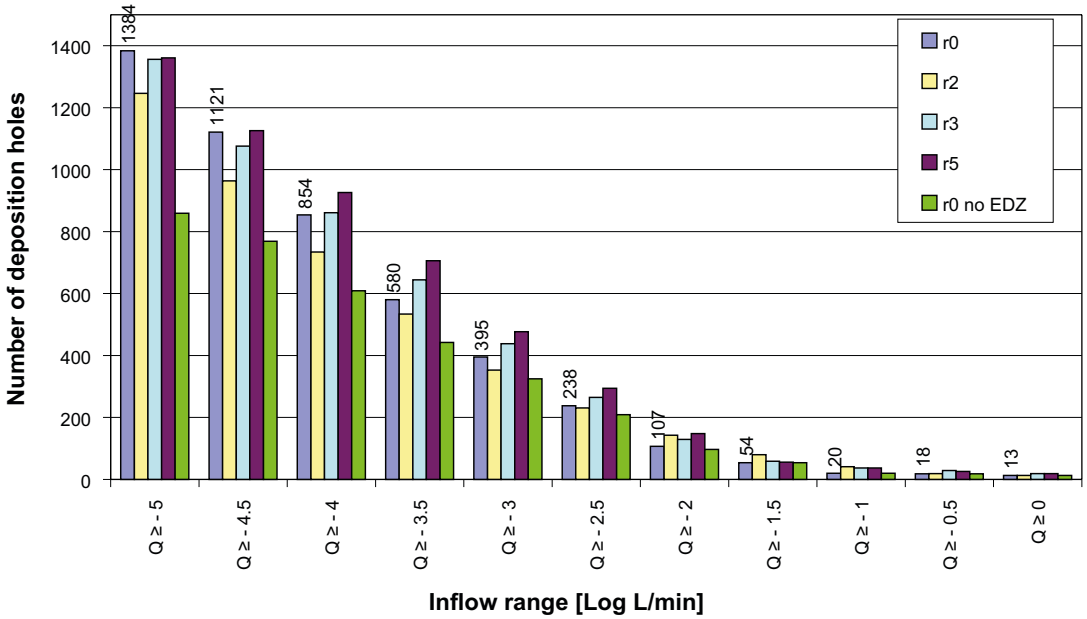

Figure 3-4. *Complementary cumulative distributions of the total inflow to each deposition hole for each case.*

Figure 3-5, shows the number of deposition holes with a particular number of inflows for each of the five cases. Only inflows from natural fractures are counted (i.e. inflows from the EDZ are excluded). The vast majority of the deposition holes have no intersecting flowing fractures, ranging from 5,753 out of 6,916 (81%) deposition holes for r5 to 5,965 (86%) for r2. Between 651 and 784 deposition holes have one intersecting fracture, falling to less than 90 deposition holes with three intersections. When there is no EDZ, the connectivity of the fracture network around the repository is reduced, although this has only a marginal affect on the numbers of inflows above the very low limit of $6 \cdot 10^{-7}$ L/min considered in this figure.

Figure 3-6 shows the number deposition holes with a certain number of inflows (i.e. inflow points), within various ranges for case r0. There is one inflow point for each fracture that interests a deposition hole. For example, there are 18 deposition holes with one inflow above 0.1 L/min, and two deposition holes with two inflows above 0.1 L/min. Figure 3-7 and Figure 3-8 show cross-plots of the total inflow to each deposition hole against the sum of the transmissivities of the intersecting fractures to that deposition hole for the cases r0 and r0 no EDZ respectively. In both plots a line depicting transmissivity, approximated to equal specific capacity (i.e. inflow/drawdown), is shown. For radial flow through a single homogeneous fracture intersecting a drill hole or tunnel orthogonally, then the specific capacity is approximately equal to the transmissivity, where the radius of influence to a fixed pressure boundary (e.g. at a high transmissivity fracture or deformation zone) is about 500 times the radius of the opening. This approximation has been used extensively in estimating a transmissivity from the specific capacity measured in the PFL tests. For these calculations a drawdown of –470 m is applied to deposition holes. However, it is recognised that a correction factor may need to be applied to the drawdown to deposition holes in a similar manner to that which is applied to radial flow to a horizontal cylinder (see Section 3.2), where the drawdown to a deposition tunnel is calculated to be 513.8 m.

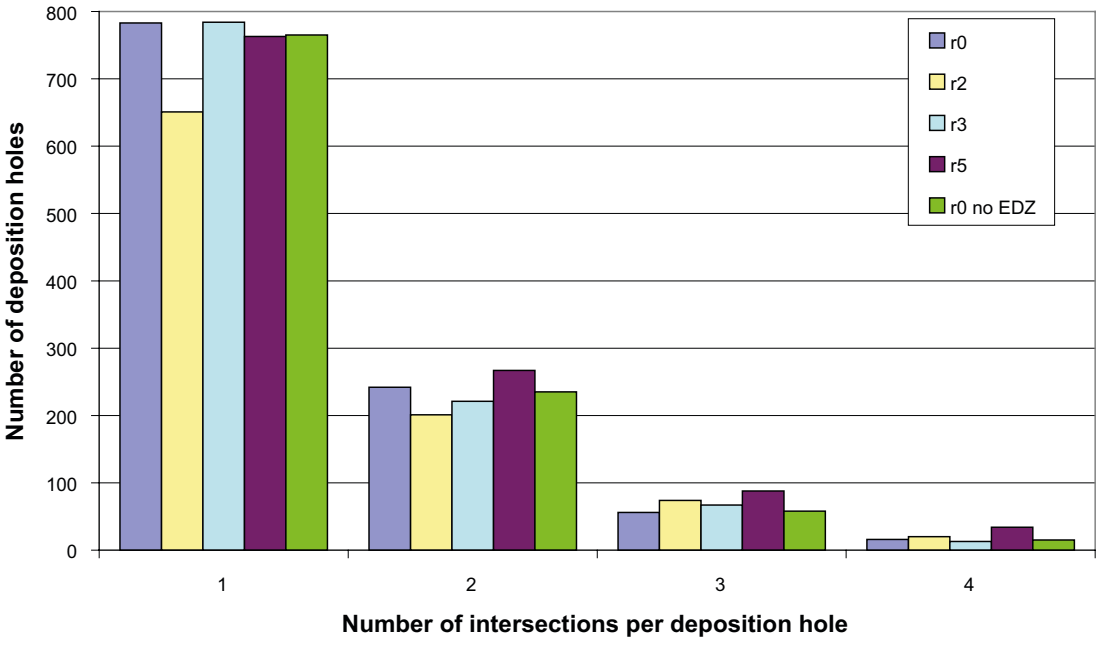

Figure 3-5. *Comparison of the number of deposition holes with a certain number of natural fractures with inflows intersecting the deposition holes, out of a total of 6,916 possible deposition holes for the five cases. Note only fractures with inflows over $6 \cdot 10^{-7}$ L/min are counted. For the cases with an EDZ only natural flowing fractures are included.*

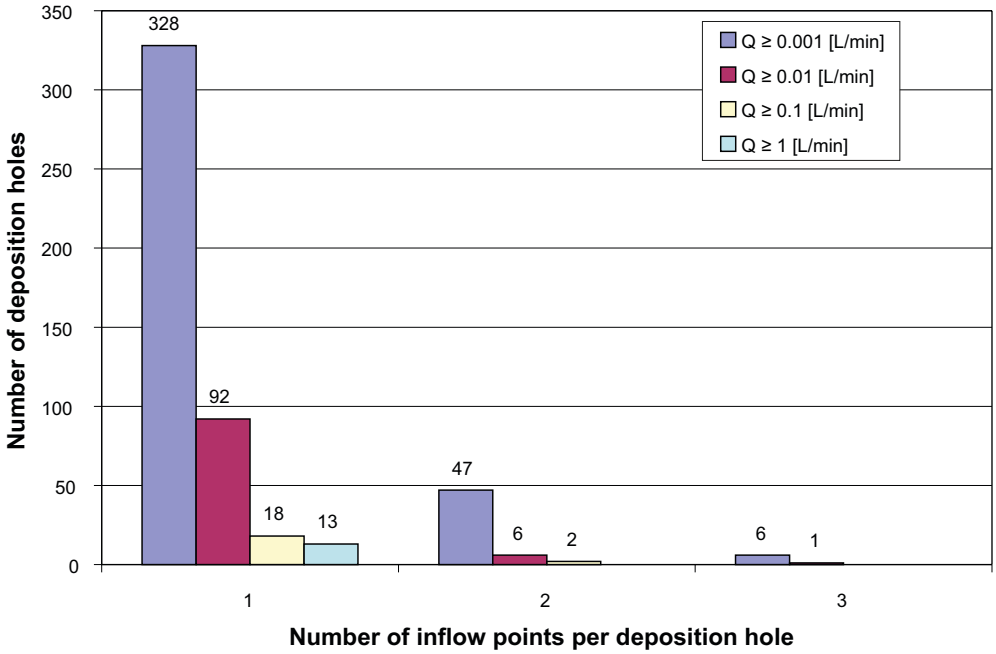

Figure 3-6. *Plot of the number of deposition holes that have a certain number of inflow points for a range of inflow limits for case r0.*

Figure 3-7 shows a cross-plot of the total inflow to deposition holes against the sum of the transmissivities of the intersecting fractures. There are very few points below a transmissivity of $1 \cdot 10^{-8}$ m^2/s since this is the transmissivity of the EDZ, which intersects all deposition holes. There are four distinct bands around transmissivities ~$3 \cdot 10^{-8}$ m^2/s across a wide inflow range. These bands are due to inflows to the deposition holes via the EDZ fractures, where the transmissivity of the EDZ is $1 \cdot 10^{-8}$ m^2/s. The EDZ is represented by a set of fractures parallel to the tunnel bottom and a set of small cross fractures connecting these fractures to the tunnel base (the adjusted transmissivity is $9 \cdot 10^{-9}$ m^2/s). The EDZ can provide between one and four fractures intersecting a deposition hole, giving rise to the four transmissivity bands that are apparent in the figure. The four transmissivity values which would result from intersections with one to four EDZ fractures are shown as orange lines in the plot. As expected, without the EDZ these bands disappear (see Figure 3-8), although some vertical series of points do remain, especially at higher transmissivities, which correspond to fractures with uniform transmissivities intersecting multiple deposition holes.

3.1.1 Spatial distribution

Figure 3-9 is a view of the repository together with the stochastic fractures and deformation zones sliced at repository elevation (–470 m) showing the spatial distribution of inflows to the deposition holes for case r0. For clarity, only total inflows to deposition holes greater than $1 \cdot 10^{-3}$ L/min are shown. Deformation zones are shown in purple and stochastic fractures in green (for sub-vertical fractures) and orange (for sub-horizontal fractures). From this figure, the higher inflows to deposition holes can be seen to occur when the deposition holes intersect with deformation zones in DA-C and sub-vertical stochastic fractures in DA-A, DA-B and DA-C. The sub-vertical fractures tend to be larger outside the deposition area due to a lower k_r value in the parameterisation of FFM04/05 compared to FFM01/06 (Table 2-1).

The spatial distribution of inflows for other cases are shown in Appendix A.1.

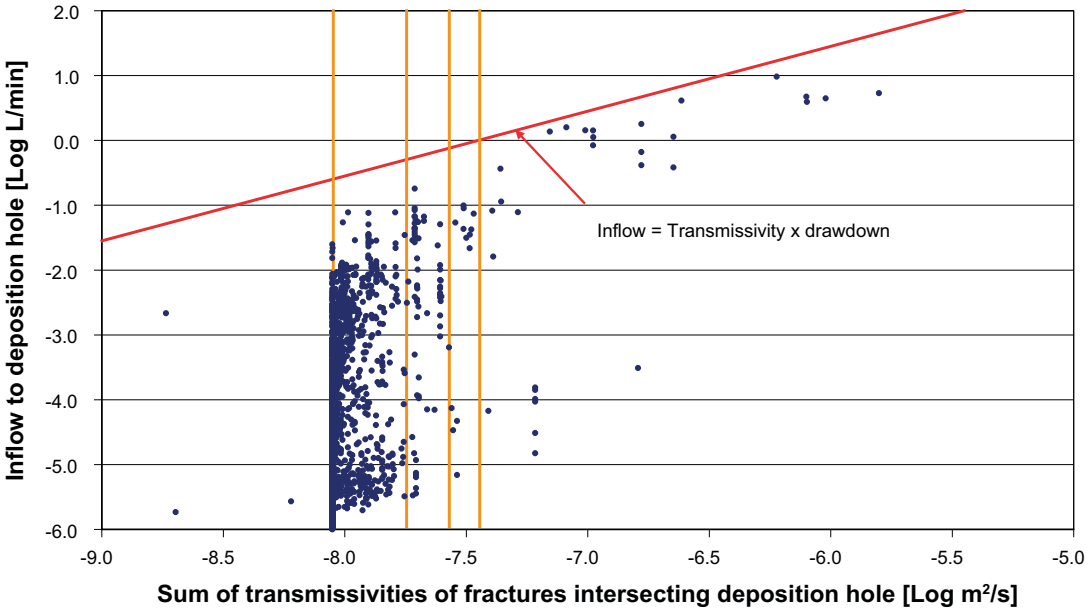

Figure 3-7. *Cross-plot of the total inflow to deposition holes out of a possible 6,916 versus the sum of the transmissivities of fractures intersecting each deposition hole for the case r0. The EDZ is included in the calculations of transmissivity and inflow. Transmissivities due to 1–4 intersections with the EDZ are indicated as orange vertical lines.*

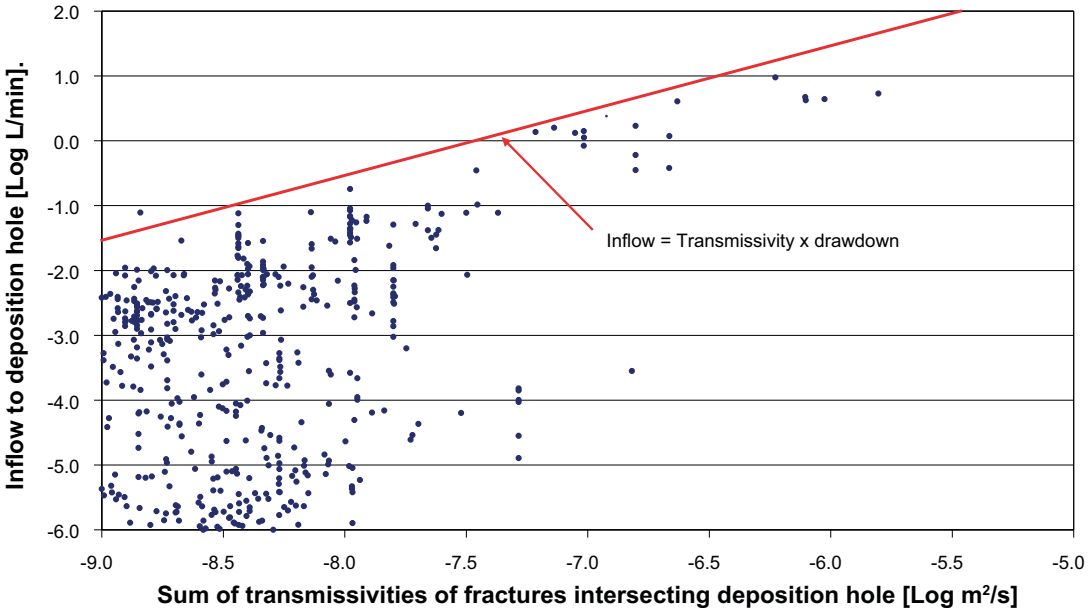

Figure 3-8. *Cross-plot of the total inflow to deposition holes out of a possible 6,916 versus the sum of the transmissivities of fractures intersecting each deposition hole for case r0 with no EDZ.*

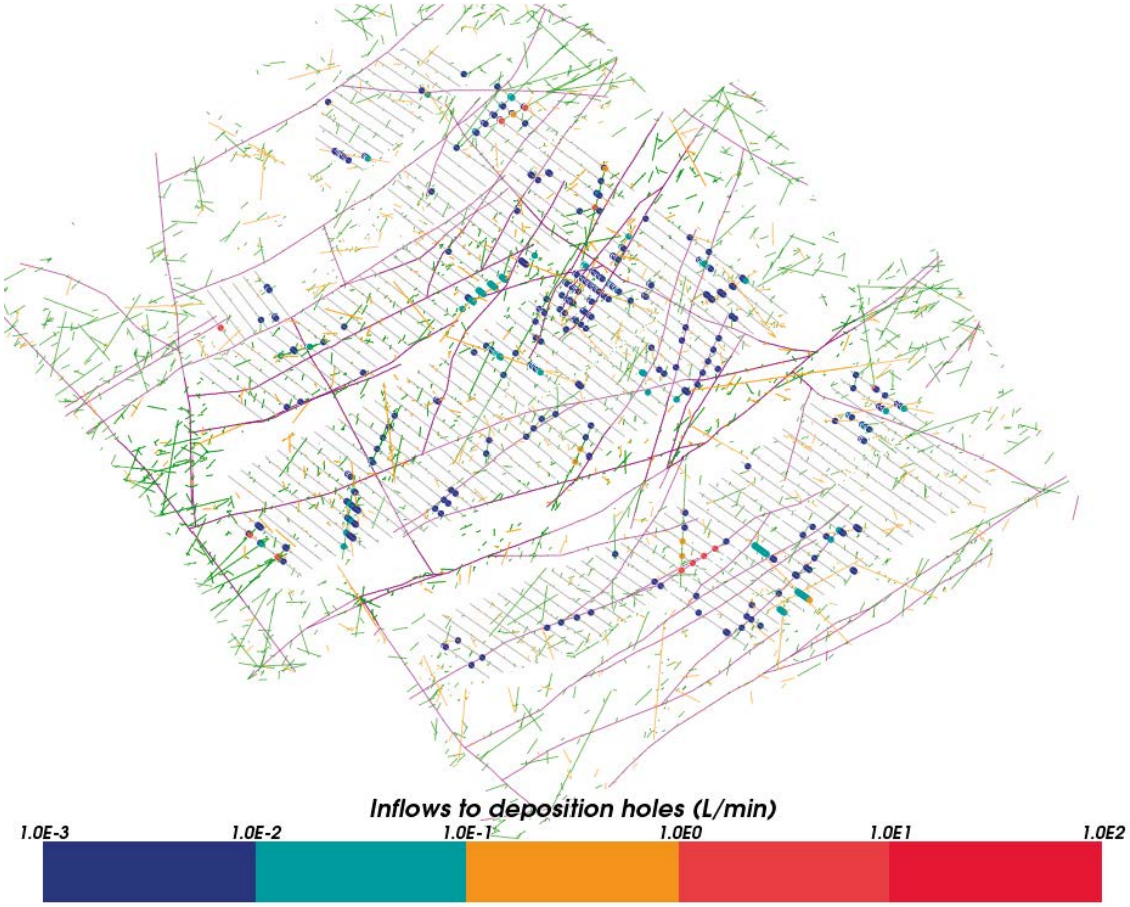

Figure 3-9. *Spatial distribution of inflows to deposition holes coloured by total inflow for case r0. Only deposition holes with inflows greater than $1 \cdot 10^{-3}$ L/min) are shown. Stochastic fractures are shown in green for sub-vertical fractures and orange for sub-horizontal fractures, deformation zones in purple and repository tunnels in grey.*

3.2 Inflows to deposition tunnels

Like inflows to deposition holes, the total inflow to a deposition tunnel depends on the total transmissivity of flowing fractures that intersect the tunnel and the flow in the surrounding fracture network.

Table 3-4 shows the total inflows to all deposition tunnels for each of the five cases considered, together with the number of intersections attributed to each fracture type, sub-divided into deformation zone, EDZ (inflows only), sub-vertical and sub-horizontal stochastic fractures. In contrast to the inflows to deposition holes, where sub-vertical fractures provided the main source of inflows (see Table 3-2), inflows to tunnels from deformation zones are dominant. Again, the high inflows for cases r3 and r5 are due to single large fractures generated for each of these two cases, as explained previously, and are shown more clearly when the inflows from sub-vertical fractures are broken down by fracture domain and depth in Table 3-5. Here, for cases r3 and r5, it is evident that the large inflows are due to a small number of intersections, from one or two large fractures centred in the top 200 m of the model.

Table 3-4. Total flow into all 207 deposition tunnels [L/min] / Count of intersections by natural fracture type and case.

Case	Deformation Zone	EDZ	Sub-horizontal	Sub-vertical	Total
r0	1,407.6 / 491	4.8	13.2 / 887	176.4 / 2,319	1,602.1 / 3,697
r2	1,961.5 / 491	4.4	10.7 / 926	359.7 / 2,352	2,336.4 / 3,769
r3	1,346.9 / 491	5.2	3.9 / 993	4,043.0 / 2,554	5,399.0 / 4,038
r5	1,491.7 / 491	4.6	31.5 / 958	68,509.0 / 2,253	70,036.8 / 3,702
r0 no EDZ	1,410.9 / 491	0.0	13.4 / 836	177.0 / 1,736	1,601.2 / 3,063

Table 3-5. Total flow into deposition tunnels from sub-vertical fractures [L/min] / Count of intersections with natural fractures by fracture domain and depth of fracture centre.

Case	FFM01/6 0–200 m	FFM01/6 200–400 m	FFM01/6 >400 m	FFM04/5 0–800 m
r0	0.0 / 0	53.4 / 50	3.3 / 2,250	119.8 / 19
r2	0.0 / 0	22.3 / 57	3.7 / 2,272	333.7 / 23
r3	3,774.3 / 8	64.3 / 59	3.6 / 2,455	200.8 / 32
r5	68,464.7 / 12	21.4 / 28	7.3 / 2,198	15.5 / 15
r0 no EDZ	0.0 / 0	53.7 / 50	3.4 / 1,667	119.9 / 19

Figure 3-10 shows the complementary cumulative distribution of the transmissivity of fractures intersecting deposition tunnels. A comparison of the complementary cumulative distribution of total inflows to each deposition tunnel over an ensemble of deposition tunnels between all five cases is shown in Figure 3-11. For cases r0, r2, r3 and r5, the number of natural fractures which intersect the deposition tunnels and have transmissivities above $1 \cdot 10^{-9}$ m^2/s is relatively constant across the four cases (~ 1,050) and the distribution of their transmissivities is also very similar. Removing the EDZ increases the number of fractures intersecting the tunnels with flow above the cut-off threshold.

Figure 3-12 shows the complementary cumulative distribution function of inflows from individual natural fractures into deposition tunnels, while Figure 3-13 shows a complementary cumulative plot of the number of inflow points in a deposition tunnel above various inflow limits, both for case r0. Figure 3-13 shows that for case r0, 194 tunnels out of 207 (i.e. 94%) have at least one inflow above $1 \cdot 10^{-3}$ L/min, falling to only 123 (59%) of all tunnels where there are at least five inflows above $1 \cdot 10^{-3}$ L/min. For higher inflow rates, the picture is even more marked, with 131 tunnels having at least one inflow above 0.1 L/min, falling rapidly to only 6 tunnels (3%) in which there are five or more inflows above 0.1 L/min. In Figure 3-14 the cross-plot is presented of the sum of the inflows to each deposition tunnel against the sum of the transmissivities of fractures which intersect that tunnel for case r0. The solid red line shown in the plot is where the inflow is calculated as the transmissivity multiplied by the drawdown (taken to be 470 m). However, for steady-state flow towards a circular tunnel in a semi-infinite isotropic and homogeneous aquifer, Goodman et al. (1965) have calculated that the radial flow from a fracture to a tunnel, Q, is given by:

$$Q = 2 \pi T d / ln(2d/r) \quad (3\text{-}1)$$

where T is the transmissivity of the fracture, r the radius of the tunnel and d is a radius of influence. Inserting values for d of 470 m (the repository depth below sea level) and for r of 3 m (the radius of the tunnel from Joyce et al. (2010a, Table 4.2)), the estimated inflow to a tunnel becomes:

$$Q = 513.8m\ T \quad (3\text{-}2)$$

Some points on the plot lie above this estimate, which suggests that some inflows to tunnels are being influenced by the close proximity of deformation zones, which would have the effect of reducing the value for d and increasing the inflow. The inflows for lower transmissivity fractures fall below the line indicating that flow is being restricted because these are generally smaller, poorly connected fractures.

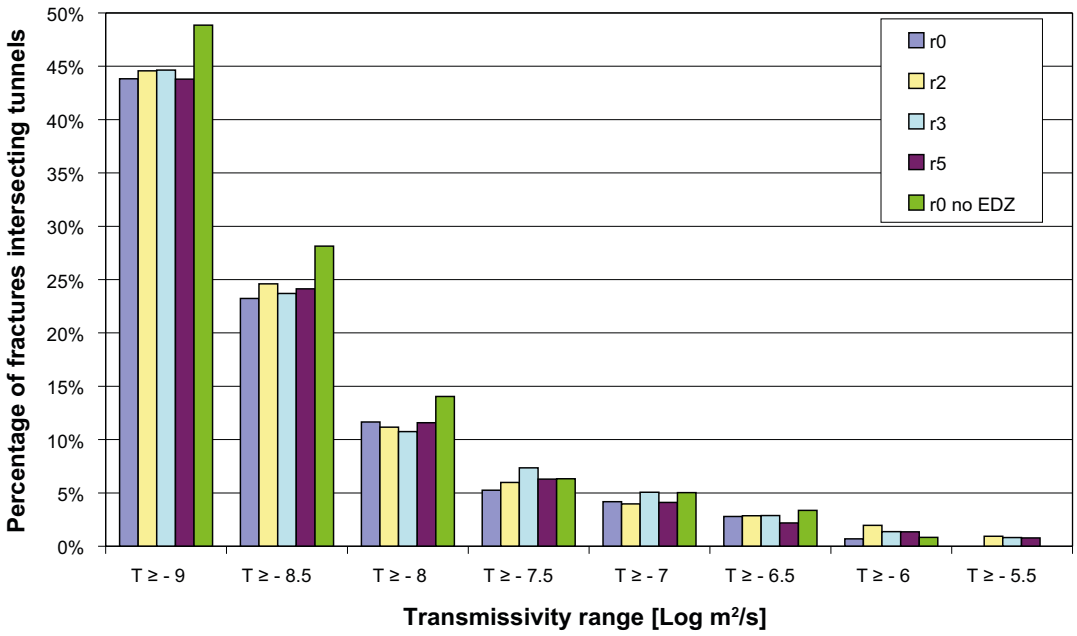

Figure 3-10. *Comparison of the complementary cumulative distribution of the transmissivity of fractures intersecting the deposition tunnels for all five cases. The transmissivities of EDZ fractures are not included.*

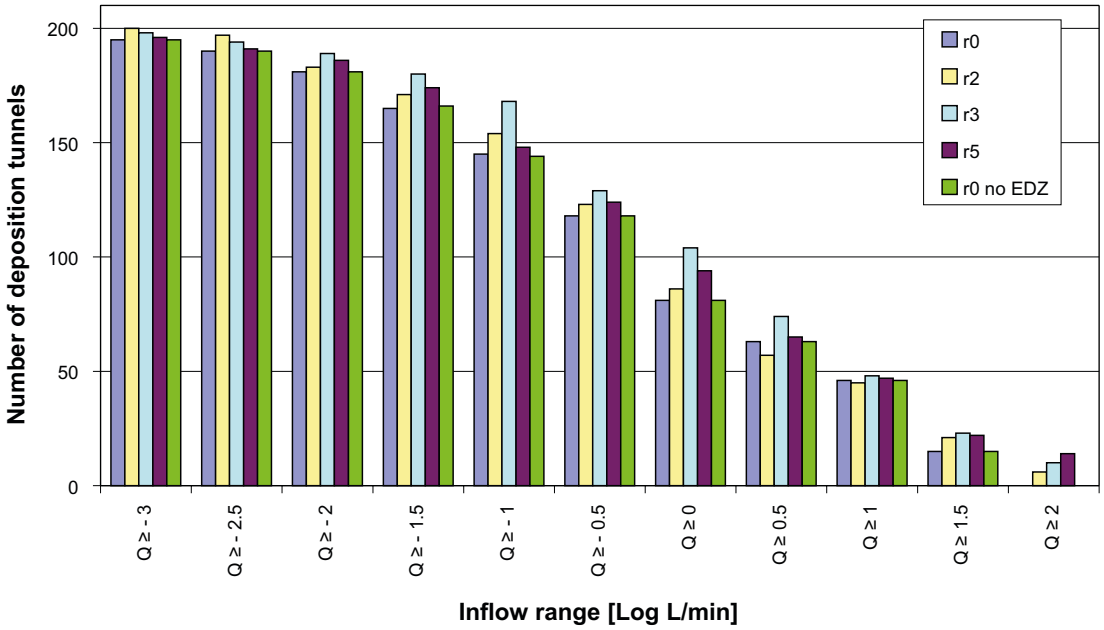

Figure 3-11. *Comparison of the complementary cumulative distributions of the total inflow to each deposition tunnel (207 tunnels in total) for all five cases.*

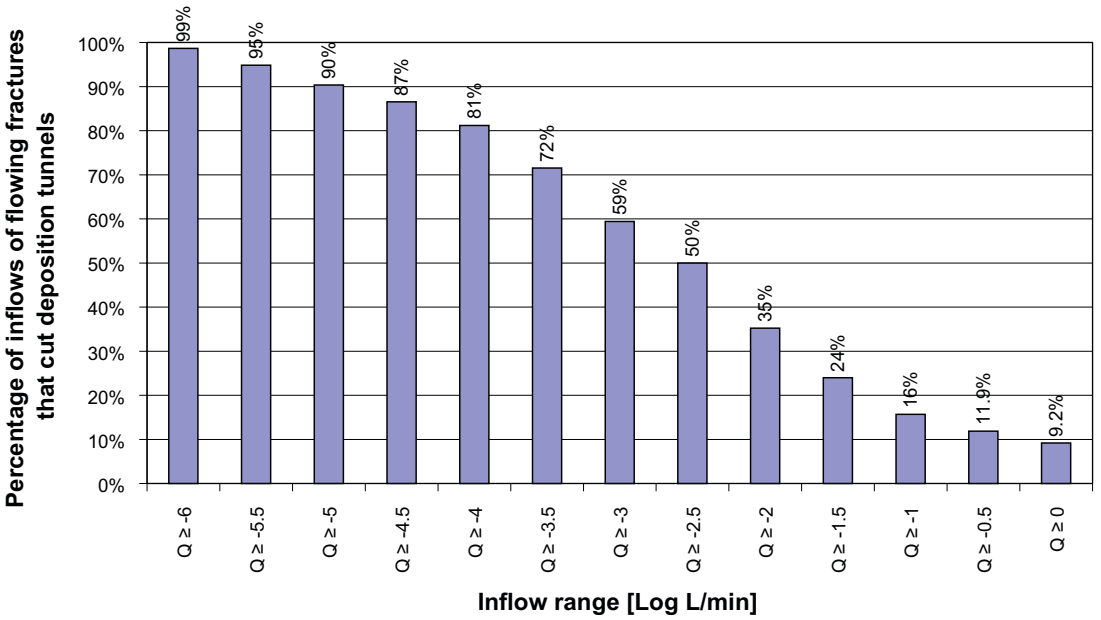

Figure 3-12. *Complementary cumulative distribution function of all inflows into deposition tunnels (207 tunnels in total) from natural fractures for case r0.*

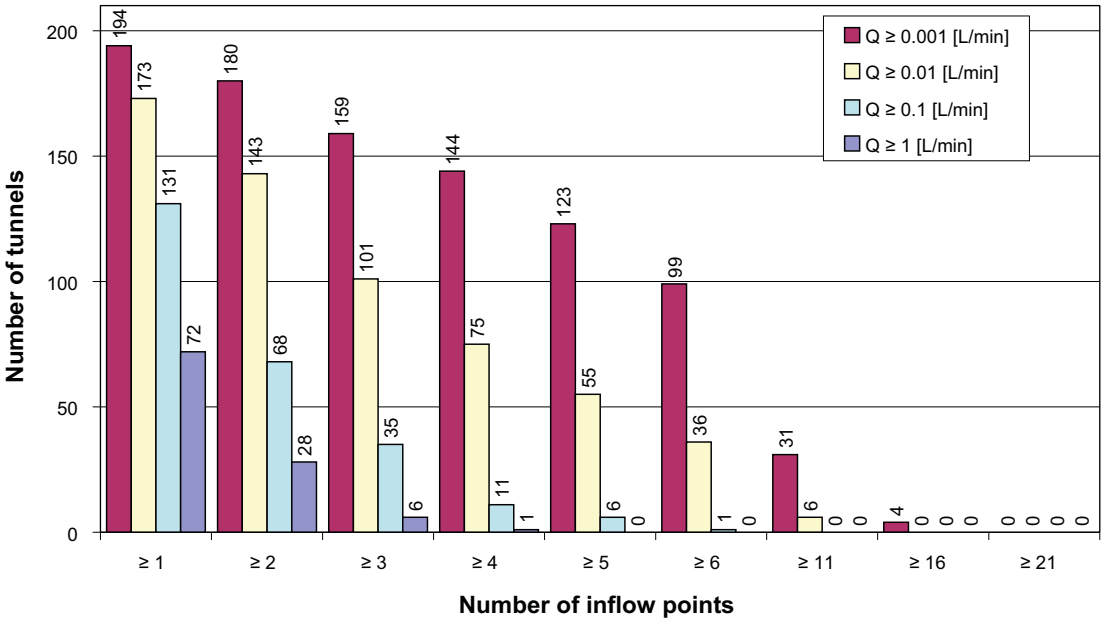

Figure 3-13. *Complementary cumulative plot of the number of tunnels that have a certain number of inflow points for a range of inflow limits for case r0.*

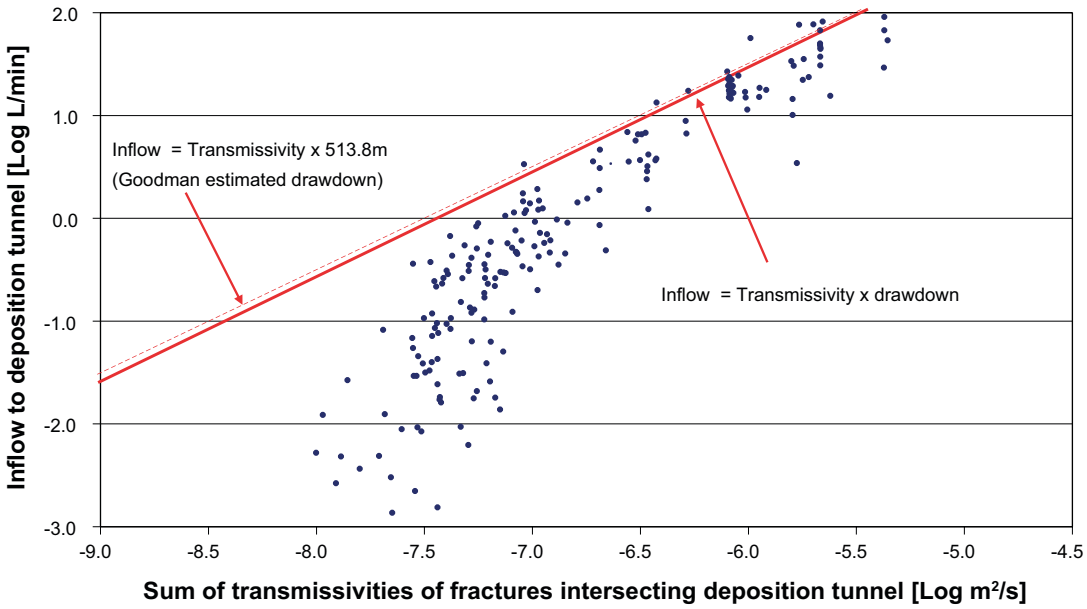

Figure 3-14. *Cross-plot of the total inflow to each deposition tunnel (207 tunnels in total) versus the sum of the transmissivities of fractures intersecting the same tunnel for the case r0. Both inflows and transmissivities include contributions from fractures representing the EDZ. The solid red line indicates inflow calculated as transmissivity times the drawdown where drawdown is set to –470 m. The dotted red line represents the inflow based on analytic expressions for radial flow to a tunnel with a corrected value of the drawdown of 513.8 m.*

3.2.1 Spatial distribution

Each tunnel is divided into a number of tunnel sections, where each tunnel section represents the area of the tunnel above a deposition hole. The tunnel sections start and end at the mid-points between deposition holes or at the tunnel ends. This means that some tunnel sections are longer than others where deposition hole locations have been omitted due to the repository design deliberately avoiding deformation zones in locating deposition holes. Figure 3-15 shows the total inflow into each tunnel section for case r0. For clarity, inflows to tunnel sections below $1 \cdot 10^{-3}$ L/min are excluded. Total inflows to each of the 207 deposition tunnels are shown in Figure 3-16.

Comparing Figure 3-9 for the inflows to deposition holes with Figure 3-15 indicates that there are many more tunnel sections with inflows above $1 \cdot 10^{-3}$ L/min than there are for the corresponding deposition holes under the tunnel section. The locations of deposition holes with high inflows are generally similar locations to where high inflows to tunnel sections are also found. The higher number of tunnel sections with high inflows compared to deposition holes can be attributed to two factors. Firstly, it was shown in Table 3-4 that the bulk of inflows to deposition tunnels came from intersections with deformation zones and sub-vertical fractures. In contrast, because deposition hole locations deliberately avoid deformation zones in the repository design, the contribution of inflows from deformation zones to deposition holes is much lower (see Table 3-2) with the main contributor to inflows to deposition holes being from sub-vertical fractures. Secondly, the volumes of the tunnel sections are larger than the volumes of the deposition hole and therefore are more likely to intersect fractures, leading to higher inflows.

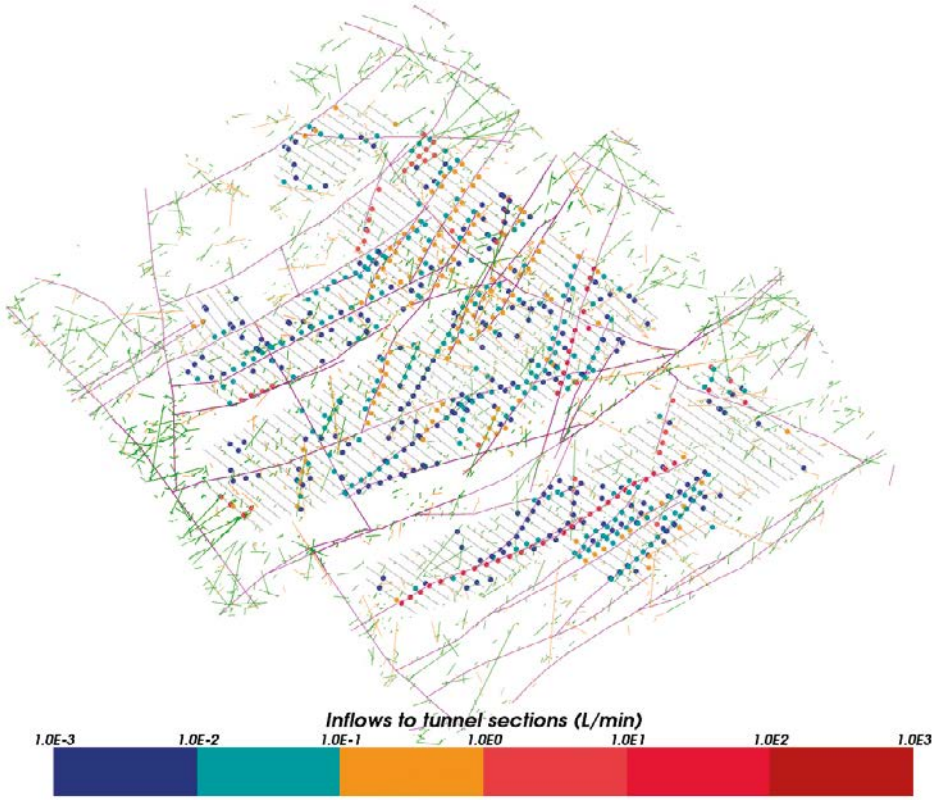

Figure 3-15. *Inflows greater than $1 \cdot 10^{-3}$ L/min to tunnel sections for case r0. Stochastic fractures are shown in green (sub-vertical) and orange (sub-horizontal). Deformation zones are shown in purple and the repository tunnels in grey.*

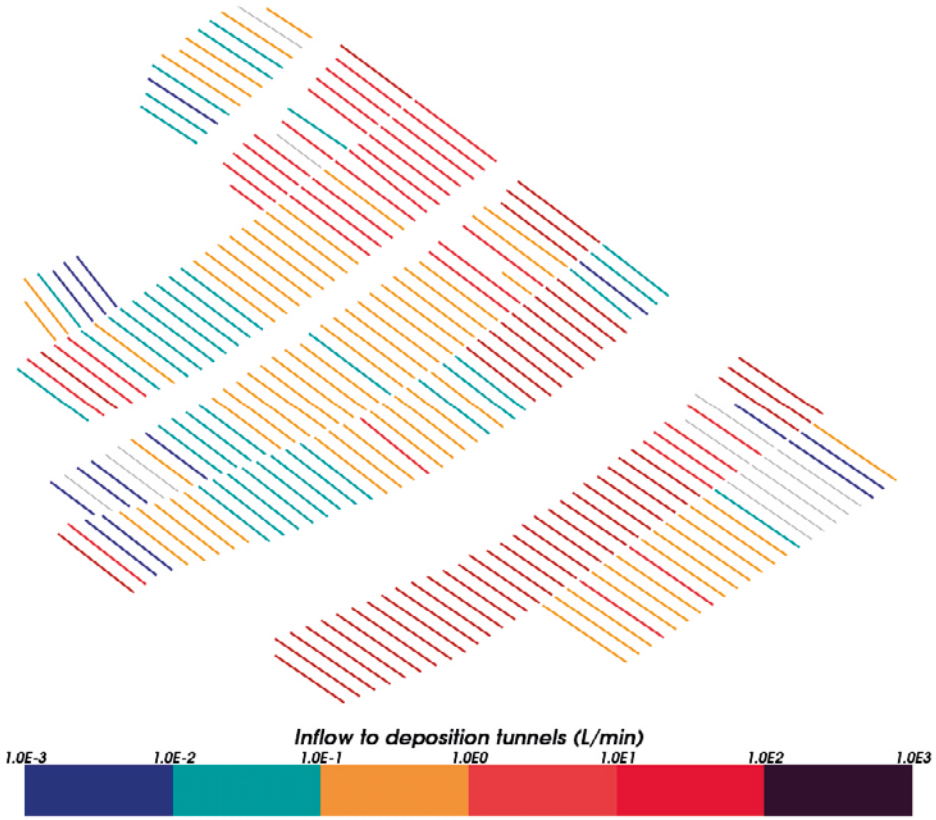

Figure 3-16. *Total inflows to deposition tunnels for inflows greater than $1 \cdot 10^{-3}$ L/min for case r0. Inflows to deposition holes are not included. Tunnels with total inflows less than $1 \cdot 10^{-3}$ L/min are shown in grey.*

3.3 Correlation between inflows to deposition tunnels and deposition holes

In this section, the correlation between inflows to deposition tunnels and inflows to deposition holes is explored, to help understand if inflows to deposition tunnels, as measured perhaps during the construction phase, can be used as a reliable estimate of the possible inflows to deposition holes.

The spatial distribution of inflows to deposition holes and tunnel sections has already been presented (Figure 3-9 and Figure 3-15 respectively). Figure 3-17 shows a plot of the number of deposition holes with inflows above certain limits against the total inflow to the deposition tunnel for case r0. From this figure it can be seen that 191 deposition tunnels (92%) do not have any deposition holes whose inflow exceeds 0.1 L/min falling to 86 (42%) that do not have any deposition holes with inflows greater than 0.001 L/min. For those deposition tunnels which do have deposition holes with inflows, 13 deposition tunnels have a single deposition hole with an inflow greater than 0.1 L/min, falling to two tunnels with two deposition holes and only one tunnel with three deposition holes with inflows greater than 0.1 L/min. There are no deposition tunnels with more than three deposition holes with inflows greater than 0.1 L/min.

Figure 3-18 shows a cross plot of the inflows to deposition holes versus the inflows to the corresponding tunnel sections (usually around 6 m long) above each deposition hole for case r0. The cross plot shows a large variability such that no real correlation between the two can be established, although it can be seen that inflows to tunnel sections are generally higher than inflows to their corresponding deposition holes.

Figure 3-19 shows the number of deposition holes with inflows greater than the inflows to the corresponding tunnel section. Thus, there are 20 deposition holes with inflows above 0.1 L/min but of these only 8 have inflows greater than the corresponding tunnel section above the deposition hole and 4 where the inflow to the deposition hole is over 1,000 times greater than the inflow to the tunnel section.

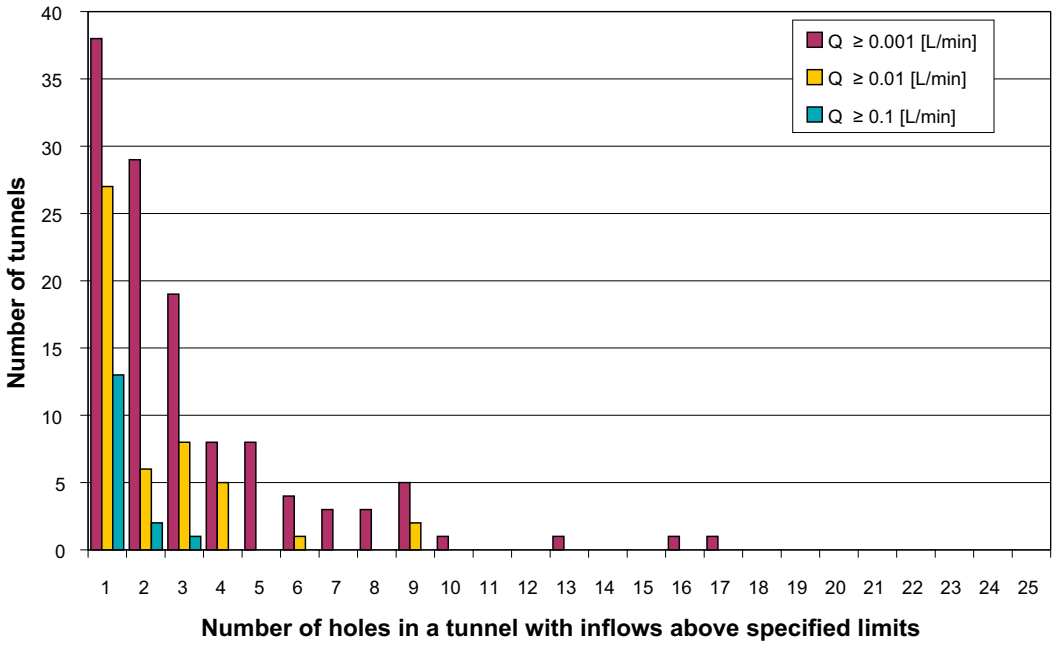

Figure 3-17. *Number of tunnels (out of 207) that have a number of deposition holes with inflows greater than specified flow limits for case r0.*

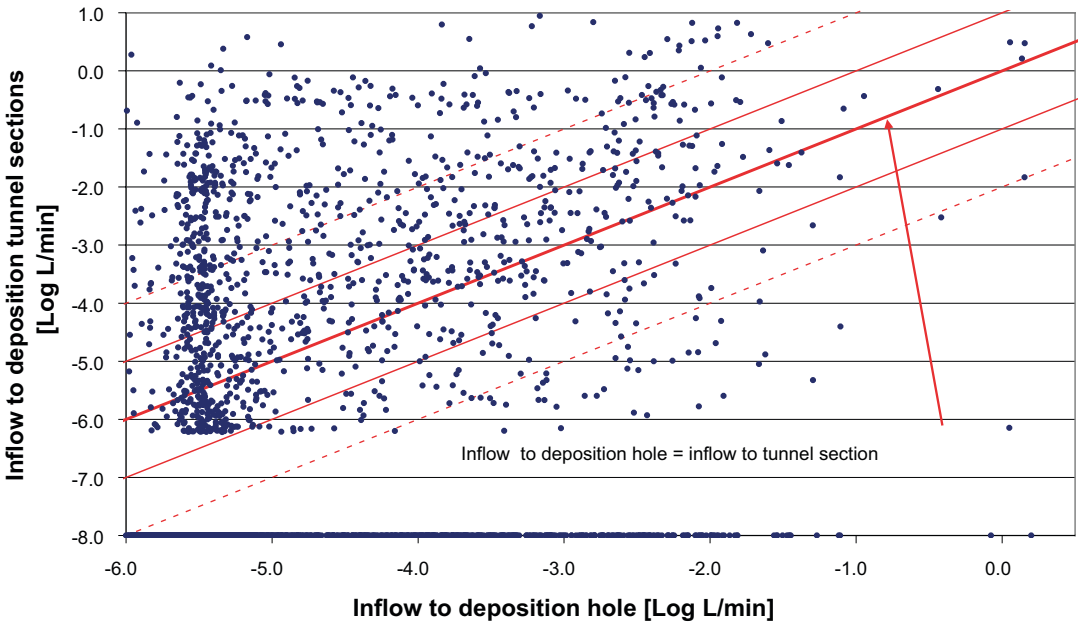

Figure 3-18. *Cross plot of the total inflow to each tunnel section (~6 m long, above each deposition hole) versus the total inflow to the corresponding deposition hole for case r0. For deposition holes with inflow and associated tunnel section with no inflow, the tunnel section inflow is set to $1 \cdot 10^{-8}$ L/min. The dotted red lines are one and two orders of magnitude from the solid red line indicating where the inflow to the deposition hole is equal to the inflow to the tunnel section immediately above the deposition hole.*

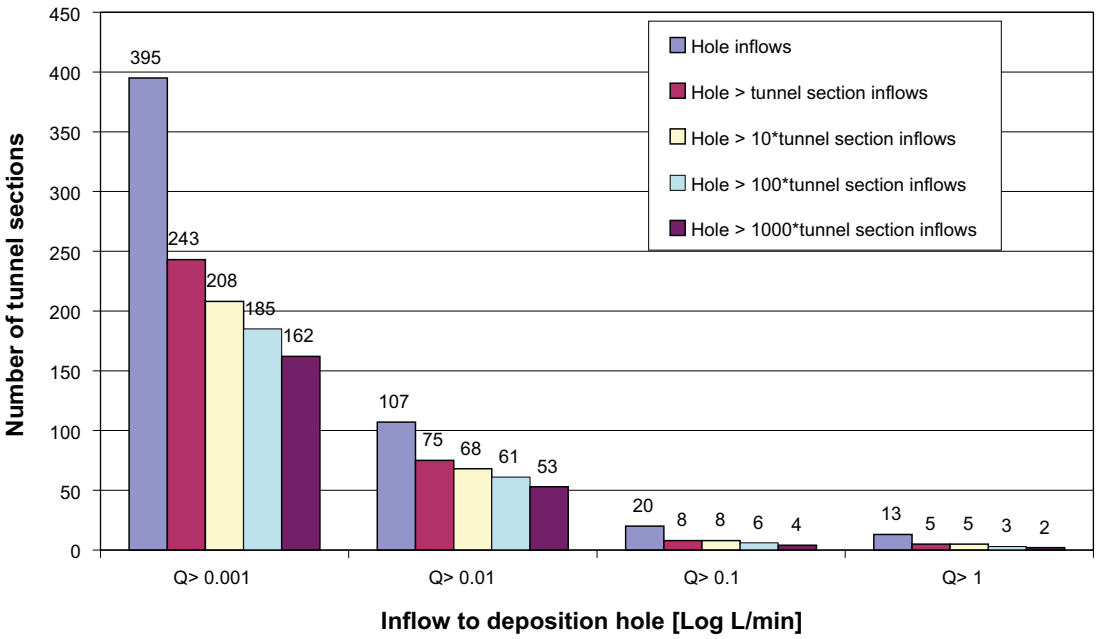

Figure 3-19. *Number of tunnel sections (out of 6,916) where the deposition hole inflow is greater than the corresponding tunnel section inflow for various ratios of the hole to tunnel inflows for case r0.*

Figure 3-20 shows a cross plot of the total inflow into each deposition tunnel against the maximum inflow into any deposition hole within that tunnel. The tunnel inflows are scaled according to the average tunnel length to remove any bias due to different tunnels having a different number of deposition holes and total tunnel inflows. There is reasonable correlation between the two quantities at the maximum inflows to deposition holes above 0.1 L/min, but at lower maximum inflows any correlation between the two quantities disappears. For most tunnels, the maximum inflow to a deposition hole in a tunnel is less than the scaled inflow to the tunnel, but in a small number the maximum inflow to a deposition hole is larger than the inflow to the tunnel.

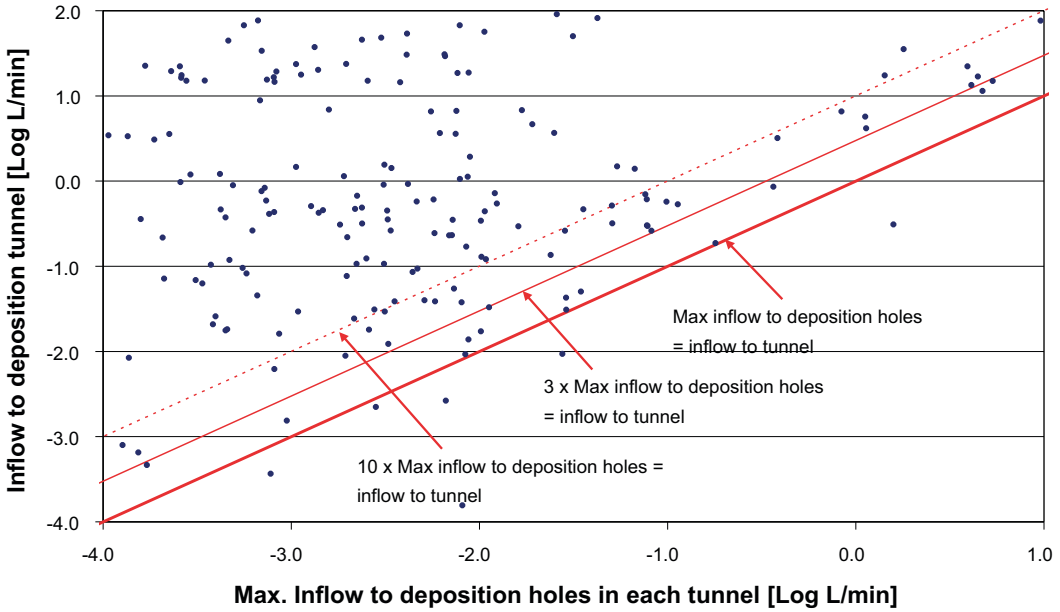

Figure 3-20. *Cross plot of the total inflow to each deposition tunnel versus the inflow to the deposition hole that has the maximum inflow of all deposition holes in that tunnel for case r0. Tunnel inflows are scaled according to the average tunnel length.*

Figure 3-21 shows a cross plot of the total inflow of all deposition holes in a tunnel against the total inflow to that tunnel for case r0. The main observation from this plot is that there is little correlation between the total inflow of all deposition holes in a tunnel and the total inflow to the tunnel. For many of the tunnels, inflows occur at intersections of the tunnel with deformation zones. These deformation zones tend to have higher inflows than those from the natural background fractures, resulting in high total tunnel inflows. Moreover, in many instances, deposition holes are excluded in locations immediately below tunnel sections where it is known that a deformation zone intersects a particular tunnel section. Thus, although the inflow to the tunnel section above a location where there is no deposition hole is included, there is no equivalent inflow to the deposition hole, thus reducing the correlation between the inflows to deposition holes and the inflows to the tunnel sections above the deposition holes even further. Improved correlation between the total inflow to a tunnel and the total inflows to all deposition holes in a tunnel is found if the inflows to tunnels associated with deformation zones are excluded. When these inflows are excluded, the total inflow to all tunnels falls from 1,602 L/min to 291 L/min, indicating the substantial inflows to tunnels from the deformation zones, as shown in Table 3-4. The total inflow to all deposition holes is unchanged. Figure 3-22 shows the equivalent plot to Figure 3-21, but with the inflows to tunnels from deformation zones excluded. Although the correlation in Figure 3-22 is improved, compared to Figure 3-21, there is still a considerable variability between the total tunnel inflow and the inflows to deposition holes for individual tunnels, suggesting that other factors may also be important.

3.4 Hydraulic rejection criteria

In this section the number of deposition holes whose inflows exceed a certain limit are considered. Svensson and Follin (2010, Section 5.6) reported both the number and spatial distribution of deposition holes that would be excluded based on a combination of criteria including deposition hole inflows, Full Perimeter Criteria (FPC) and Extended Full Perimeter Criteria (EFPC) (see Joyce et al. 2010a, Section 3.2.7). In this work, we consider those deposition holes with inflows greater than 0.1 L/min (equivalent to Variant I in Svensson and Follin (2010, Table 5.3)) and then apply FPC and EFPC to these deposition holes to determine how applicable these criteria are to screening out deposition holes with high inflows.

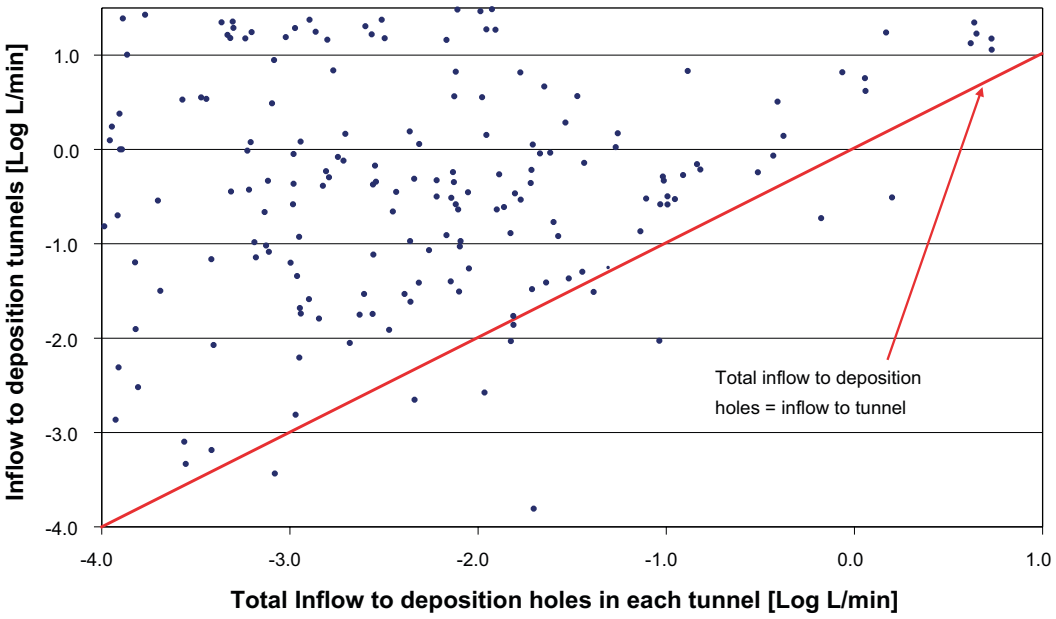

Figure 3-21. *Cross plot of the total inflow to each deposition tunnel versus the total inflow to all deposition holes in that tunnel for case r0.*

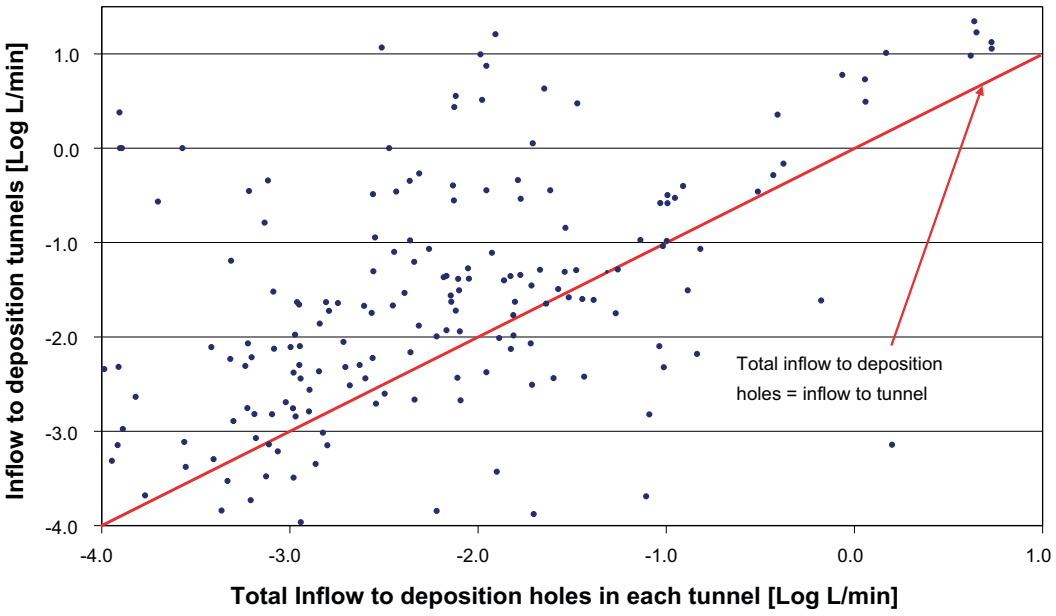

Figure 3-22. *Cross plot of the total inflow to each deposition tunnel versus the total inflow to all deposition holes in that tunnel for case r0, where inflows from deformation zones are excluded.*

Table 3-6 presents the number of deposition holes with inflows greater than 0.1 L/min by block for each case. For comparison, the table also includes the number of deposition holes with inflows greater than 0.1 L/min found by Svensson and Follin (2010). In their calculations, Svensson and Follin used two modelling approaches: an equivalent continuous porous medium approach (ECPM) and an alternative approach in which grid cells not intersected by fractures are removed from the computational grid rather than giving them arbitrary low values as in the ECPM method. This approach is described as an equivalent discontinuous porous medium (EDPM) in Svensson and Follin (2010, Appendix E). In both models, Svensson and Follin included grouting by setting the maximum value of the hydraulic conductivity of all cells in contact with the repository to $1 \cdot 10^{-8}$ m/s.

Table 3-6. Comparison of the number of deposition holes in each block with inflows above 0.1 L/min for each case, together with the corresponding number of deposition holes with inflows above 0.1 L/min found by Svensson and Follin (2010).

Case	DA-A	DA-B	DA-C	Total
r0	6	5	9	20
r2	20	13	8	41
r3	4	21	12	37
r5	4	8	5	17
r0 no EDZ	6	5	9	20
ECPM(1)				157
EDPM(1)				88

(1) Values taken from Svensson and Follin (2010, Figure E-5) for deposition holes with inflows greater than 0.1 L/min.

It is clear from Table 3-6 that the number of deposition holes with inflows that exceed 0.1 L/min from this study is much lower than that found by Svensson and Follin for either of their two modelling approaches. However, in terms of their spatial distribution, comparison of Figure 3-23 and Figure 3-24 for those holes which exceed 0.1 L/min in this study and the Svensson and Follin study respectively, indicate that while this study suggests fewer deposition holes with high inflows, their locations are generally in good agreement.

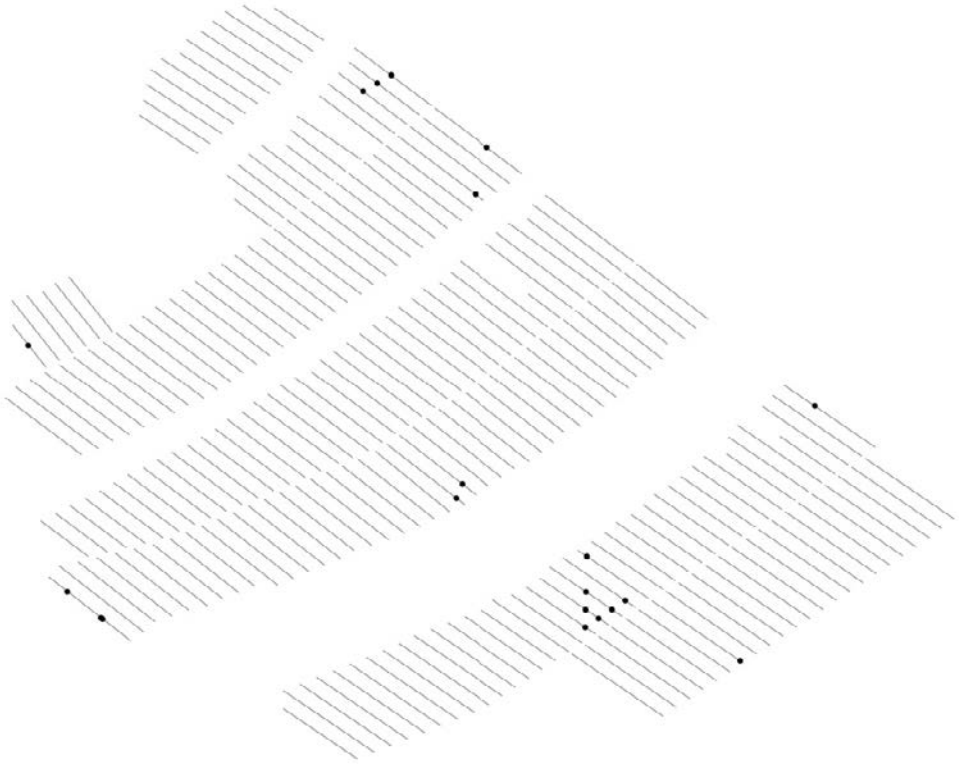

Figure 3-23. *Spatial distribution of deposition holes with inflows greater than 0.1 L/min for case r0.*

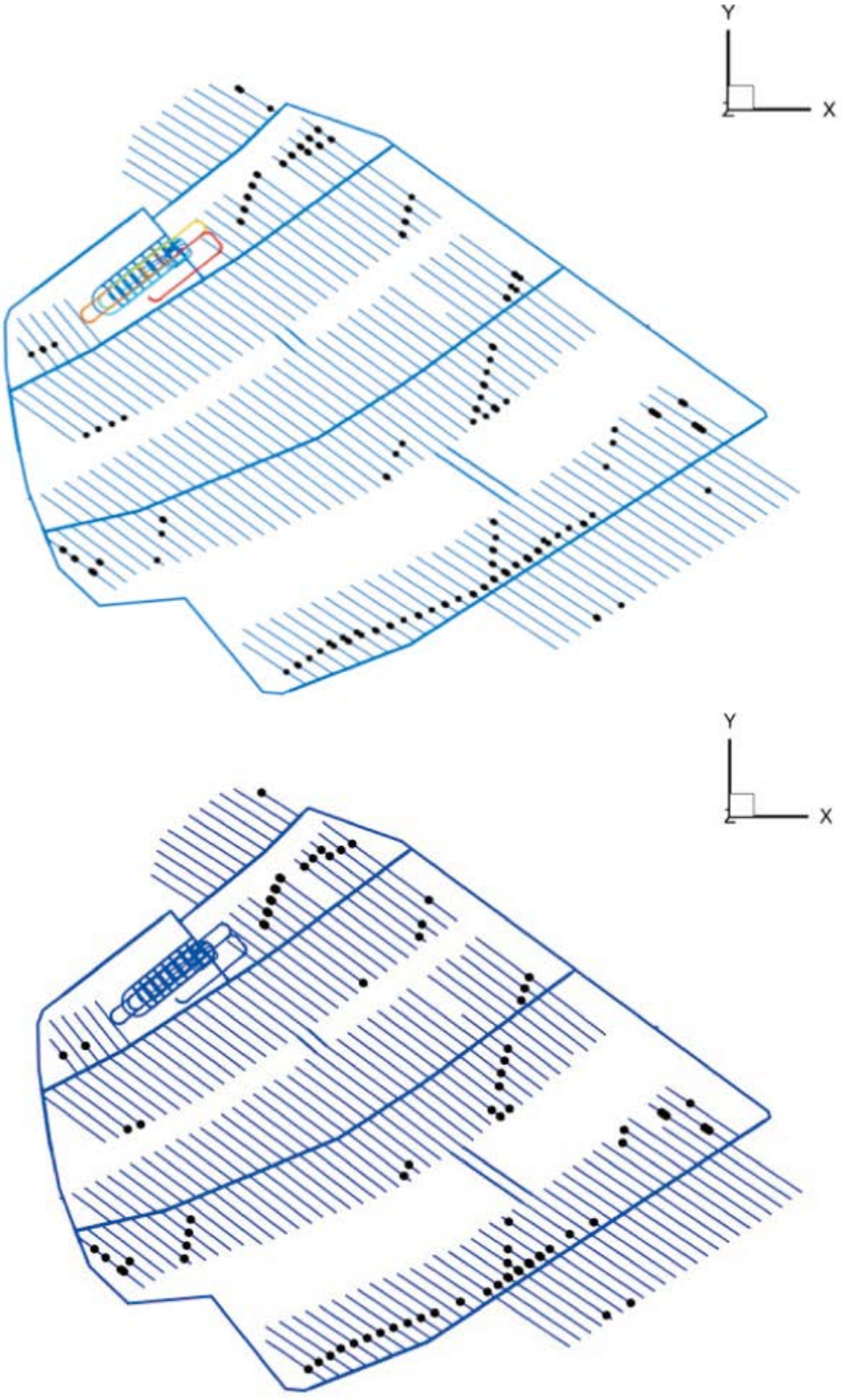

Figure 3-24. *Illustration of the spatial distribution of deposition holes with inflows greater than 0.1 L/min. The top picture is based on the ECPM approach (157 deposition holes) and the bottom picture is based on the EDPM approach (88 deposition holes). (Svensson and Follin 2010, Figure E-5).*

The lower number of deposition holes with inflows greater than 0.1 L/min found in this study compared to Svensson and Follin's results, is likely to be attributed to the different conceptual models and tools used. In this work using the DFN approach, stochastic fractures can be generated very close to a deposition hole but not actually intersect the hole and therefore will not contribute an inflow to the hole. In the ECPM approach, it is not as easy to distinguish between fractures which are very close to a deposition hole but do not intersect the hole and those that do intersect the deposition hole, unless very small grid cells are used. Without these very small grid cells, the flow in a fracture which is very close to a deposition hole but does not intersect it is likely to be attributed as an inflow to the deposition hole, leading to an over estimate of the inflow to that deposition hole. When grid cells not intersected by fractures are removed with the EDPM approach and smaller grid cells are used, this over estimate is reduced and the results for the EDPM model are closer to the DFN results, although still higher.

Other criteria for identifying deposition holes for possible exclusion have also been used, notably the Full Perimeter Criteria (FPC) and Extended Full Perimeter Criteria (EFPC) (see Joyce et al. 2010a, Sections 3.2.7 and 6.2.5).

Table 3-7 shows the effect of applying the FPC (Full Perimeter Criteria) and EFPC (Extended Full Perimeter Criteria) to those deposition holes with inflows greater than 0.1 L/min. Thus for case r0, there are 20 deposition holes with inflows greater than 0.1 L/min and of those, 16 of them have an FPC value of 1 (excluded due to background fracture) or 2 (excluded due to deformation zone). In other words, if deposition holes were excluded using FPC alone, then this would exclude 16 of the twenty deposition holes with inflows greater than 0.1 L/min, suggesting FPC is a reasonable indicator for deposition holes with high inflows. A similar picture can be seen for the other cases.

For EFPC, however, the situation is different, so that for case r0 only one of the deposition holes with high inflows would be excluded if only EFPC were applied (where a single sub-horizontal fracture intersects more than four adjacent deposition holes). This finding is entirely consistent with Table 3-2 which indicates that inflows to deposition holes from sub-horizontal fractures are small compared to inflows from sub-vertical fractures and deformation zones. This suggests EFPC would be a poor indicator of deposition holes with inflows greater than 0.1 L/min. In fact, for r2, r3 and r5 all of the inflows excluded by EFPC would also have been excluded by FPC alone.

3.4.1 Effect on performance measures

In this section, the effect of excluding deposition holes with inflows greater than 0.1 L/min is considered on two performance measures, the initial equivalent flux in the rock (U_r) and the flow-related transport resistance in the rock (F_r), as described in Joyce et al. (2010a, Section 3.2.6).

The calculation of the performance measures presented here is based on the number of particles released from deposition holes into fractures (one particle per deposition hole) under closed repository conditions, as described for SR-Site in Joyce et al. (2010a, Section 4.3.3), for the various cases considered. An additional filter is then applied to these SR-Site results to exclude those deposition holes with inflows greater than 0.1 L/min as determined under open repository conditions.

Table 3-7. The number of deposition holes with inflows greater than 0.1 L/min and FPC and/or EFPC applied.

Case	Inflows > 0.1 L/min	Inflows > 0.1 L/min and FPC	Inflows > 0.1 L/min and EFPC	Inflows > 0.1 L/min and FPC and EFPC
r0	20	16	1	0
r2	41	32	2	2
r3	37	33	4	4
r5	17	16	1	1
r0 no EDZ	20	16	1	0

Figure 3-25 and Figure 3-26 show cross plots of the inflows to deposition holes under open repository conditions against the initial equivalent flux (U_r) and the flow-related transport resistance (F_r) under closed repository conditions. Figure 3-25 shows that deposition holes with inflows greater than 0.1 L/min have higher values for U_r. A corresponding but weaker correlation can be observed for the flow-related transport resistance (F_r) in Figure 3-26, where the F_r values are observed to be lower for those deposition holes with the higher inflows, implying good connection to the surface.

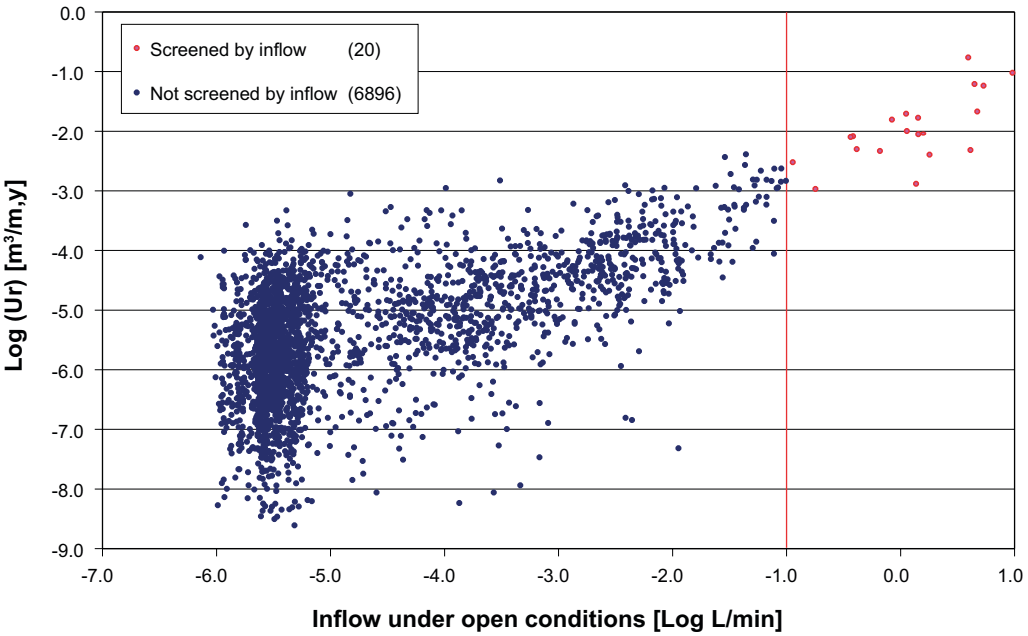

Figure 3-25. *Cross plot of inflows to all 6,916 deposition holes under open repository conditions against U_r, the initial equivalent flux into the fractured rock adjacent to the deposition holes under closed repository conditions at 2000 AD, for case r0. Deposition holes with inflows greater than 0.1 L/min are shown in red and those with lower inflows in blue.*

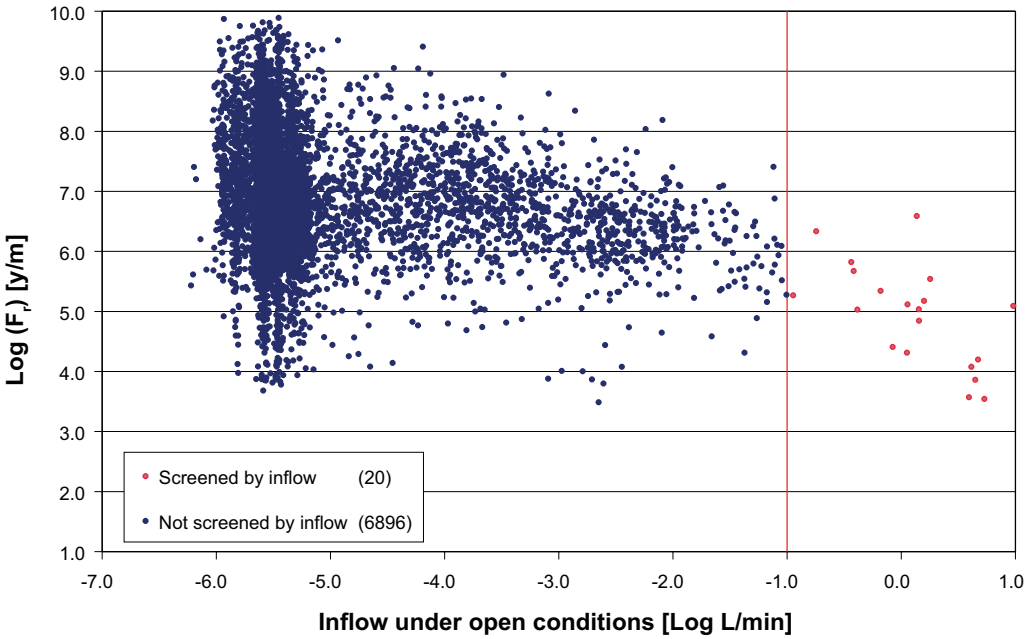

Figure 3-26. *Cross plot of inflows to all 6,916 deposition holes under open repository conditions against F_r, the flow-related transport resistance in the rock under closed repository conditions at 2000 AD, for case r0. Deposition holes with inflows greater than 0.1 L/min are shown in red and those with lower inflows in blue.*

4 Inflows to pilot holes

In Section 3, inflows to deposition holes are calculated when all the tunnels in a block are open. The results are analysed statistically and the calculated inflows to deposition holes used to identify those deposition holes with high inflows (i.e. those with inflows above 0.1 L/min).

In practice, however, during the construction of the repository it is unlikely that the repository will be constructed with all the tunnels (and their associated deposition holes) in a block (i.e. DA-A, DA-B or DA-C) open at the same time and at atmospheric pressure. Instead, it is postulated that as the repository is constructed, and deposition holes are filled, tunnels will be closed and backfilled and new tunnels excavated in a progressive manner. As the new tunnels are opened, inflows to potential locations for deposition holes will initially be estimated by measuring the inflows into pilot holes within the newly excavated tunnels and the decision to create a deposition hole in that location will be based on those pilot hole inflows. In this section, the model used in Section 3 is adapted in order to model the progressive opening of tunnels as described above. Deposition holes are replaced by pilot holes and the inflows to the pilot holes in the open tunnels are calculated and compared to the corresponding inflows to deposition holes calculated in Section 3, for both the case where tunnels are opened progressively as well as the case where all deposition holes are replaced by pilot holes in a block.

4.1 Model description

An area of the repository was selected in which there are a significant number of inflows to deposition holes above $1 \cdot 10^{-3}$ L/min (see Figure 3-9) calculated under open repository conditions for the case r0. The area selected is in block DA-B and is shown in Figure 4-1. The selected area comprises 20 tunnels in the south west of the block (shown in dark blue) which are closed and backfilled. New tunnels are then opened two at a time in a north easterly direction in six phases (referred to as phases m1 – m6) such that by the sixth phase twelve tunnels in total are open. The tunnels that are opened in such a way are shown in Figure 4-1 in red or green. All other tunnels in block DA-B previously described as open in Section 3 are considered unexcavated and are modelled as background rock.

The deposition tunnels and deposition holes in the closed and backfilled tunnels are represented as CPM, in the same way that these tunnels and deposition holes were modelled in Section 3. The hydraulic conductivity and porosity values for these deposition tunnels and holes are set to the backfilled values as in Joyce et al. (2010a, Table 4.2). The newly excavated tunnels in m1–m6 are also represented as high conductivity CPM but, in order to model inflows to pilot holes in the newly opened tunnels, each pilot hole is represented as a single long, thin fracture of width 0.076 m extending from the base of the tunnel to the length of the pilot hole (8 m). Each pilot hole fracture is given a transmissivity of $3 \cdot 10^{-4}$ m^2/s (to represent a high transmissivity). This provides a connection between fractures intersecting the pilot hole with the base of the tunnel and an atmospheric boundary condition. The high transmissivity means that there is effectively no hydraulic resistance along the hole.

4.2 Phased opening of tunnels

In this section the effects of opening new deposition tunnels, two tunnels at a time, on the inflows to pilot holes in the newly opened tunnels are examined. Seven simulations are performed, the first where no new tunnels are open and then six more simulations corresponding to the six phases m1 through to m6 as the new tunnels are opened, two at a time. For each phase, the inflows to the pilot holes in the open tunnels are calculated and the impact of the opening of the new tunnels assessed.

The total number of pilot holes in the newly opened tunnels in all six phases m1 to m6 is 448. When all twelve tunnels are open the total inflow to the 448 pilot holes is 0.42 L/min. This compares with a total inflow of 0.48 L/min for the corresponding deposition holes, when the whole of block DA-B is under open conditions as calculated in Section 3. Given that the pilot holes are smaller than the corresponding deposition holes it might be expected that the ratio of inflows to deposition holes and

pilot holes would be larger (about a factor of 1.4 based on their relative radii). However, the calculation of inflows to deposition holes is based on the case where all the tunnels in block DA-B are open, so that for a given quantity of water attempting to inflow to the open tunnels and deposition holes, the inflows will be spread over a larger number of tunnels and deposition holes, resulting in lower inflows per tunnel and deposition hole under these circumstances. The total inflows to the 448 pilot holes compared to the corresponding total inflows to the deposition holes suggest that these two competing effects (the smaller diameter of the pilot holes vs. the more concentrated open repository area for inflows) tend to balance each other out.

In Figure 4-2 the effect of opening new tunnels on the inflows to newly opened pilot holes and those previously opened can be seen. Figure 4-2 indicates that the sums of inflows to pilot holes for individual tunnels change as additional tunnels are opened. For example, in tunnel m1b which is the second tunnel to be opened, the inflows to pilot holes in that tunnel with just tunnels m1a and m1b open total just over 0.18 L/min. As new tunnels are opened in phases m2 through to m6, the inflows to the pilot holes in m1b decrease, falling to ~0.11 L/min by phase m6 (although these inflows are still higher than when all tunnels and pilot holes in the block are open). A similar picture is found for the inflows to tunnel sections above each pilot hole. Figure 4-3 shows the inflows to the tunnel sections above each pilot hole in each open tunnel. Considering tunnel m1b again, the inflows to the tunnel sections in this tunnel once again are highest when only the first two tunnels are open, but as further tunnels are opened, then the inflows to the tunnel sections decrease in a similar manner to that seen for pilot holes in Figure 4-2, but show a much closer correlation with the inflows to tunnels when all tunnels in the block are open.

Figure 4-4 shows the cross plot of the total inflows to deposition holes under open conditions as calculated in Section 3 versus the corresponding inflows to the 448 pilot holes when all twelve tunnels are open. For some pilot holes there are no inflows and for these holes the inflow value is set to a log value of –7. The plot shows that there is a reasonable correlation between inflows to pilot holes and inflows to deposition holes across a wide range of pilot hole inflows. It is noted that Figure 4-4 also shows that none of the 448 deposition holes had inflows greater than 0.1 L/min under open repository conditions as calculated in Section 3. Under conditions where most tunnels are either closed and backfilled or not yet excavated, with only a very small number of tunnels open, it might be expected that inflows to the open areas would be higher and for some holes this is indeed observed, but even so no inflows to the pilot holes exceed 0.1 L/min.

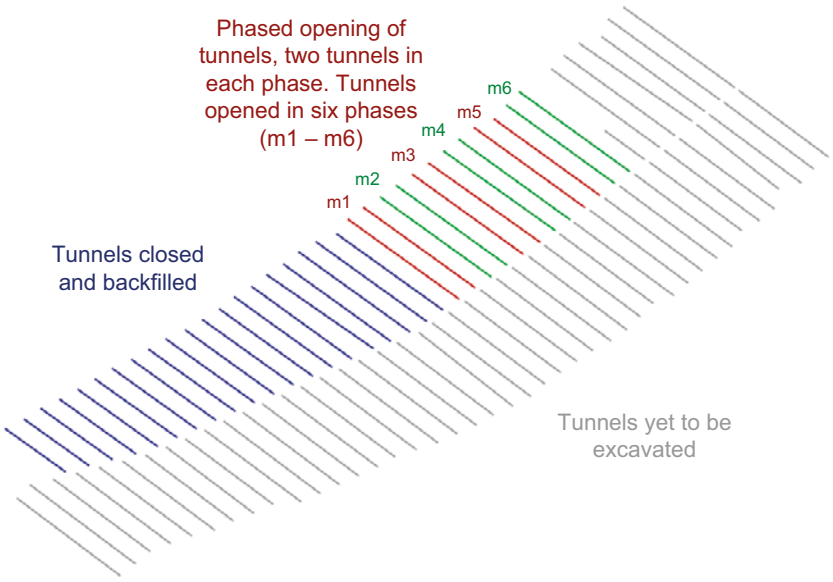

Figure 4-1. *Block DA-B showing the phasing of the tunnel excavations as new tunnels are opened progressively. The tunnels coloured dark blue are closed and backfilled. Tunnels are then excavated in six phases (m1–m6) with two tunnels opened at each phase and are shown in red or green. Tunnels yet to be excavated are shown in grey.*

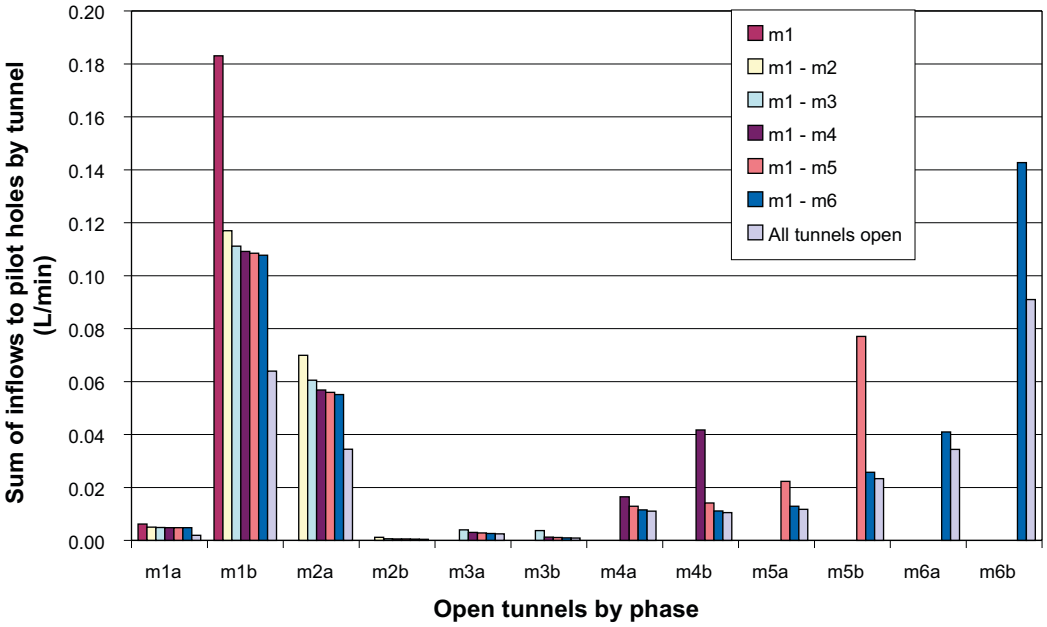

Figure 4-2. *Illustrations of the sensitivity of total inflows to pilot holes under each tunnel as new tunnels are excavated. Tunnels opened in phases m1 to m6 are opened two at a time with the first tunnel opened labelled "a" and the second with "b". The sums of inflows to the pilot holes when all the tunnels in block DA-B are open are shown in All Tunnels Open.*

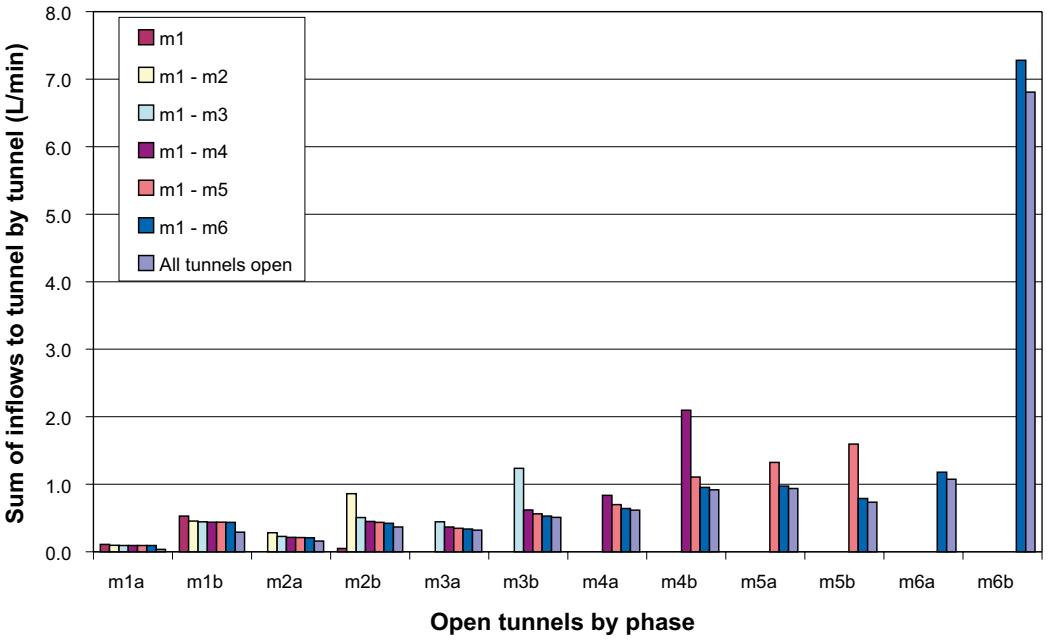

Figure 4-3. *Illustrations of the sensitivity of total inflows to tunnels as new tunnels are excavated. Tunnels opened in phases m1 to m6 are opened two at a time with the first tunnel opened labelled "a" and the second with "b". The sums of inflows to the tunnels when all the tunnels in block DA-B are open are shown in All Tunnels Open.*

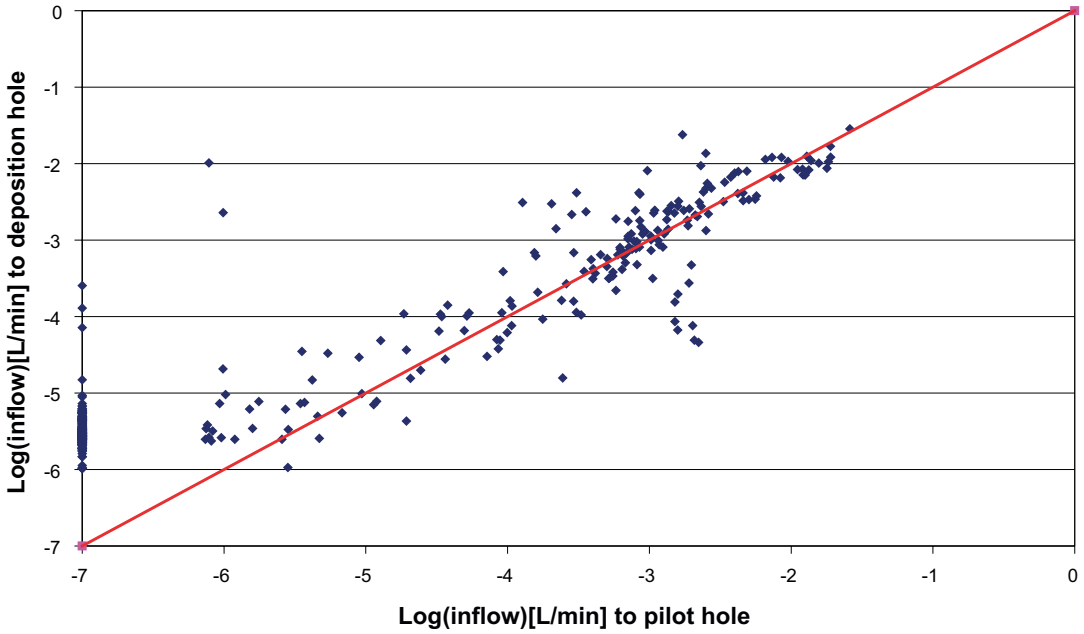

Figure 4-4. *Cross plot of the total inflow to each deposition hole versus the total inflow into the corresponding pilot hole for the 448 holes under the twelve open tunnels in phase m6. The red line indicates where inflows to deposition holes are equal to inflows to pilot holes.*

Figure 4-5 shows the complementary cumulative distribution of the total inflow to 448 pilot holes when all twelve tunnels are open, compared to the inflows to deposition holes calculated for the same 448 holes in Section 3 when the whole of the block DA-B was under open conditions. Many of the pilot holes do not have an inflow and this is reflected in the number of pilot holes compared to the number of deposition holes with inflows of $1 \cdot 10^{-6}$ L/min. However, at inflows above $1 \cdot 10^{-5}$ L/min, there is little difference between the inflows to pilot holes and the inflows to deposition holes.

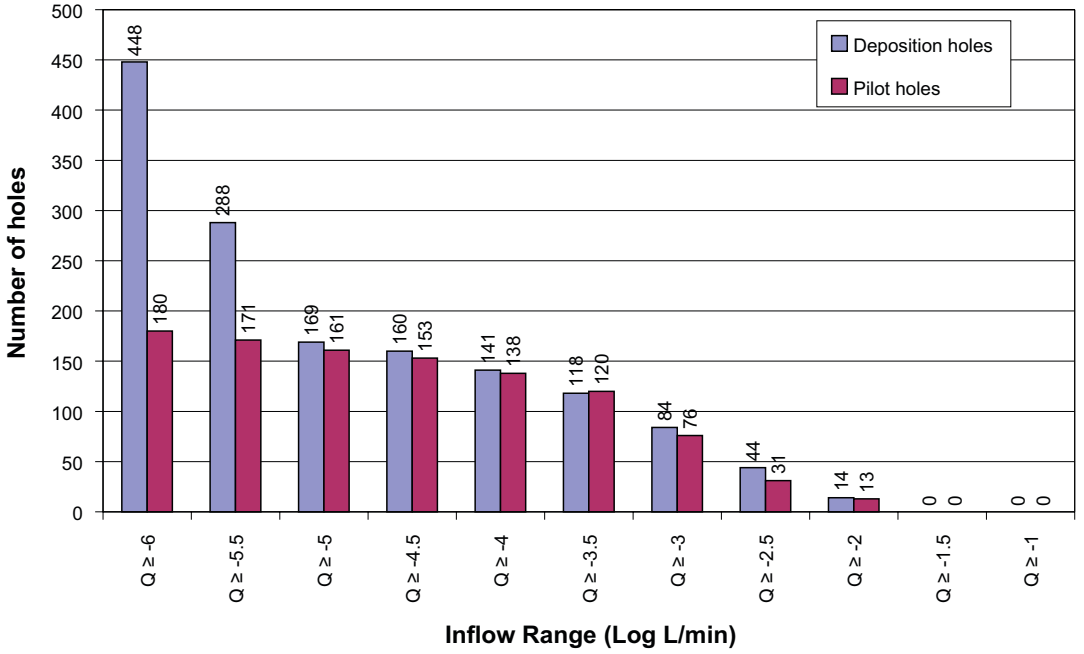

Figure 4-5. *Complementary cumulative distribution of the total inflow to each deposition hole and to each pilot hole for the 448 holes beneath the twelve tunnels open in phase m6. The deposition hole inflows are calculated with all tunnels open.*

4.3 Comparison of inflows to deposition holes vs pilot holes

In Section 3, the statistical analysis is based on calculated inflows to deposition holes for each of the three blocks (DA-A, DA-B and DA-C) under open conditions. To compare directly the inflows to pilot holes with those to deposition holes under the same conditions, we consider the case when all the holes in block DA-B are modelled as pilot holes and the atmospheric pressure boundary conditions applied in block DA-B are the same as applied in Section 3, i.e. the whole repository block is open. Here we present the comparison of inflows calculated to deposition holes and inflows calculated to pilot holes for block DA-B.

Figure 4-6 compares the transmissivity range of the fractures intersecting the deposition holes and pilot holes. Because the pilot holes are smaller than the deposition holes, the number of intersections with pilot holes is less (438) than the number of intersections with the corresponding deposition holes (705). However, from Figure 4-6, the transmissivity ranges of fractures intersecting the deposition holes and pilot holes is broadly similar, although there is a slightly larger percentage of fractures with lower transmissivities intersecting deposition holes than intersect the corresponding pilot holes. A comparison of the cross plots for the total inflow to deposition/pilot holes in block DA-B versus the sum of the transmissivities of natural intersecting fractures to the deposition or pilot holes is shown in Figure 4-7.

The comparison of the number of holes with certain inflows between deposition and pilot holes is shown in Figure 4-8 and indicates significant differences. This is to be expected, given that many of the pilot holes do not have an intersecting fracture at all and therefore have no inflow, whereas virtually all the deposition holes have an inflow. The majority of intersections with deposition holes and pilot holes arise from intersections with the EDZ. For example, out of a total 3,431 intersections with deposition holes only about 20% (705) of the intersections are those with natural fractures. When the deposition holes are replaced by pilot holes then the percentage of natural fractures intersecting with the pilot holes rises to about 43% (438) of all intersections (1,021). Figure 4-9 shows the number of deposition/pilot holes with multiple intersections with natural fractures. For similar reasons as described earlier regarding the relative sizes of the deposition hole versus the pilot hole, it is not surprising that the number of deposition holes having both single and multiple intersections with natural fractures is higher than for the corresponding pilot holes.

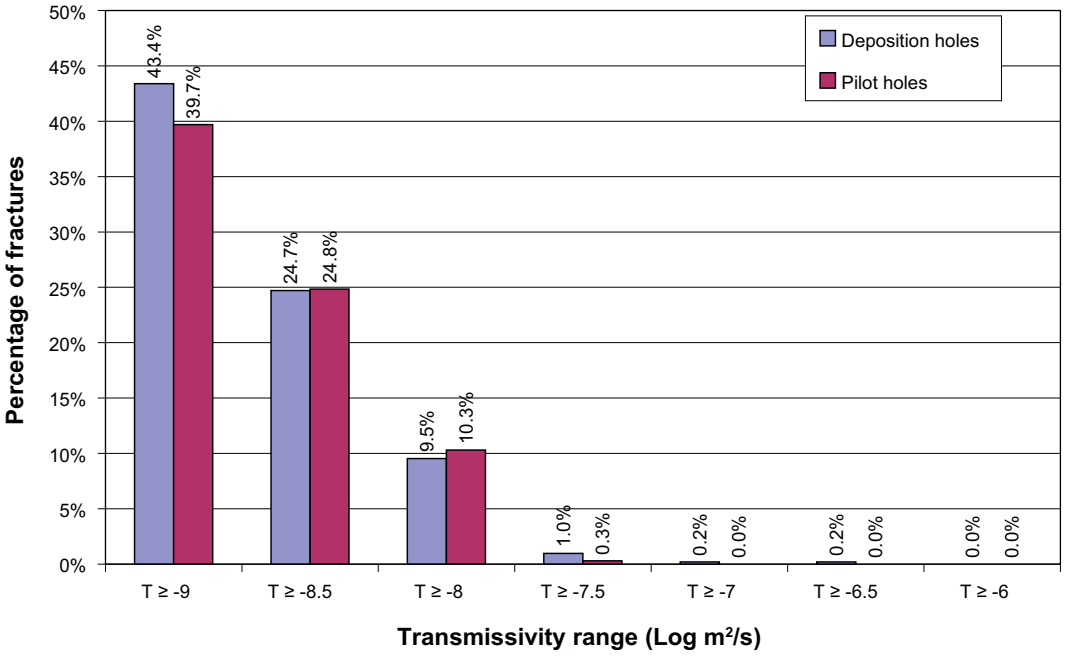

Figure 4-6. *Comparison of the complementary cumulative distributions of the transmissivity of natural fractures with inflows intersecting deposition and pilot holes in block DA-B.*

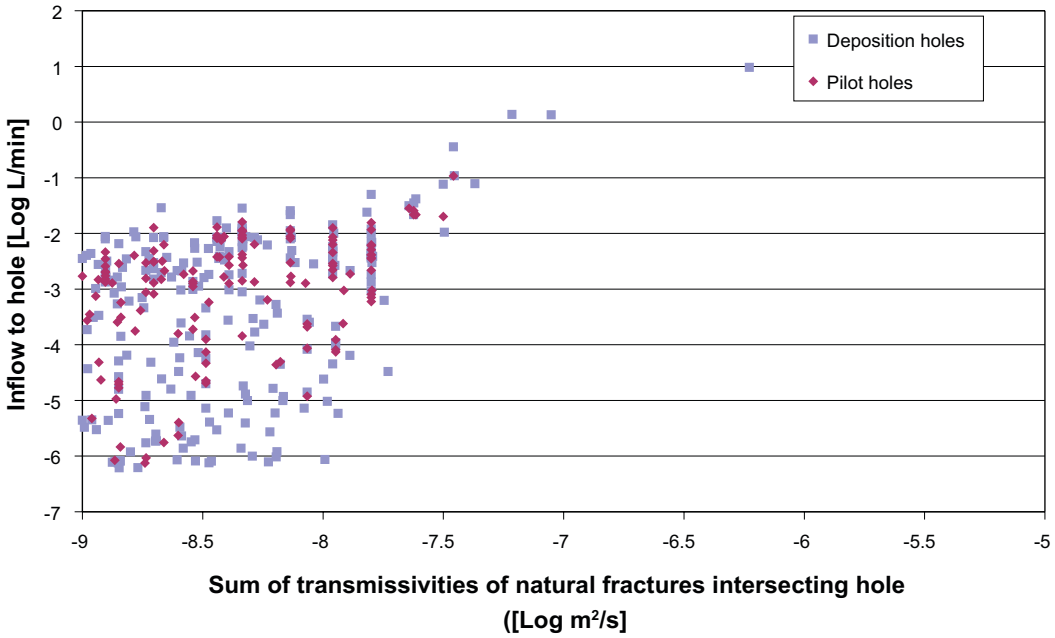

Figure 4-7. *Comparison of the cross plot of the total inflow to deposition and pilot holes out of a possible 2,769 pilot holes in block DA-B versus the sum of the transmissivities of fractures intersecting each deposition/pilot hole. The EDZ transmissivities and inflows are not included.*

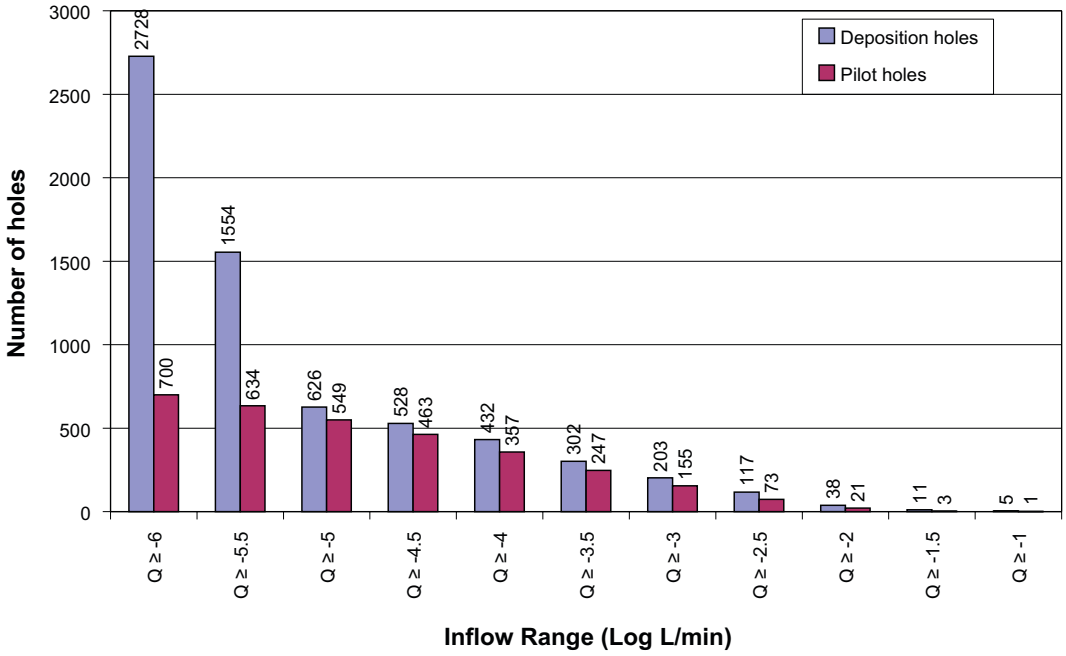

Figure 4-8. *Comparison of the complementary cumulative distributions of the total flow to each deposition and pilot hole in block DA-B.*

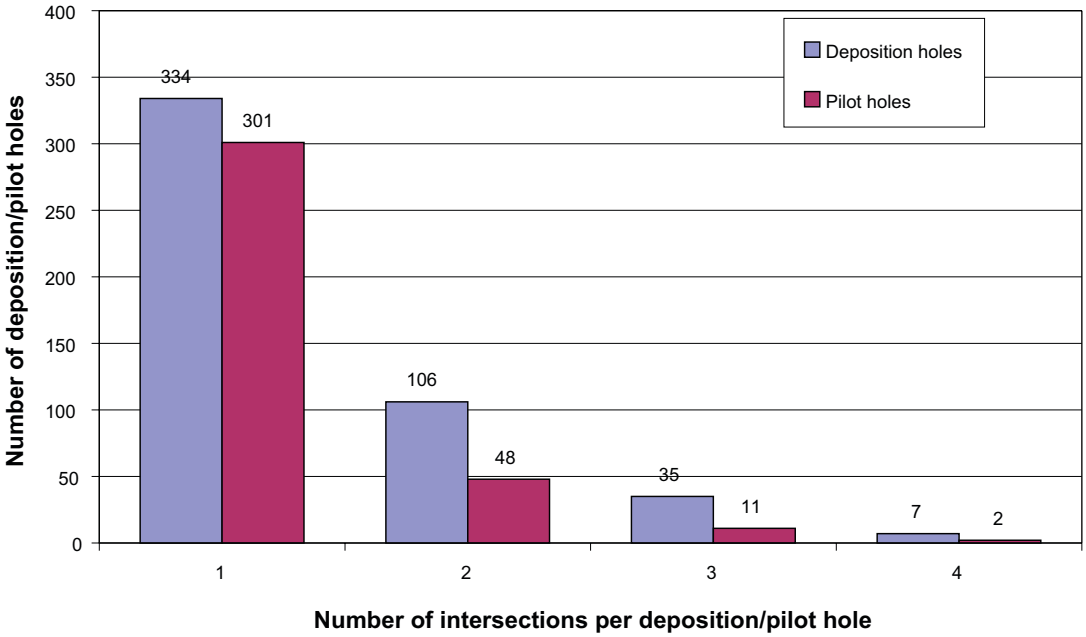

Figure 4-9. *Comparison of the number of deposition/ pilot holes with a certain number of natural fractures intersecting the deposition/ pilot hole in block DA-B.*

Figure 4-10 shows a cross plot of the inflows to pilot holes versus the inflows to deposition holes for all the holes in block DA-B under open repository conditions. A default log inflow value of –7 is assigned to those pilot holes which have no inflow but for which there is an inflow to the corresponding deposition hole. This plot should be compared with Figure 4-4, when block DA-B was only partially open and only 448 pilot holes were under open repository conditions. With all 2,769 holes now included, the correlation between inflows to deposition holes and inflows to pilot holes shows a small but noticeable improvement compared to Figure 4-4. Generally, the inflows to deposition holes are higher than to the corresponding pilot holes due to the greater number of fracture intersections. However, in a some cases the pilot hole inflows are higher due to redistribution of flows.

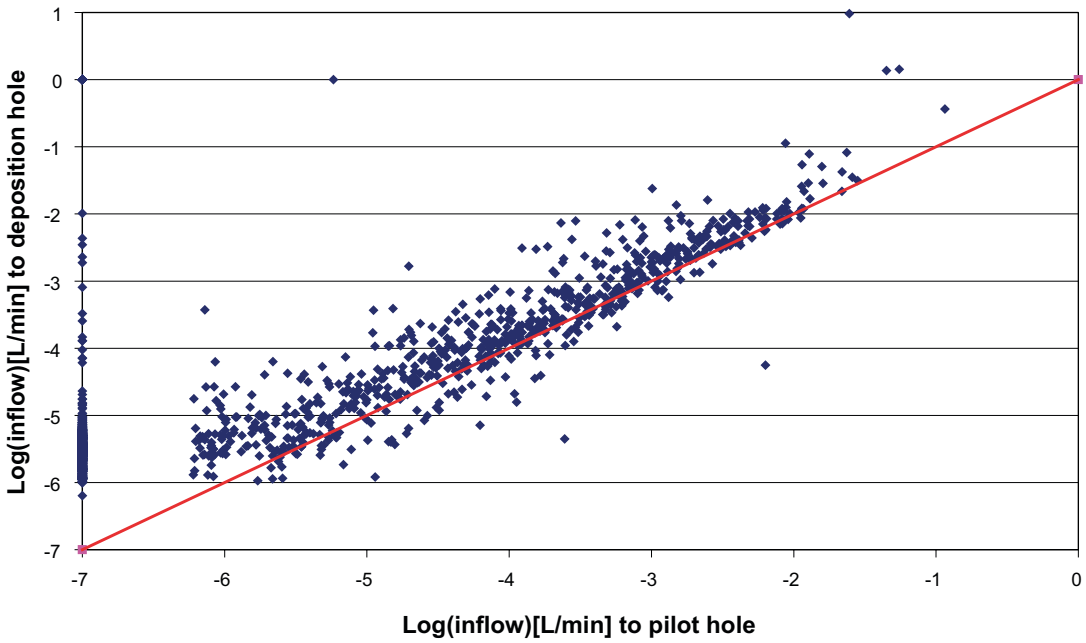

Figure 4-10. *Cross plot of the total inflow to each deposition hole versus the total inflow into the corresponding pilot hole for the holes in block DA-B. The red line indicates where inflows to deposition holes would be equal to inflows to pilot holes.*

5 Hydraulic injection tests

In this section, we consider the case where, instead of calculating the inflow to deposition/pilot holes from fractures, selected pilot holes are subjected to an overpressure and the induced flow rate into the surrounding bedrock, as well as the pressure changes in neighbouring pilot holes are calculated.

5.1 Model description

For these injection tests, the same repository block (block DA-B) is used with all deposition tunnels and main tunnels open and at atmospheric pressure and pilot holes positioned at the proposed locations of each deposition hole. Each pilot hole is represented as a cylindrical hole with a radius of 0.038 m and an overall depth of 8 m, and where the upper 0.5 m of each pilot hole is packed off. Each pilot hole is given a high hydraulic conductivity of $1 \cdot 10^{-3}$ m/s to allow flow along the pilot hole and to give a uniform pressure within it.

Ideally, individual injection tests should be simulated for each pilot hole in the repository, but given the number of pilot holes (6,916), this is not practical. Therefore for the purposes of illustration, up to three pilot holes are selected from each deposition tunnel as injection pilot holes. Clearly, if a pilot hole is not intersected by a natural fracture, then the application of an overpressure to the pilot hole will have no effect on any neighbouring pilot holes. Thus, only those pilot holes that have an intersection with a natural fracture are considered. Three simulation cases are considered each with one injection pilot hole per tunnel. One with injection pilot holes corresponding to the pilot holes furthest from the main tunnel in each deposition tunnel with a natural fracture intersection is selected; one with injection pilot holes corresponding to the pilot holes closest to the main tunnel in each deposition tunnel with a natural fracture intersection is selected; and a third injection pilot hole corresponding to a pilot hole with a natural fracture intersection between the two outermost injection pilot holes. Thus, for example, if there are nine pilot holes with a natural fracture intersection in a tunnel, then pilot holes 1, 5 and 9 would be selected to be injection pilot holes. It should be noted that some deposition tunnels do not have any pilot holes which intersect with natural fractures, whilst a few others only have one or two pilot holes which intersect natural fractures. Selecting injection pilot holes in this way gives rise to a total number of injection pilot holes of 215 over the three simulations. The locations of the injection pilot holes are shown in Figure 5-1, where the injection pilot holes are shown as large red, green and orange dots (to differentiate the three injection holes in each deposition tunnel), and other pilot holes with natural fracture intersections shown as blue dots.

Four simulations are performed. In the first simulation, atmospheric pressure boundary conditions are applied to the deposition tunnels and main tunnels. The results from this simulation provide the baseline pressures for each pilot hole prior to any injection tests being performed.

A further three simulations are then performed, in which a single injection pilot hole from each tunnel is selected, according to the selection criteria described above. For example, the first simulation uses the injection pilot holes shown in red in Figure 5-1, the second uses the injection pilot holes shown in green and the third uses the injection pilot holes shown in orange. For each injection pilot hole, a fixed overpressure of 5 bar (i.e. 5 bar pressure over and above the baseline pressure calculated for the pilot hole in the first simulation), is applied. All other pilot holes in the tunnel have no boundary conditions applied. It is further assumed that there is minimal interference between tunnels given the ~40 m spacing, although this may be hard to avoid and could lead to a lower injection rate when injecting into adjacent tunnels. The steady-state flow from the injection pilot hole and the flows and pressure changes in neighbouring pilot holes in the same tunnel are then calculated.

The number of pilot holes in a particular tunnel that would exhibit a change in pressure to an overpressure applied to a single pilot hole in the same tunnel will clearly depend on the fracture connectivity between the pilot holes. As Figure 5-1 shows, not all pilot holes are intersected by natural fractures, and thus their pressures will not respond to an injection pilot hole in the same tunnel (or any other tunnel). However, in some cases, even where a pilot hole is intersected by a natural fracture, its connectivity to an injection pilot hole may be through a long and tortuous route such that the impact of the injection pilot hole may be minimal. In contrast, large sub-horizontal fractures can often intersect several pilot holes

within the same tunnel, or tunnels, such that the overpressure applied to the injection pilot hole is easily distributed to other pilot holes in the tunnel. Both these effects can be seen in Figure 5-2, which shows a plot of the number of pilot holes in a tunnel which exhibit a change in pressure above 100 Pa (about 0.01 m head change, i.e. commensurate with a practical detection limit) to an overpressure of 5 bar being applied to one other pilot hole in the same tunnel, aggregated over all three simulations. The plot shows that there are 74 injection pilot holes where there is no response from other pilot holes in the same tunnel, falling to 48 injection pilot holes where one other pilot hole in the same tunnel show a change in pressure and 28 where two other pilot holes in the same tunnel show a change in pressure and so on.

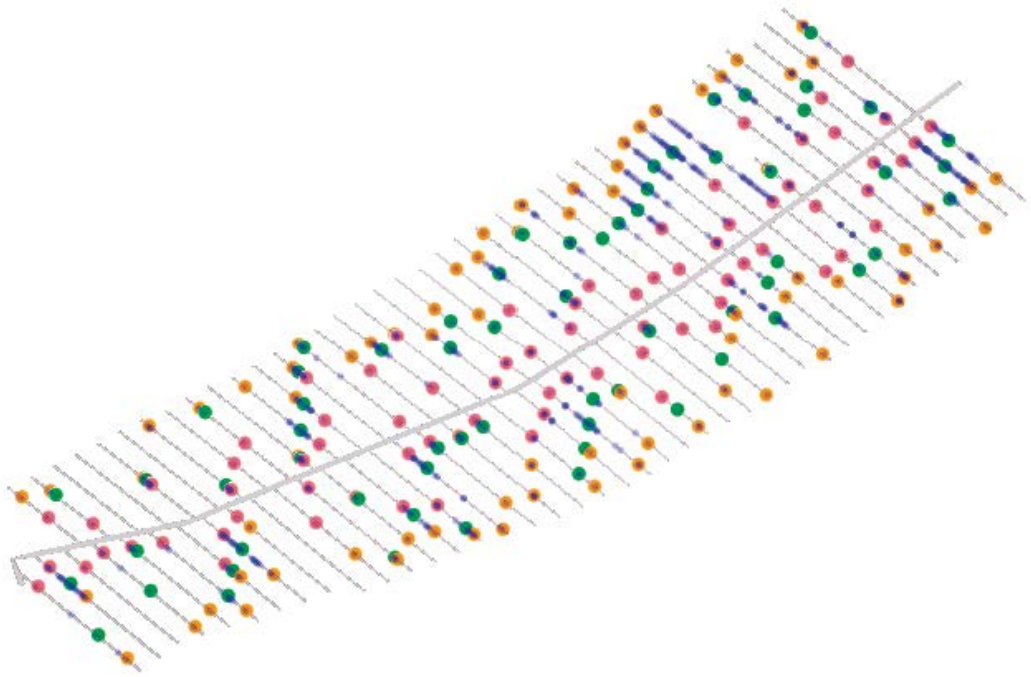

Figure 5-1. *Locations of injection pilot holes (shown as larger red, orange and green dots corresponding to the three simulations performed) in each deposition tunnel. The smaller blue dots indicate pilot holes with intersecting natural fractures. The deposition tunnels are shown in grey.*

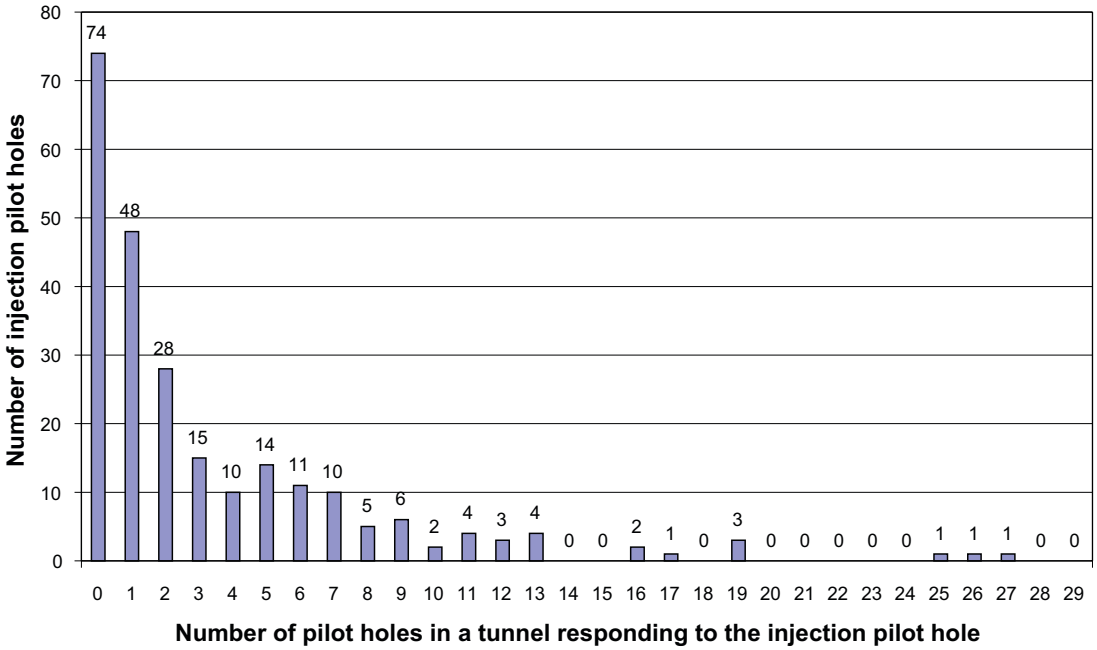

Figure 5-2. *Plot of the number of pilot holes in a tunnel with a change in pressure above 100 Pa caused by a single injection pilot hole in the same tunnel, based on 215 injection pilot holes over three simulations.*

The plot also indicates some tunnels in which there are a particularly large number of pilot holes which show a change in pressure. These can be attributed to large sub-horizontal fractures which intersect several pilot holes in the same tunnel. For instance, in one particular tunnel where three large sub-horizontal fractures intersect the pilot holes, the number of pilot holes which show a change in pressure is found to be 25, 26 and 27 for the three injection pilot holes in that tunnel, respectively.

It is considered that such characteristics are determined by the intensity-size distribution of open fractures and connectivity of open channels within fractures of the network. Any such data acquired of this type might provide a means to confirm model concepts relating to size distribution, intensity and connectivity of open fractures, and channelling. It might also shed some light on issues relating to performing PFL-f tests underground and associated detection limits.

In another case, a single large sub-horizontal fracture gives rise to 19 pilot holes with a change in pressure for each of the three injection pilot holes in that tunnel as illustrated in Figure 5-3. In this figure, pilot holes in the tunnel are shown together with the large sub-horizontal fracture intersecting many of the pilot holes. It should be noted that, in each of the three simulations performed, one injection pilot hole is selected from each tunnel, thus the head values in both the fracture and the pilot holes may be influenced by injection pilot holes in neighbouring tunnels, especially when, as in this case, the fracture extends across more than one deposition tunnel.

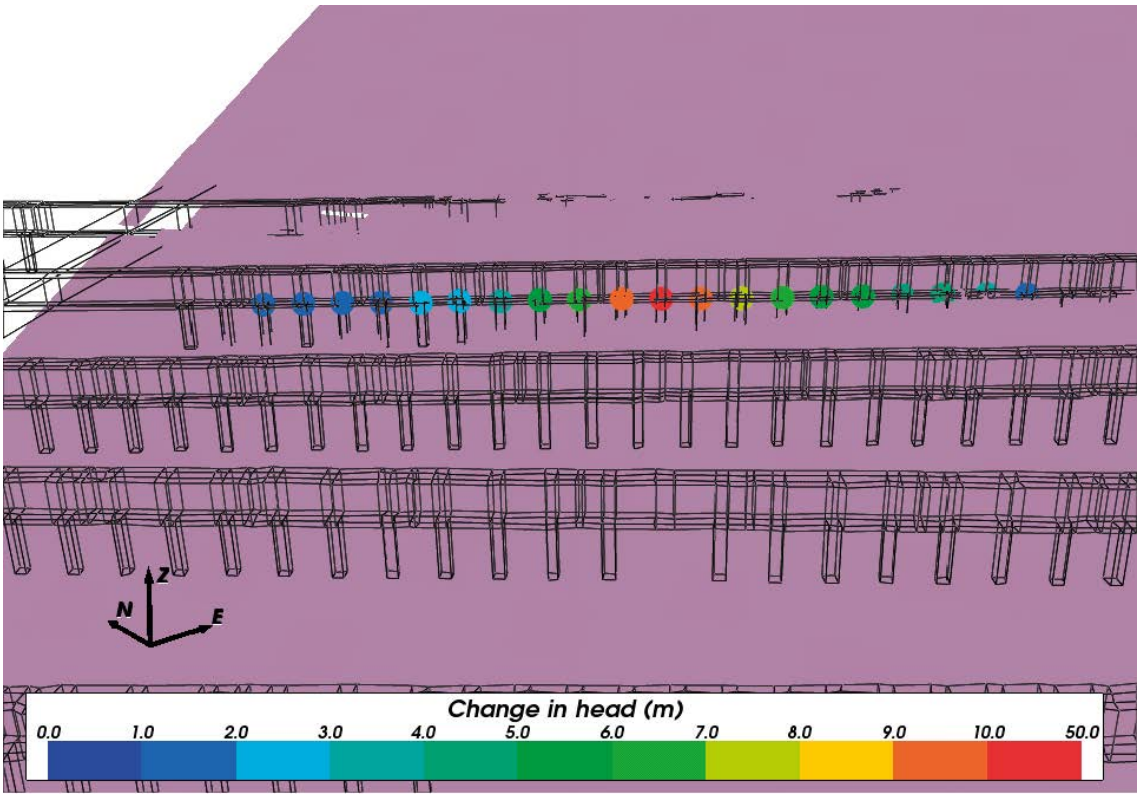

Figure 5-3. *Illustration of a single large sub-horizontal fracture (coloured purple) that intersects several pilot holes in a single tunnel. The head changes in the pilot holes due to injection are indicated by filled circles, coloured by the head change, at the top of each responding pilot hole. The injection pilot hole is the one with the red circle. Note the non-linear colour scale above 10.0 m head change. The deposition tunnels and pilot holes are coloured black.*

Figure 5-4 shows a cross plot of the injected specific capacity (the outflow divided by the injection head, 50 m) from the 215 injection pilot holes against the corresponding specific capacity (the inflow divided by the head change between packed off and open conditions, which varies between holes) to pilot holes in block DA-B, as calculated in Section 4 when all pilot holes in DA-B are open. Both flow-rates are divided by the change in head resulting from either injection or opening of the pilot holes relative to the case where the tunnels are open, but the pilot holes are closed. In this way the flow-rate resulting from the disturbance from the pilot holes is discerned from the disturbance resulting from the opening of the tunnel. Whilst there is reasonable correlation between the two quantities there is also some scatter of the points. In the injection tests only one pilot hole is tested per tunnel per simulation, whereas the inflows calculations have all holes open and there is more interaction between the responses to conditions in each hole. This difference in boundary conditions is thought to be why often the injected specific capacity is higher than the inflow to an open hole specific capacity. Due to the different way in which the pilot holes are modelled in this section compared to Section 4, some of the injection pilot holes do not have a corresponding inflow as calculated in Section 4, leading to a reduced number of points on the plot.

However, better correlations than Figure 5-4 are found in Figure 5-5 and Figure 5-6, showing cross plots between injected specific capacity from injection pilot holes for the open repository block against U_r and F_r for deposition holes in the closed repository block at 2000 AD, respectively. In Figure 5-5, two outlying points at low injected specific capacity and high U_r values can be seen. These outlying points can be explained by the greater number of intersections of natural fractures with deposition holes compared to the much narrower pilot holes.

An injection specific capacity (or effective transmissivity) for each injection pilot hole is calculated as the total outflow from the injection pilot hole divided by the applied change in head for the injection pilot hole. Figure 5-7 shows a cross plot of the injected specific capacity against the sum of the transmissivities of fractures intersecting the injected pilot hole. This plot shows a reasonable correlation between the two quantities, particularly at higher transmissivities, with a scatter of about an order of magnitude over a range of four orders of magnitude. In most cases, however, the scatter suggests that the measured injected specific capacity tends to underestimate the actual sum of transmissivities of the intersecting fractures, indicating that for these injection pilot holes the transmissivities of the connected fractures in the wider fracture network are limiting the outflow from the injected pilot hole.

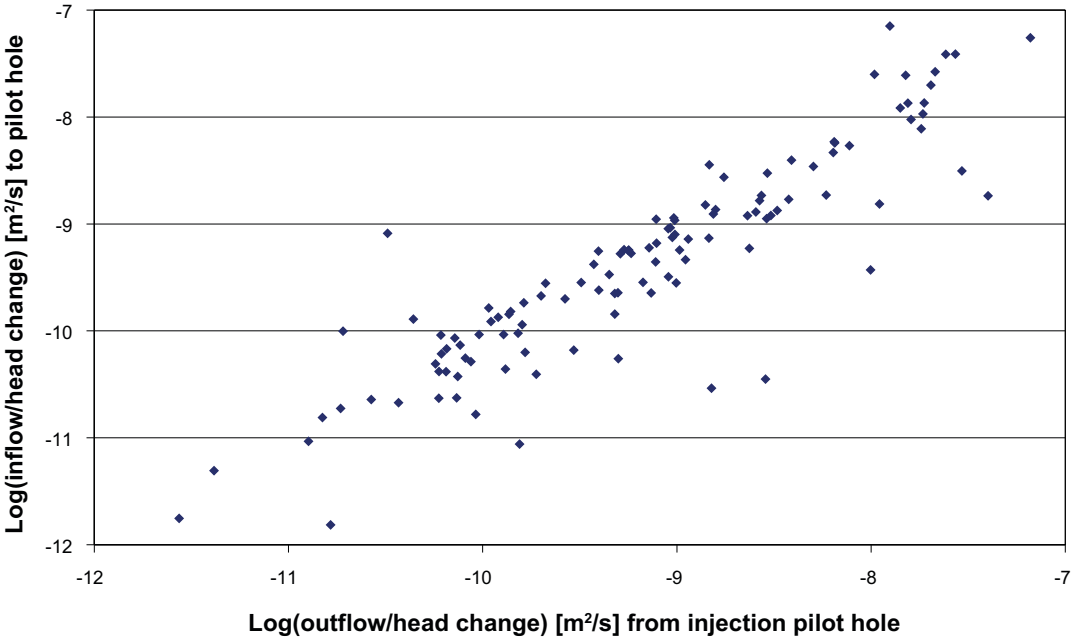

Figure 5-4. *Cross plot of the injected specific capacity from 215 injection pilot holes versus the specific capacity from natural fractures to the corresponding pilot hole under open repository conditions for case r0.*

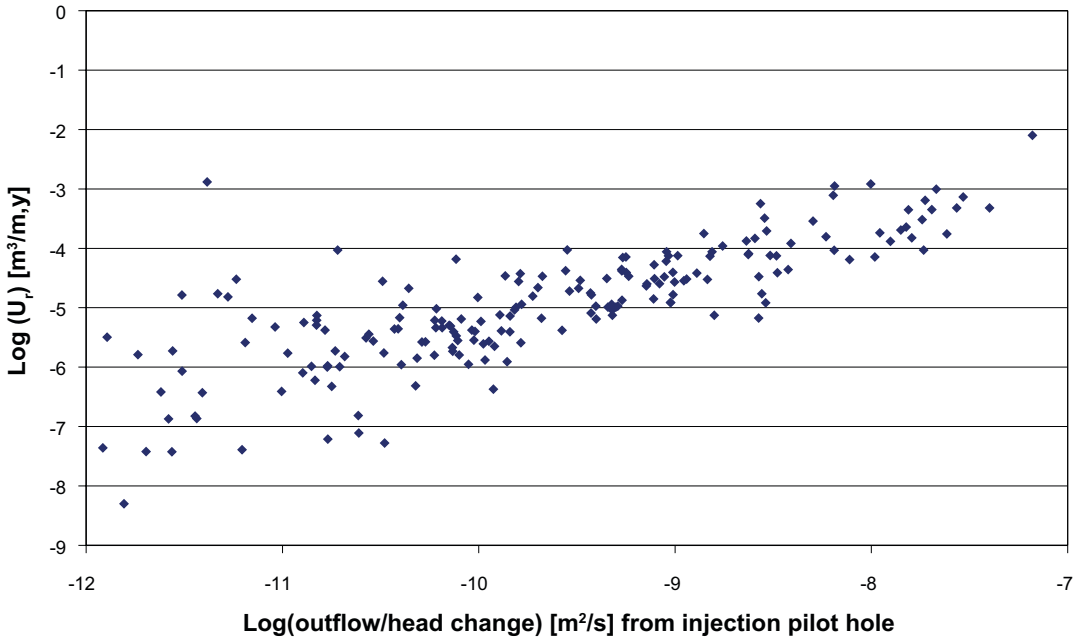

Figure 5-5. *Cross plot of the injected specific capacity from 215 injection pilot holes under open repository conditions against U_r, the initial equivalent flux into the fractured rock adjacent to the corresponding deposition holes under closed repository conditions at 2000 AD, for case r0.*

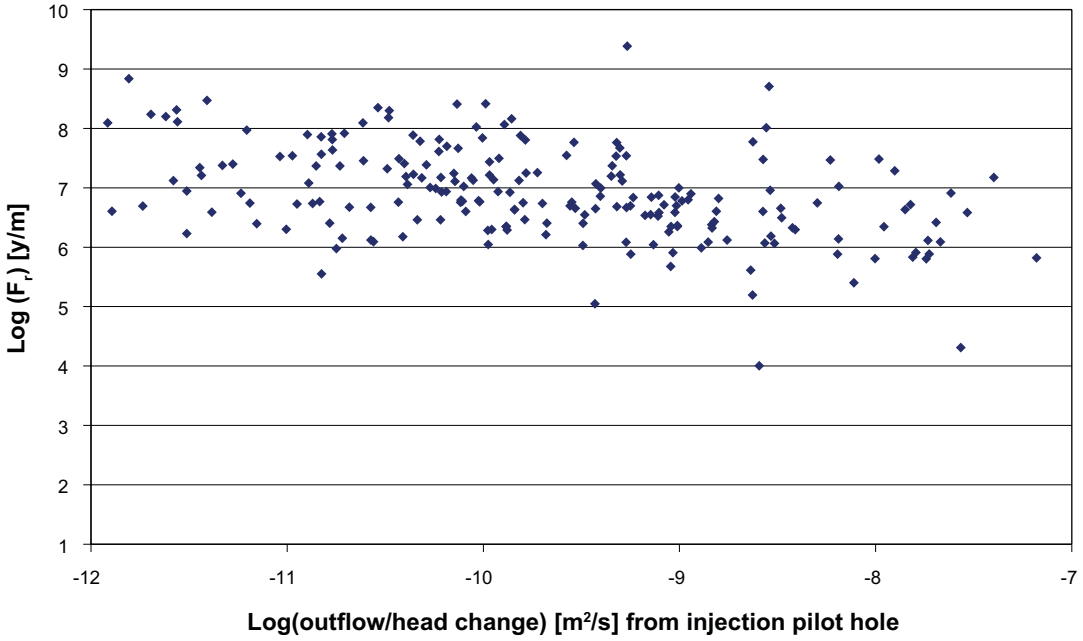

Figure 5-6. *Cross plot of the injected specific capacity from 215 injection pilot holes under open repository conditions against F_r, the flow-related transport resistance in the rock under closed repository conditions at 2000 AD, for case r0.*

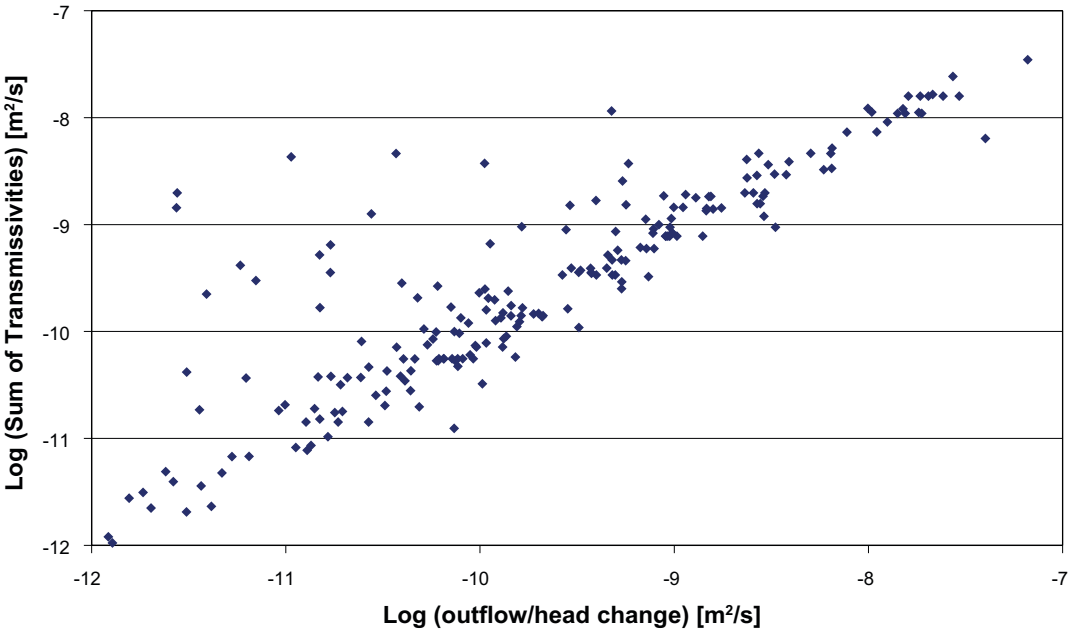

Figure 5-7. *Cross plot of the injected specific capacity against the sum of the transmissivities of the fractures intersecting the injection pilot holes for case r0.*

6 Conclusions

The work reported here describes the application of the SR-Site modelling methodology to the calculation of inflows to deposition holes, deposition tunnels and pilot holes under open repository conditions and hydraulic injection tests to selected pilot holes drilled in advance of deposition holes.

6.1 Inflows to deposition holes and tunnels

A study has been carried out of inflows to deposition tunnels and deposition holes under open repository conditions using the SDM-Site Forsmark hydrogeological discrete fracture network (Hydro-DFN) model. The modelling divides the repository structures into three separate blocks to represent the phased opening of repository panels one at a time. Within each block, the inflows to the deposition tunnels and deposition holes are calculated and analysed statistically.

The main conclusions arising from the inflows to deposition tunnels and deposition holes are:

- Inflows to deposition tunnel sections are mostly higher than the inflows to the corresponding deposition holes in the same tunnel due to inflows from deformation zones.
- Approximately half of all inflow to deposition holes is from sub-vertical natural fractures and about a third from deformation zones.
- Many of the high total inflows from stochastic fractures result from sub-vertical fractures with centres at relatively shallow depths or in bordering fracture domains with high uniform transmissivity.
- Over 80% of total inflows to deposition tunnels are from deformation zones and about 10% from sub-vertical fractures.
- Based on four realisations, between 20 and 41 deposition holes have an inflow greater than 0.1 L/min. This compares with 88 or 157 calculated by Svensson and Follin (2010) using either an EDPM or ECPM model respectively in which they included grouting in their models.
- For the base case realisation, of 20 deposition holes with inflows greater than 0.1 L/min, 16 of these would be screened by applying FPC (Full Perimeter Criteria). In contrast only one of the 20 would be screened by applying EFPC (Extended Full Perimeter Criteria).
- Screening out high inflow positions during open conditions removes the majority of positions with post-closure flows, $U_r > 10^{-2}$ m/y. However, it does not remove a significant proportion of holes with relatively low values of F_r.

6.2 Inflows to pilot holes

In practice, during the construction of the repository, it is unlikely that the repository will be constructed with all the tunnels (and their associated deposition holes) in a block (i.e. DA-A, DA-B or DA-C) open at the same time and at atmospheric pressure. Instead, it is postulated that as the repository is constructed, and deposition holes are filled, deposition tunnels will be closed and backfilled and new tunnels excavated in a progressive manner. As the new tunnels are opened, inflows to potential locations for deposition holes will initially be estimated by measuring the inflows into pilot holes beneath the newly excavated tunnels and the decision to create a deposition hole in that location will be based on those pilot hole inflows.

An area of the repository is selected in which there are a significant number of inflows to deposition holes calculated under open repository conditions for the base case realisation. The selected area comprises 20 tunnels in the south west of the block which are closed and backfilled. New tunnels are then opened two at a time in an easterly direction in six phases, such that by the sixth phase twelve tunnels in total are open. Inflows to the opened deposition tunnels and associated pilot holes are then calculated and compared to the inflows to the corresponding deposition holes when all deposition tunnels and deposition holes in block DA-B are open.

The main conclusions from the inflows to pilot holes are:

- As deposition tunnels are opened, initially inflows to both the tunnel and associated pilot holes are higher, but then as additional tunnels are opened the inflows to the tunnels and pilot holes opened in the earlier phases rapidly decrease.
- The median ratio of initial inflow to the pilot hole when it is located near the front of excavation relative to when all pilot holes are open is about 2. As an estimate this might imply that if inflow screening was performed based on measured inflows to pilot holes conducted shortly after construction of each tunnel, then around twice as many positions, approximately 40–50 would be rejected compared to a case based on measurements with all tunnels open.
- There is a reasonable correlation between the inflows to the 448 pilot holes in the 12 tunnels open in block DA-B and the inflows to the corresponding deposition holes when all 81 tunnels in block DA-B are open. There is a strong correlation between inflows to all 2,769 deposition holes in block DA-B compared to inflows to pilot holes in the same positions.
- For the case where all deposition holes in block DA-B are replaced by pilot holes, only one pilot hole has an inflow greater than 0.1 L/min compared to five deposition holes under the same open conditions.
- There are no significant differences between the cross plots of inflows to deposition holes and inflows to pilot holes for an open repository against the two performance measures, U_r and F_r, for a closed repository, for all 2,769 holes in block DA-B.

6.3 Hydraulic injection tests

This study has also demonstrated a modelling methodology for examining injection pilot holes, and in particular has shown that the outflows observed from the injection pilot holes under open repository conditions have a good correlation with the initial equivalent flux into the fractured rock, U_r, under closed repository conditions, although a wide diameter deposition hole can occasionally intersect hydraulically significant fractures not seen in a slim pilot hole used to perform the injection tests. It might be worth comparing the effectiveness of screening on such injection tests for single slim pilot holes against wider diameter single pilot holes, or multiple slim pilot holes. There is also a reasonable correlation between the injected specific capacity and the sum of the transmissivities of the fractures intersecting each injection pilot hole.

The number of pilot holes giving a pressure change in the same tunnel as an injection pilot hole can give an indication of the presence of sub-horizontal fractures that intersect several neighbouring pilot holes. Such characteristics are determined by the intensity-size distribution of open fractures and connectivity of open channels within fractures of the network. Any such data acquired of this type might provide a means to confirm model concepts relating to size distribution, intensity and connectivity of open fractures, and channelling. It might also shed some light on issues relating to performing PFL-f tests underground and associated detection limits.

6.4 Future work

This study has successfully demonstrated a modelling process for estimating magnitudes and spatial distributions of inflows to deposition tunnels, deposition holes and pilot holes based on DFN modelling of a repository under open conditions. It has also demonstrated a methodology for simulating injection tests in pilot holes. However, the approach could be taken further and the following future work is suggested, accepting that many of these tasks could only be performed once information becomes available from underground investigations at Forsmark:

- The effects of grouting on inflows.
- Penetration of grout from deposition tunnels to deposition hole locations and possible exclusion of those locations due to potentially adverse pH conditions.
- Investigate the effects of introducing fracture heterogeneity. This is likely to give greater variability in inflows between deposition holes. The parameterisation of the heterogeneity would benefit from additional data acquired from underground investigations.
- Simulate hydraulic tests in pilot holes for deposition tunnels.
- Association of high inflows and post-closure flows with extensive fractures seen in multiple tunnels.
- Assessment of the sensitivity of inflows to flow from low transmissivity fractures at or below the practical detection limit in deep boreholes.
- The values of total inflows to deposition tunnels were found to be sensitive to the presence of stochastic fractures originating in bordering rock domains (FFM04/FFM05). This suggests that hydraulic tests in pilot holes and probe holes ahead of extending main tunnels to the north and south may need to be factored into the construction or procedures for adaptive design.
- Revise calculations based on measurements during underground investigations.

References

SKB's (Svensk Kärnbränslehantering AB) publications can be found at www.skb.se/publications.

AMEC, 2012a. CONNECTFLOW Release 10.4 Technical summary document. AMEC/ENV/CONNECTFLOW/15, AMEC, UK.

AMEC, 2012b. NAMMU Release 10.4 Technical summary document. AMEC/ENV/CONNECTFLOW/8, AMEC, UK.

AMEC, 2012c. NAPSAC Release 10.4 Technical summary document. AMEC/ENV/CONNECTFLOW/12, AMEC, UK.

Follin S, 2008. Bedrock hydrogeology Forsmark. Site descriptive modelling, SDM-Site Forsmark. SKB R-08-95. Svensk Kärnbränslehantering AB.

Follin S, Levén J, Hartley L, Jackson P, Joyce S, Roberts D, Swift B, 2007. Hydrogeological characterisation and modelling of deformation zones and fracture domains, Forsmark modelling stage 2.2. SKB R-07-48, Svensk Kärnbränslehantering AB.

Goodman R E, Moye D G, Van Schalkwyk A, Javandel I, 1965. Ground water inflow during tunnel driving. Engineering Geology 2, 39–56.

Joyce S, Simpson T, Hartley L, Applegate D, Hoek J, Jackson P, Swan D, Marsic N and Follin S, 2010a. Groundwater flow modelling of periods with temperate climate conditions – Forsmark. SKB R-09-20, Svensk Kärnbränslehantering AB.

Joyce S, Simpson T, Hartley L, Applegate D, Hoek J, Jackson P, Roberts D, Swan D, Gylling B, Marsic N, Rhén I, 2010b. Groundwater flow modelling of periods with temperate climate conditions – Laxemar. SKB R-09-24, Svensk Kärnbränslehantering AB.

Olofsson I, Simeonov A, Stephens M, Follin S, Nilsson A-C, Röshoff K, Lindberg U, Lanaro F, Fredriksson A, Persson L, 2007. Site descriptive modelling Forsmark, stage 2.2: A fracture domain concept as a basis for the statistical modelling of fractures and minor deformation zones, and interdisciplinary coordination. SKB R-07-15, Svensk Kärnbränslehantering AB.

Rhén I, Follin S, Hermanson J, 2003. Hydrological Site Descriptive Model – a strategy for its development during Site Investigations. SKB R-03-08, Svensk Kärnbränslehantering AB.

SKB, 2008. Site description of Forsmark at completion of the site investigation phase SDM-Site Forsmark. SKB TR-08-05, Svensk Kärnbränslehantering AB.

SKB, 2010. Slutförvarsanläggning för använt kärnbränsle. Anläggningsbeskrivning layout D – Forsmark. SKB R-09-12, Svensk Kärnbränslehantering AB.

SKB, 2011. Long-term safety for the final repository for spent nuclear fuel at Forsmark. Main report of the SR-Site project. SKB TR-11-01, Svensk Kärnbränslehantering AB.

Svensson U, Follin S, 2010. Groundwater flow modelling of the excavation and operational phases – Forsmark. SKB R-09-19, Svensk Kärnbränslehantering AB.

Appendix A

Inflows to depoistion holes for other cases

A.1 Inflows to deposition holes

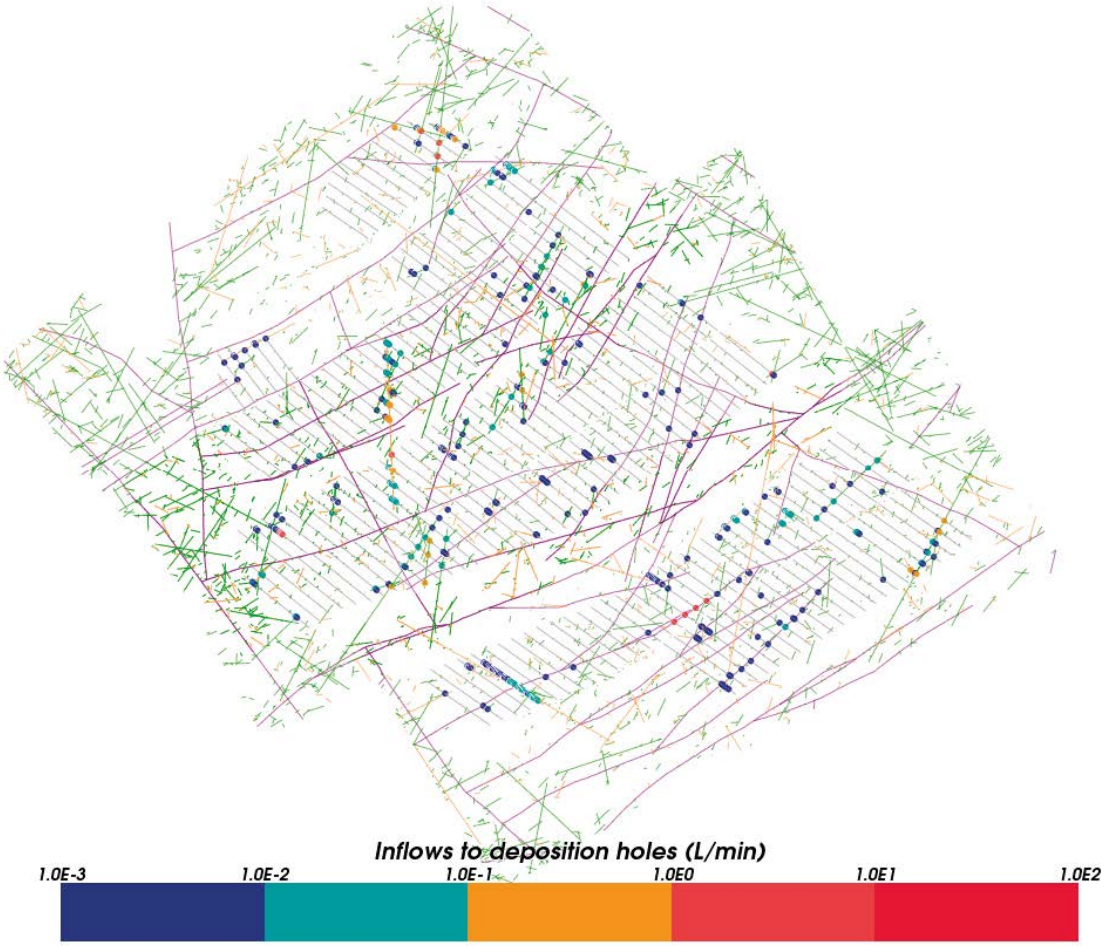

Figure A-1. *Inflows greater than $1{\cdot}10^{-3}$ L/min to deposition holes for case r2. Stochastic fractures are shown in green (sub-vertical) and orange (sub-horizontal). Deformation zones are shown in purple and the repository tunnels in grey.*

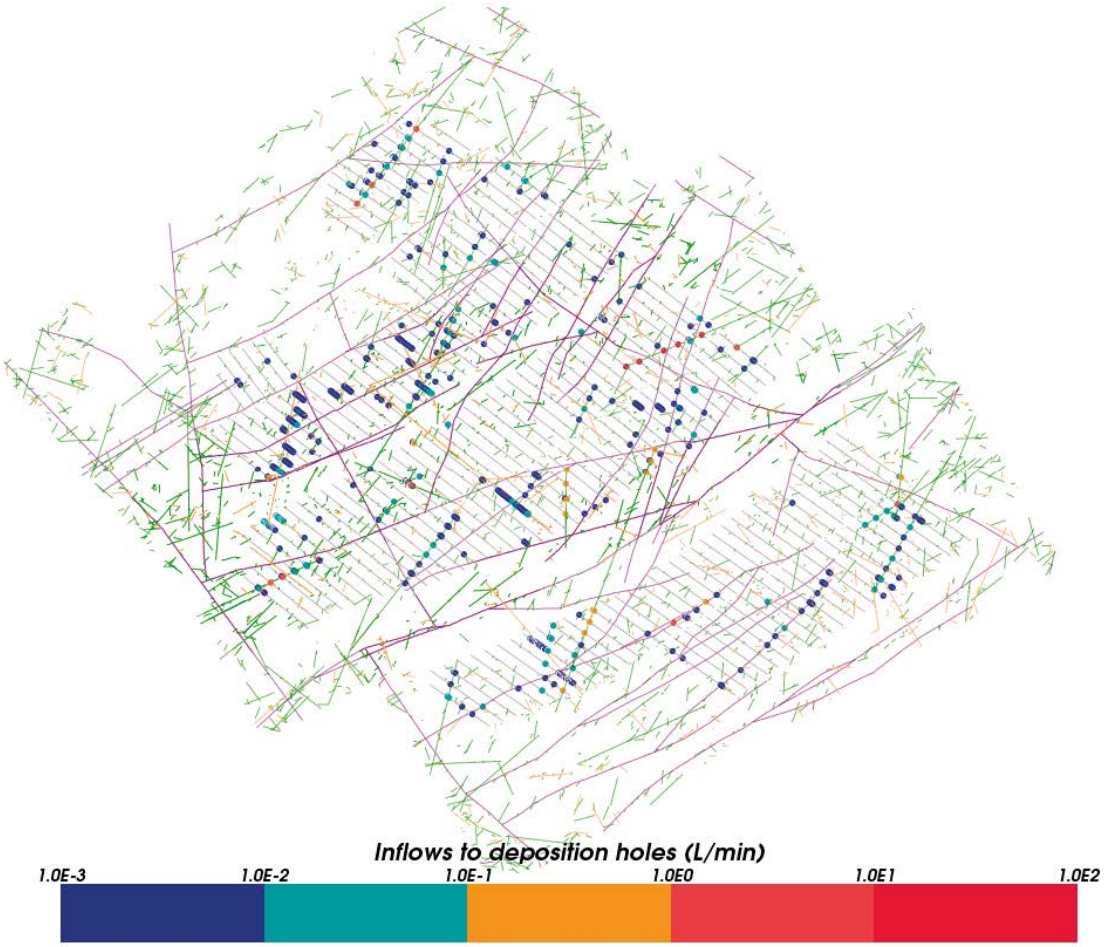

Figure A-2. *Inflows greater than $1{\cdot}10^{-3}$ L/min to deposition holes for case r3. Stochastic fractures are shown in green (sub-vertical) and orange (sub-horizontal). Deformation zones are shown in purple and the repository tunnels in grey.*

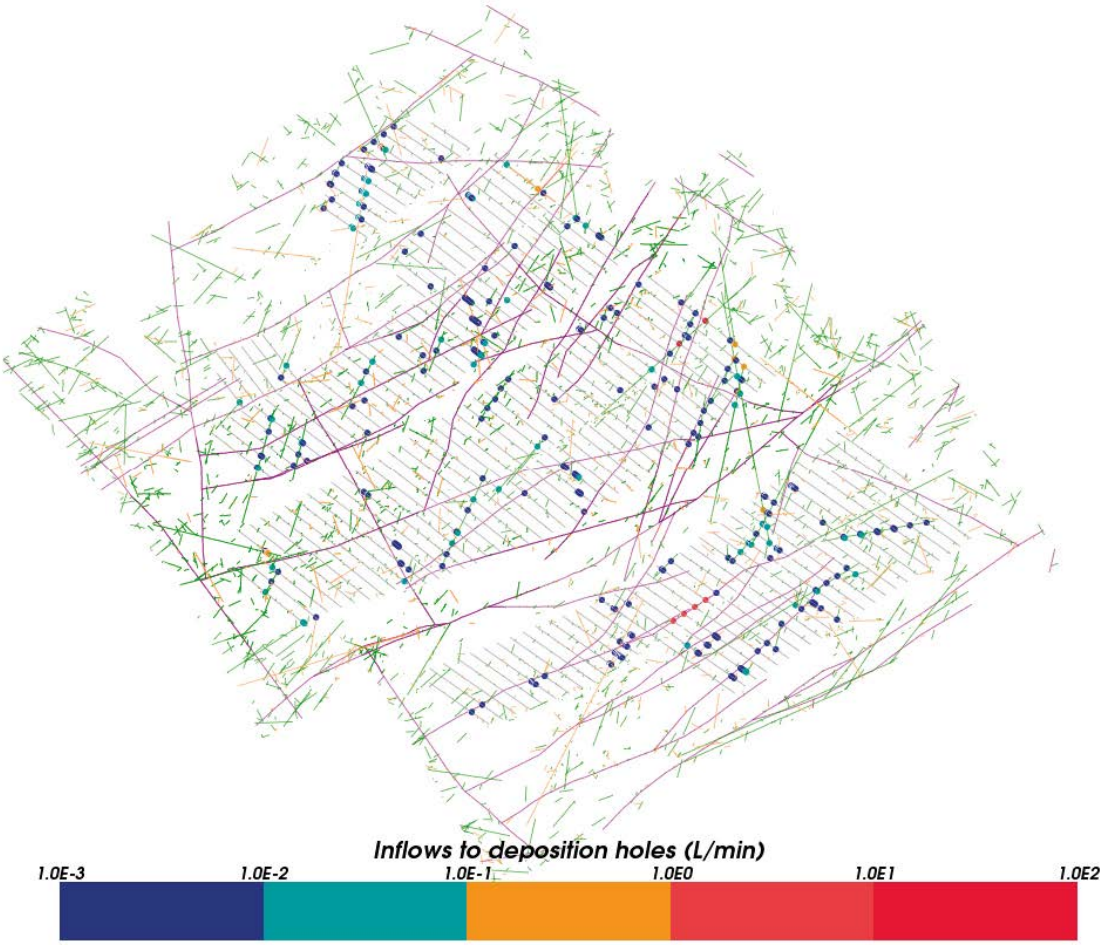

Figure A-3. *Inflows greater than $1{\cdot}10^{-3}$ L/min to deposition holes for case r5. Stochastic fractures are shown in green (sub-vertical) and orange (sub-horizontal). Deformation zones are shown in purple and the repository tunnels in grey.*

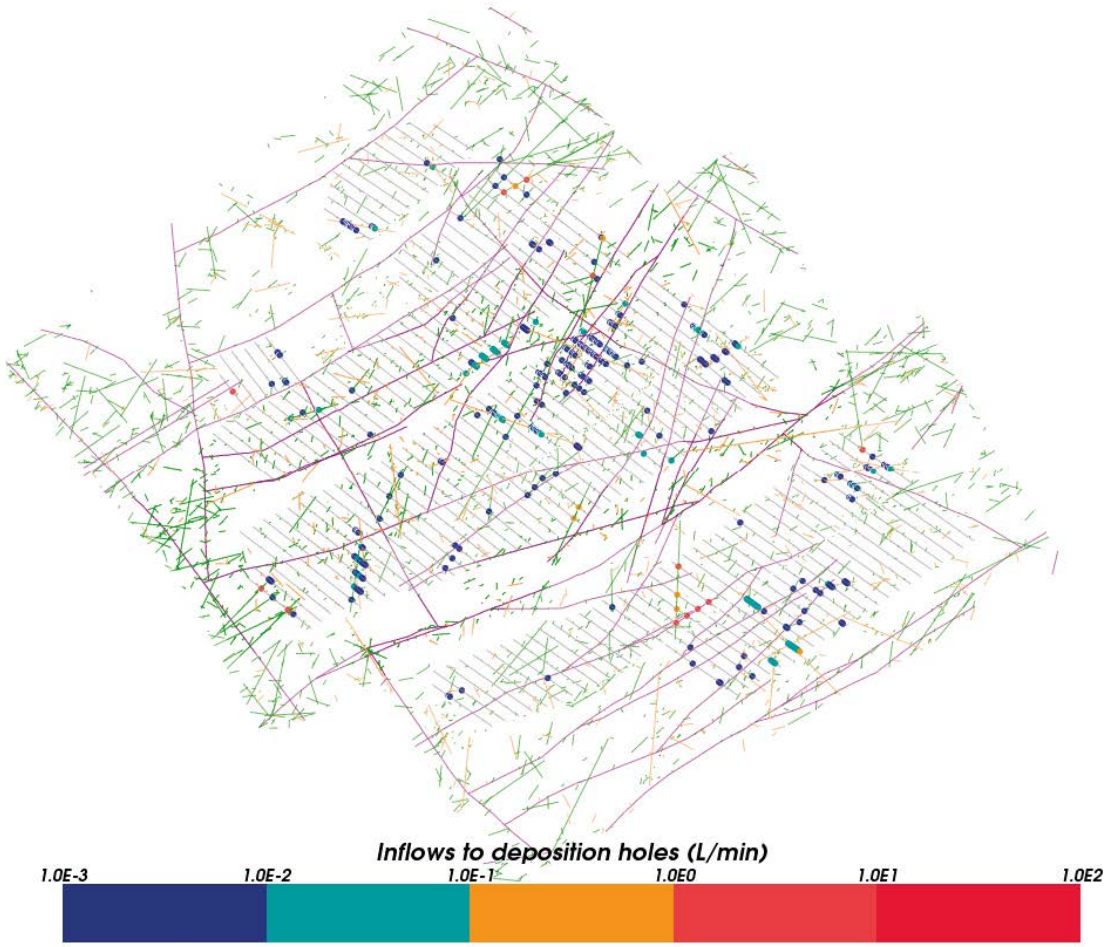

Figure A-4. *Inflows greater than $1{\cdot}10^{-3}$ L/min to deposition holes for case r0 with no EDZ. Stochastic fractures are shown in green (sub-vertical) and orange (sub-horizontal). Deformation zones are shown in purple and the repository tunnels in grey.*

A.2 Inflows to deposition tunnels

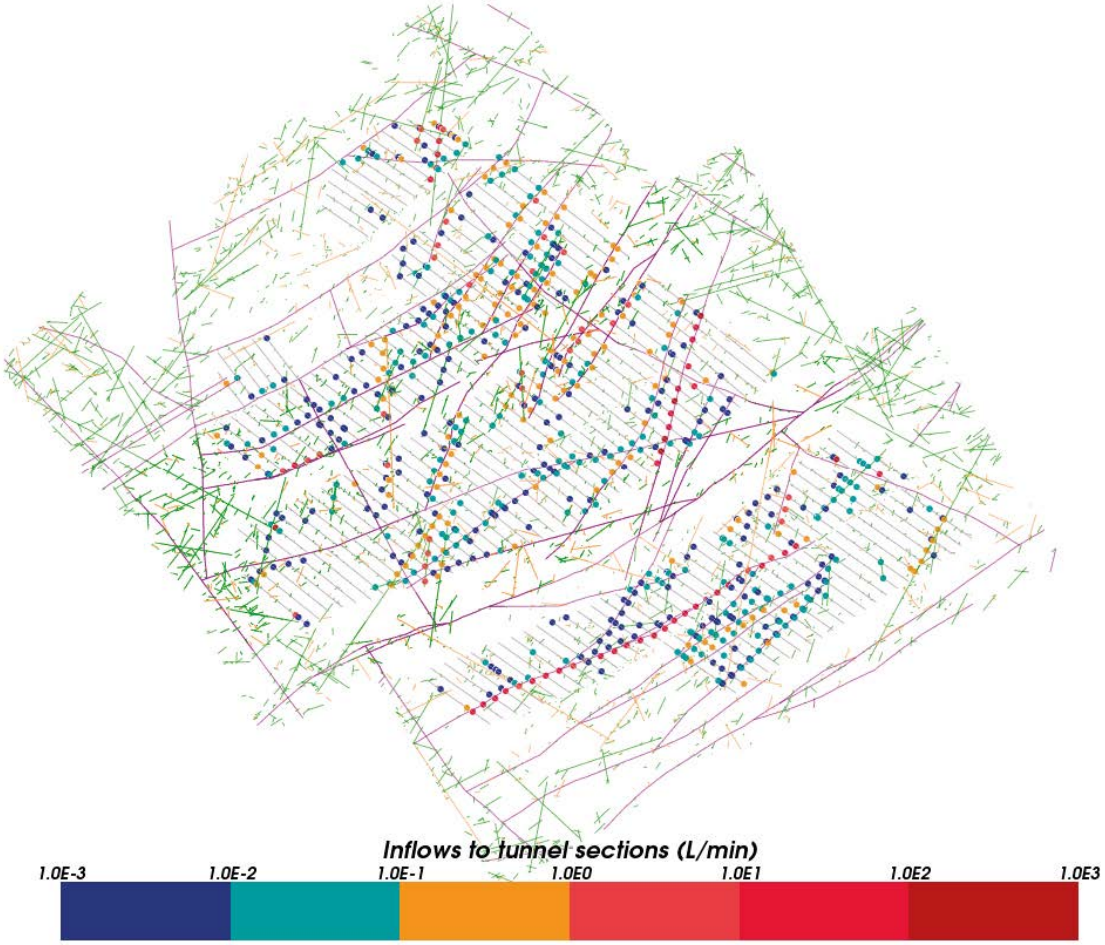

Figure A-5. *Inflows greater than $1{\cdot}10^{-3}$ L/min to tunnel sections for case r2. Stochastic fractures are shown in green (sub-vertical) and orange (sub-horizontal). Deformation zones are shown in purple and the repository tunnels in grey.*

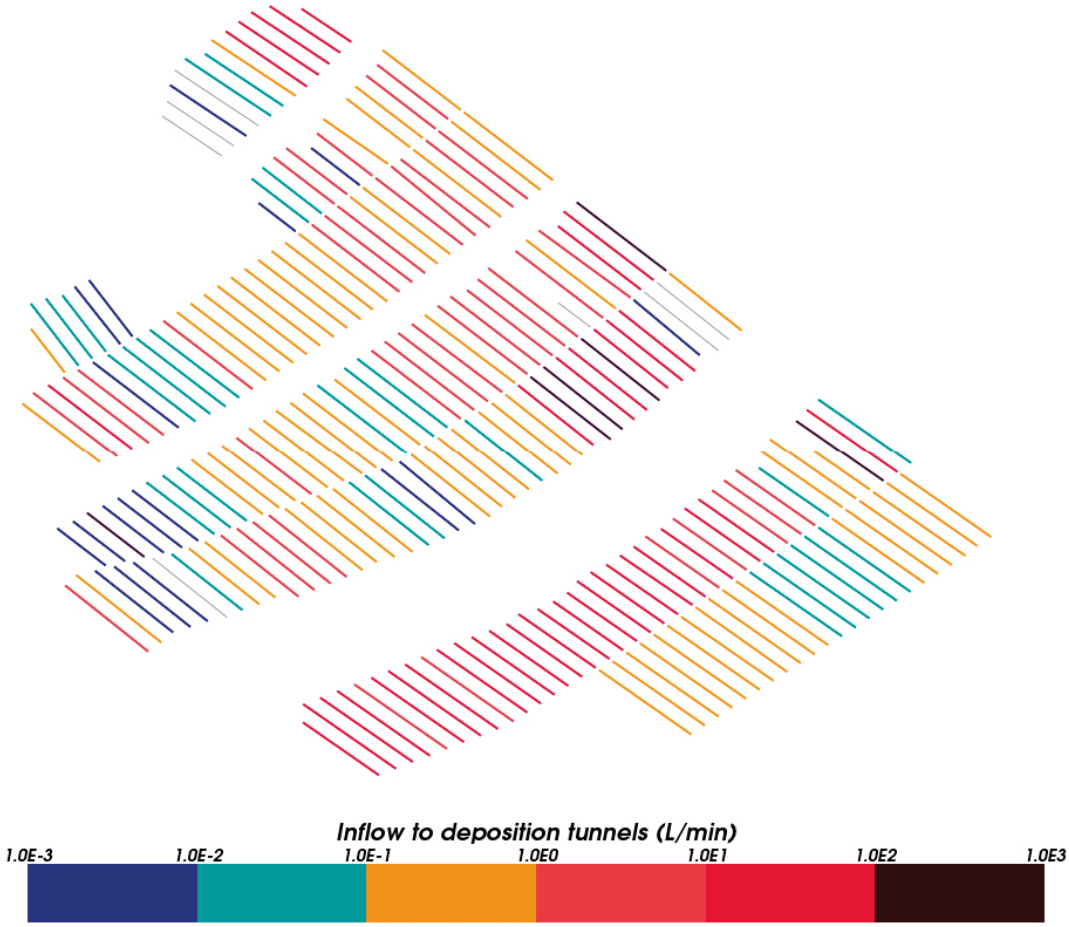

Figure A-6. *Total inflows to deposition tunnels for inflows greater than $1 \cdot 10^{-3}$ L/min for case r2. Tunnels with total inflows less than $1 \cdot 10^{-3}$ L/min are shown in grey.*

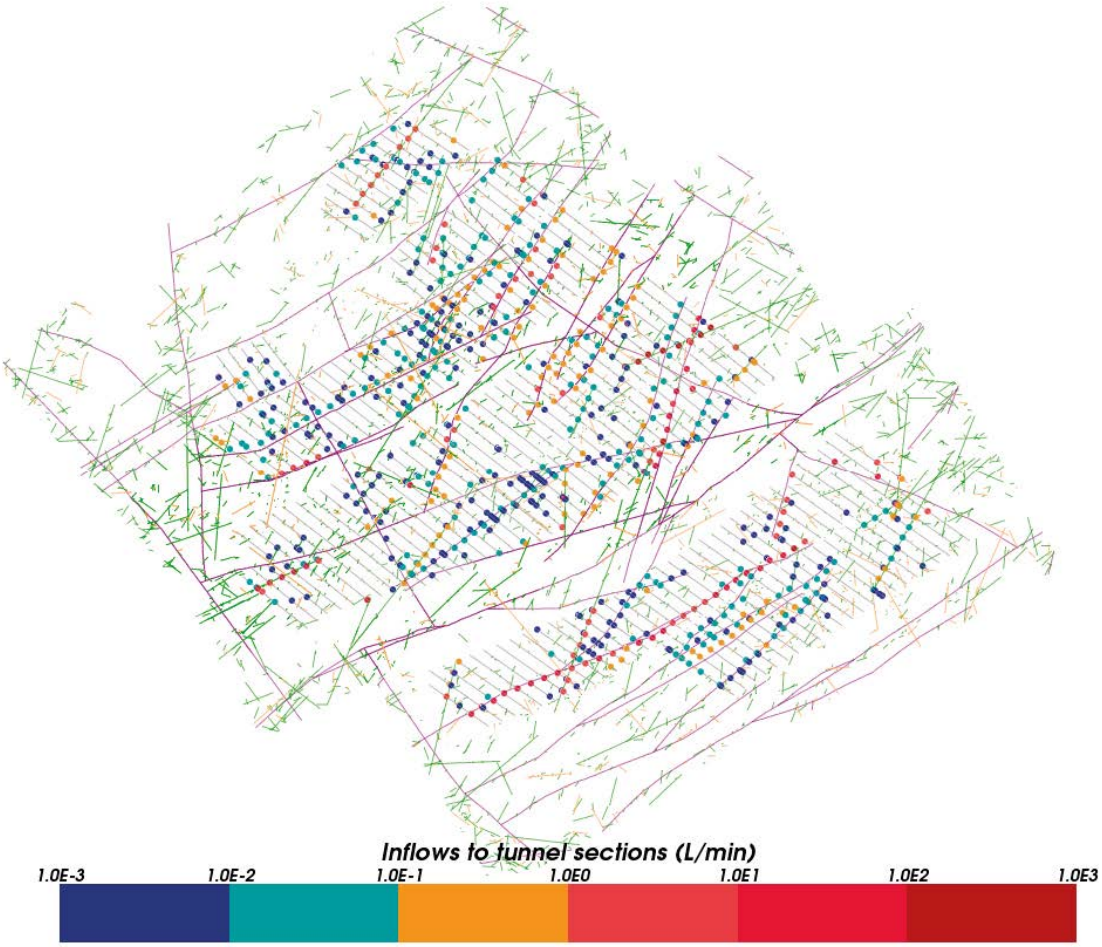

Figure A-7. *Inflows greater than 1 10^{-3} L/min to tunnel sections for case r3. Stochastic fractures are shown in green (sub-vertical) and orange (sub-horizontal). Deformation zones are shown in purple and the repository tunnels in grey.*

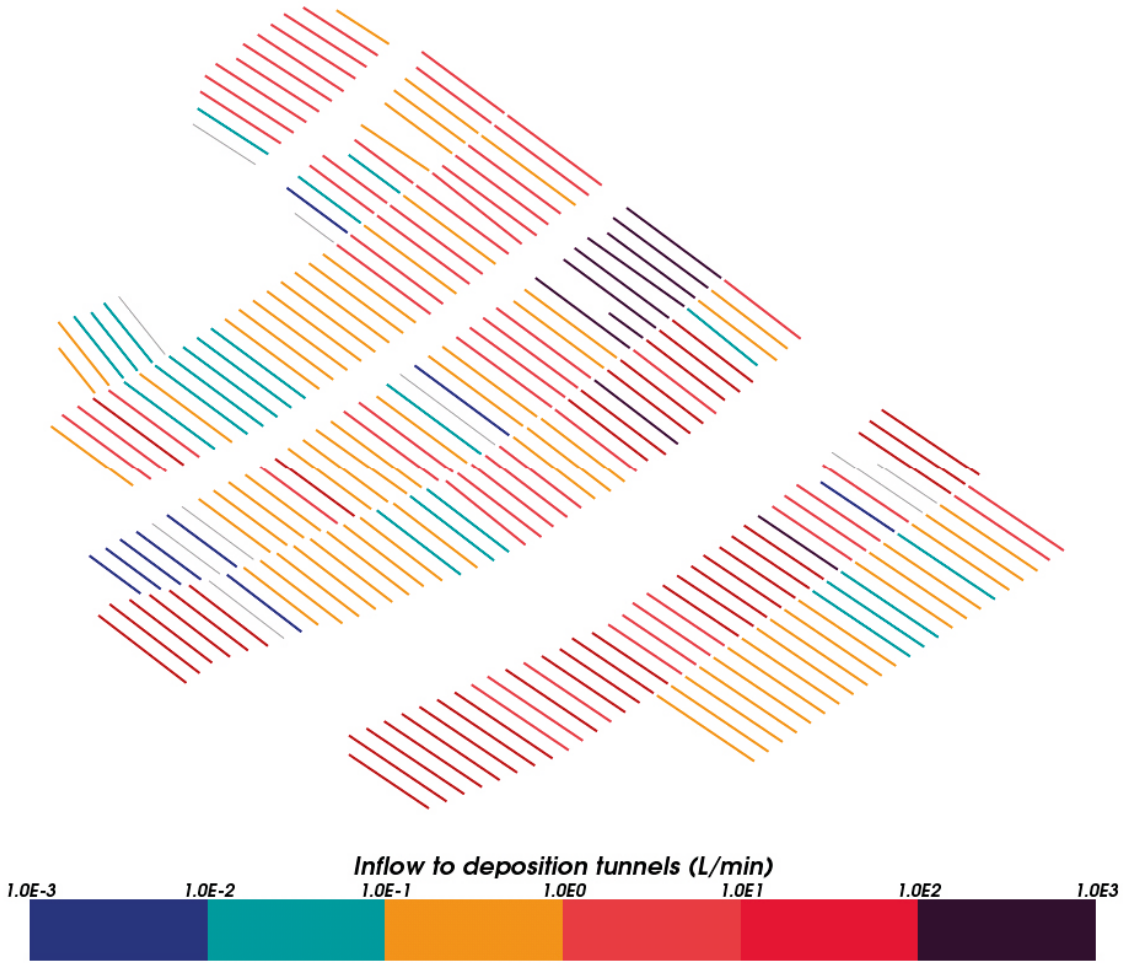

Figure A-8. *Total inflows to deposition tunnels for inflows greater than $1{\cdot}10^{-3}$ L/min for case r3. Tunnels with total inflows less than $1{\cdot}10^{-3}$ L/min are shown in grey.*

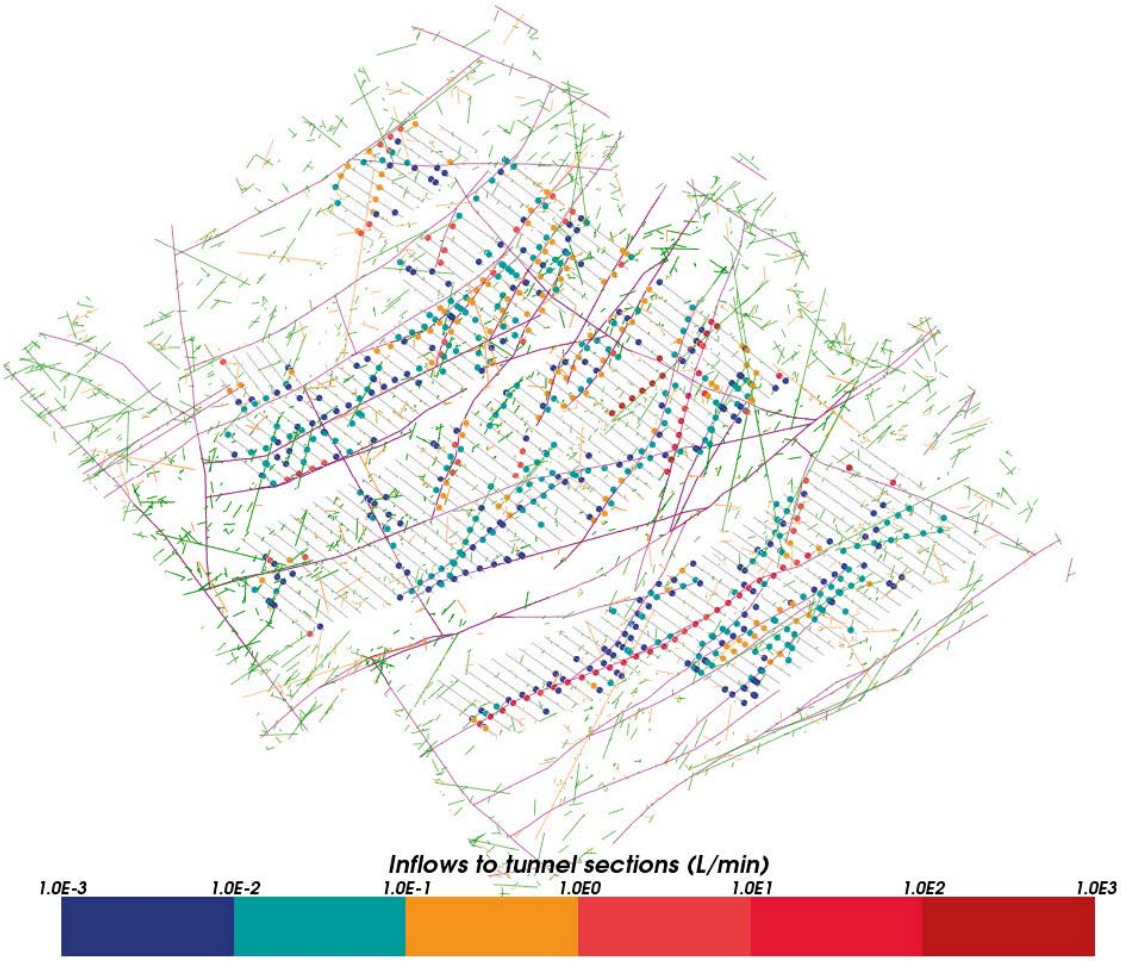

Figure A-9. *Inflows greater than 1 10^{-3} L/min to tunnel sections for case r5. Stochastic fractures are shown in green (sub-vertical) and orange (sub-horizontal). Deformation zones are shown in purple and the repository tunnels in grey.*

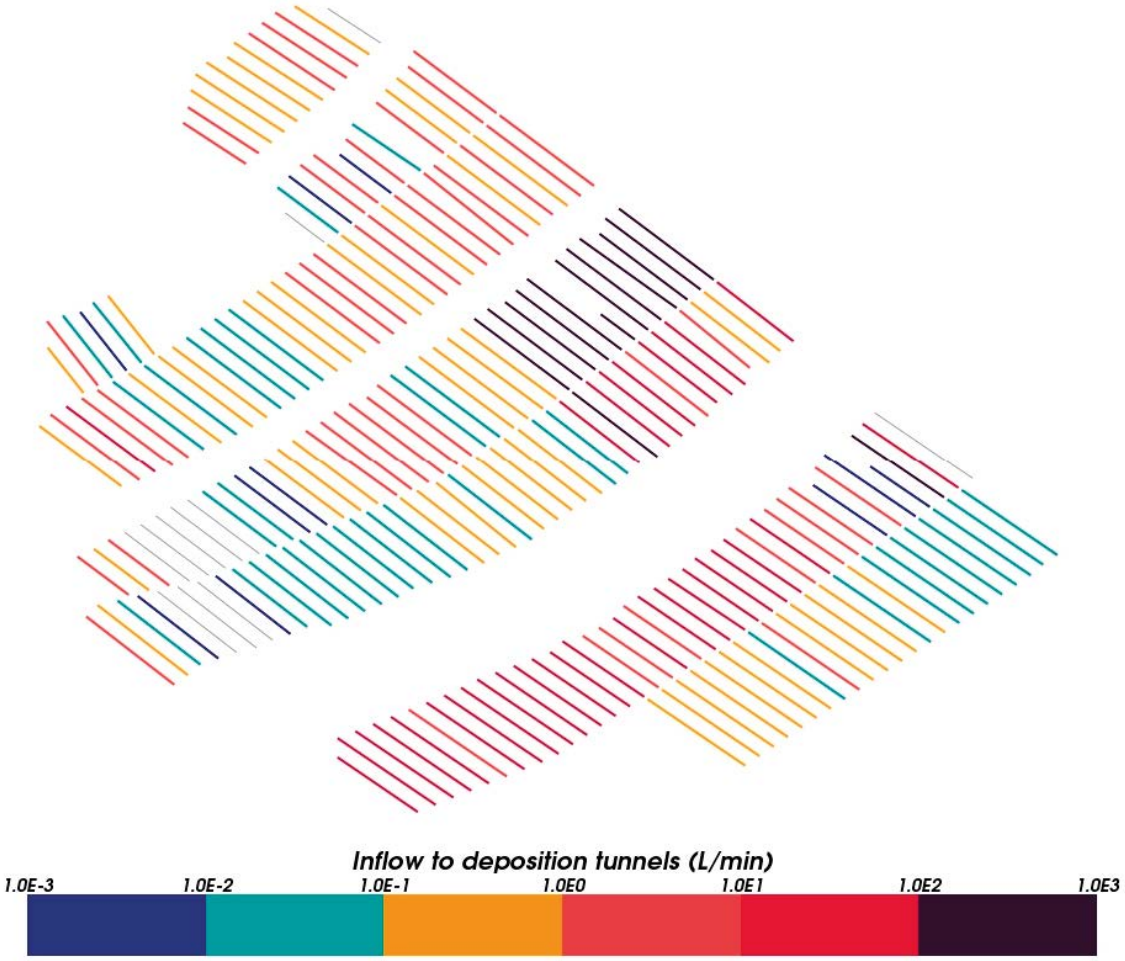

Figure A-10. *Total inflows to deposition tunnels for inflows greater than $1 \cdot 10^{-3}$ L/min for case r5. Tunnels with total inflows less than $1 \cdot 10^{-3}$ L/min are shown in grey.*

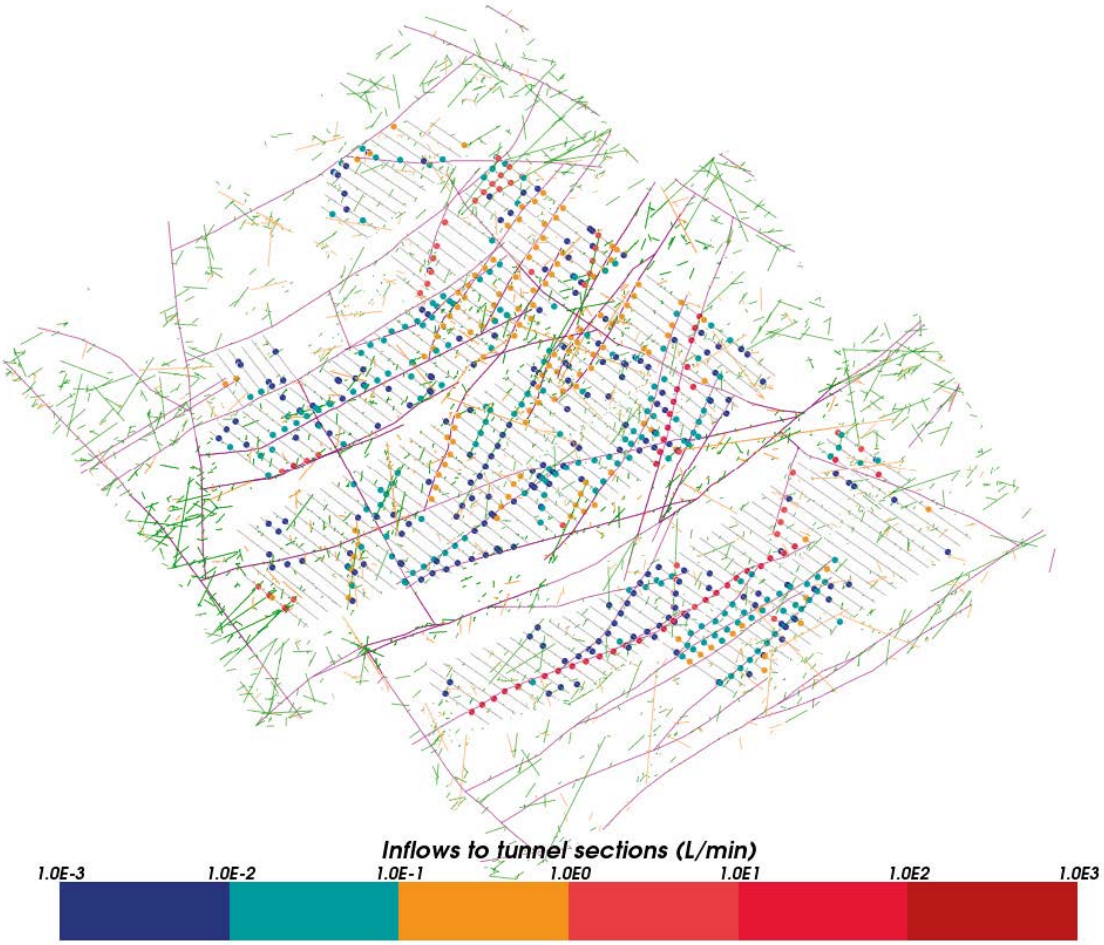

Figure A-11. *Inflows greater than $1{\cdot}10^{-3}$ L/min to tunnel sections for case r0 no EDZ. Stochastic fractures are shown in green (sub-vertical) and orange (sub-horizontal). Deformation zones are shown in purple and the repository tunnels in grey.*

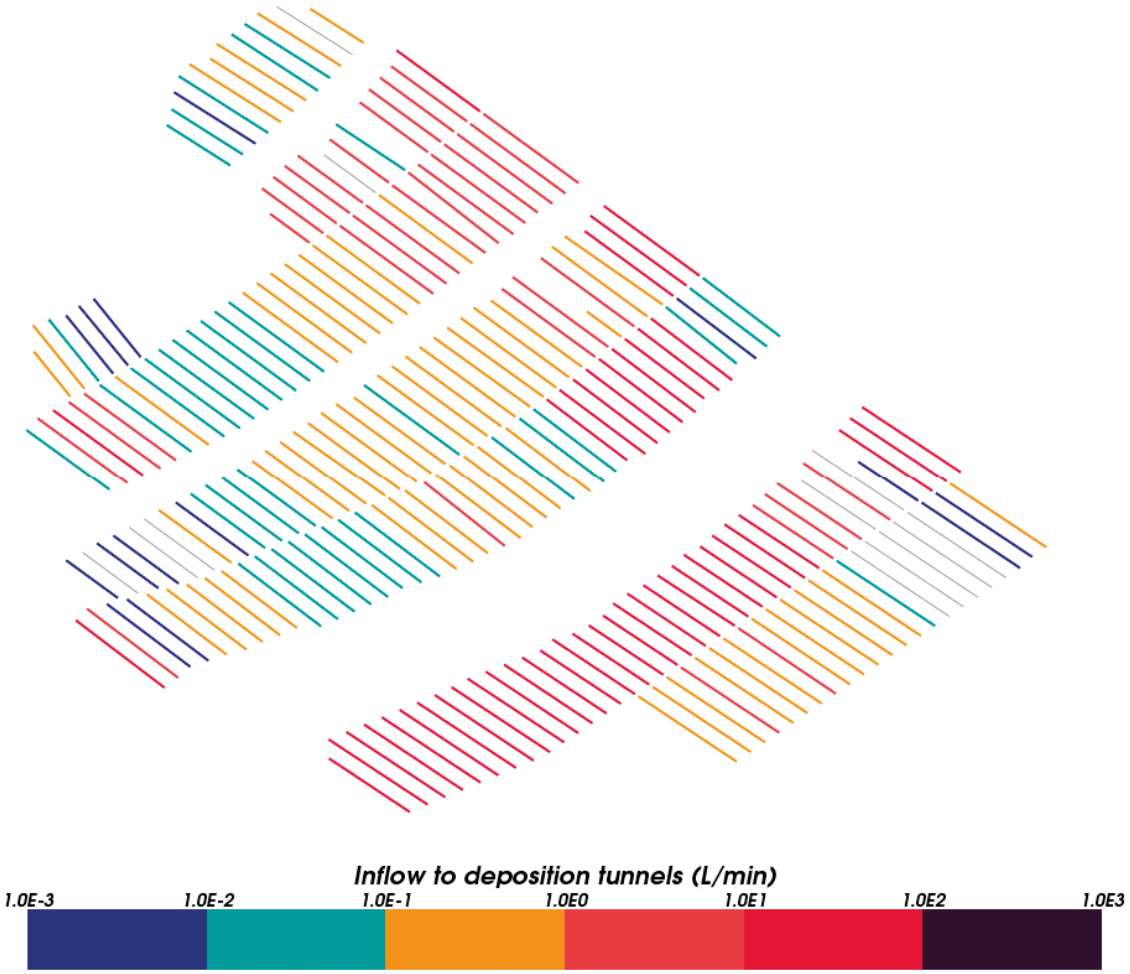

Figure A-12. *Total inflows to deposition tunnels for inflows greater than $1{\cdot}10^{-3}$ L/min for case r0 no EDZ. Tunnels with total inflows less than $1{\cdot}10^{-3}$ L/min are shown in grey.*

A.3 Hydraulic rejection criteria

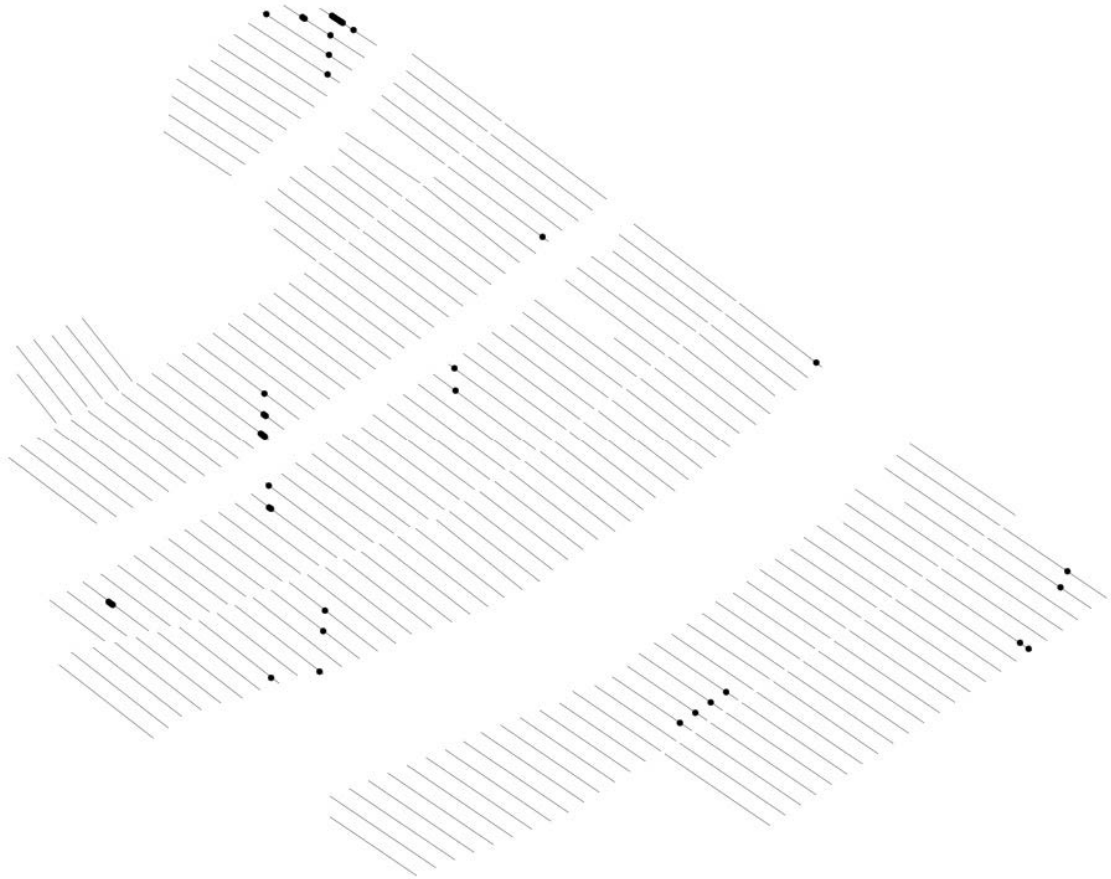

Figure A-13. *Spatial distribution of deposition holes with inflows greater than 0.1 L/min for case r2.*

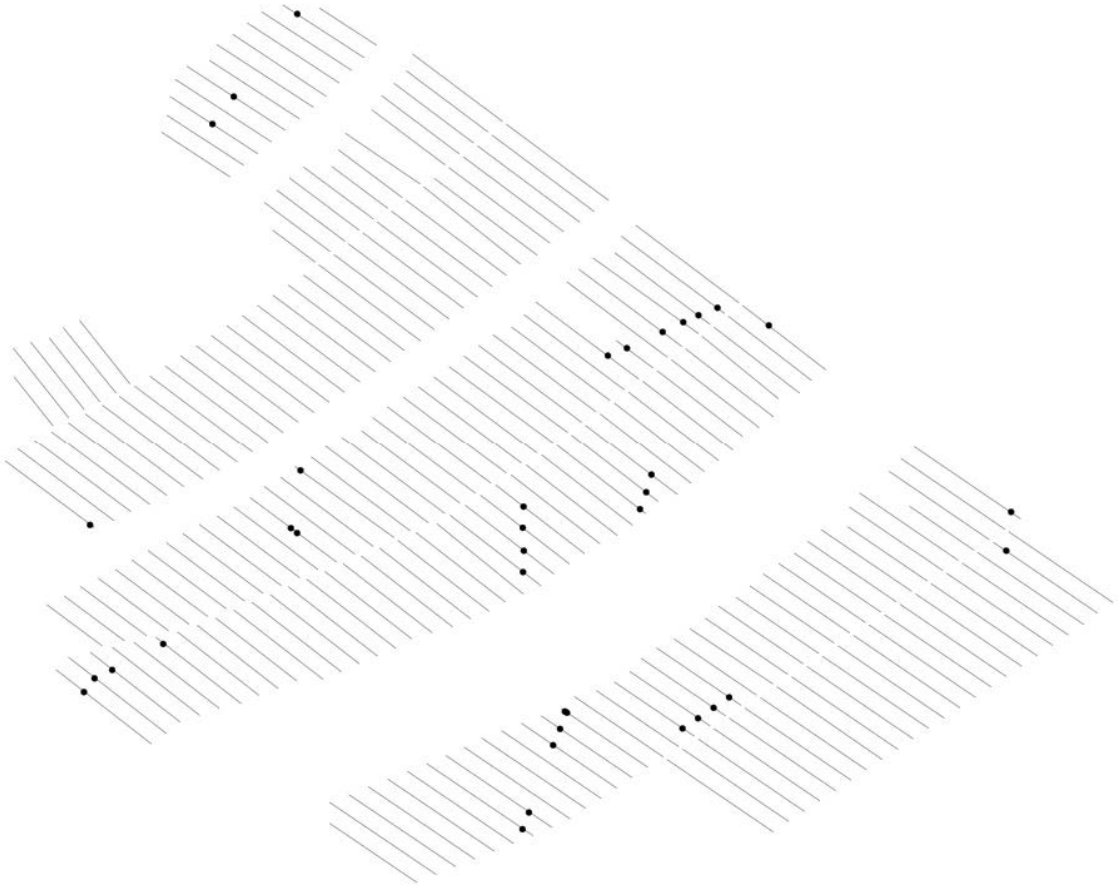

Figure A-14. *Spatial distribution of deposition holes with inflows greater than 0.1 L/min for case r3.*

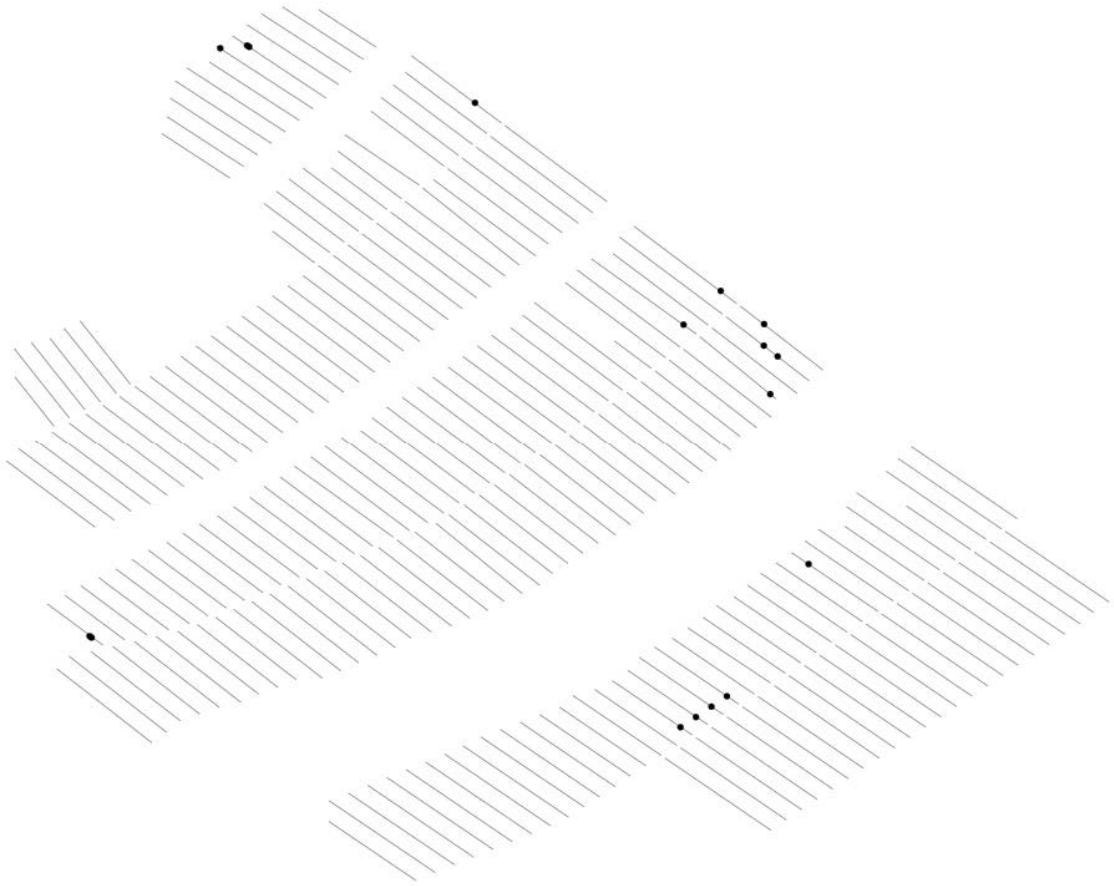

Figure A-15. *Spatial distribution of deposition holes with inflows greater than 0.1 L/min for case r5.*

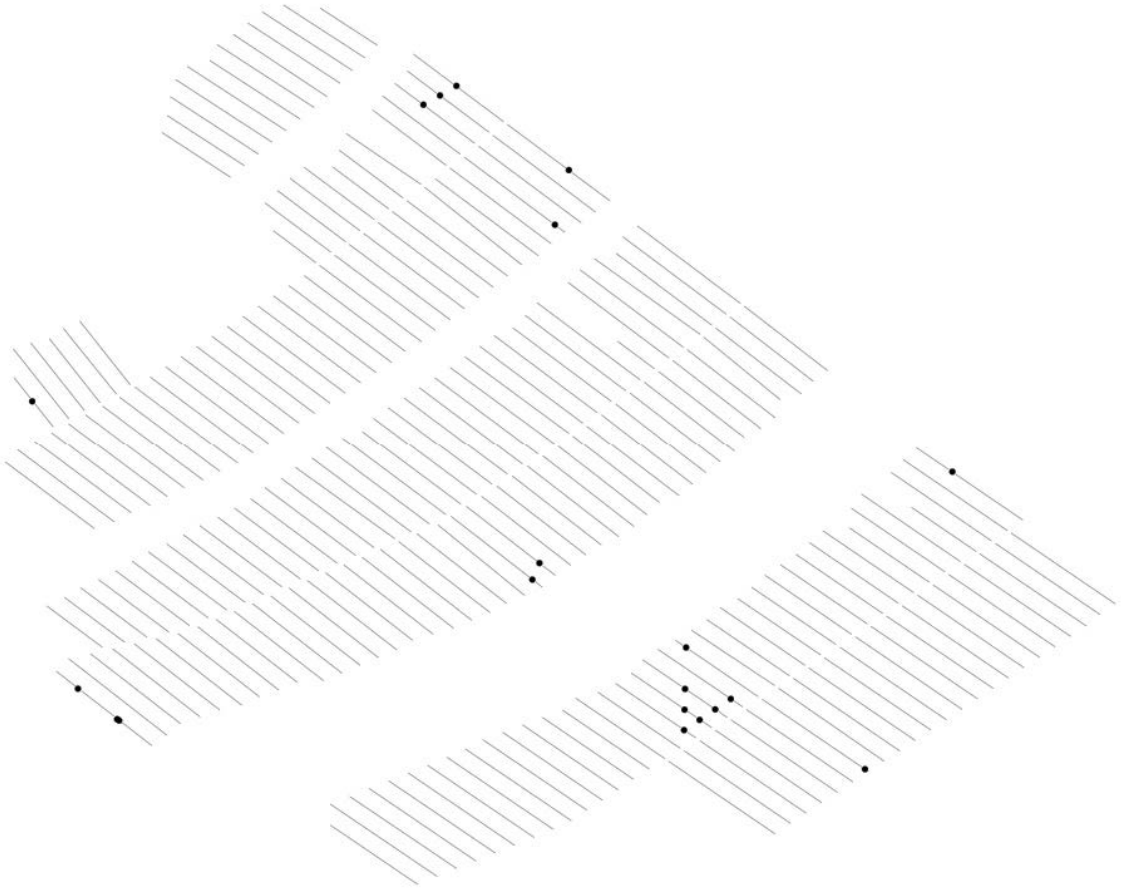

Figure A-16. *Spatial distribution of deposition holes with inflows greater than 0.1 L/min for case r0 with no EDZ.*

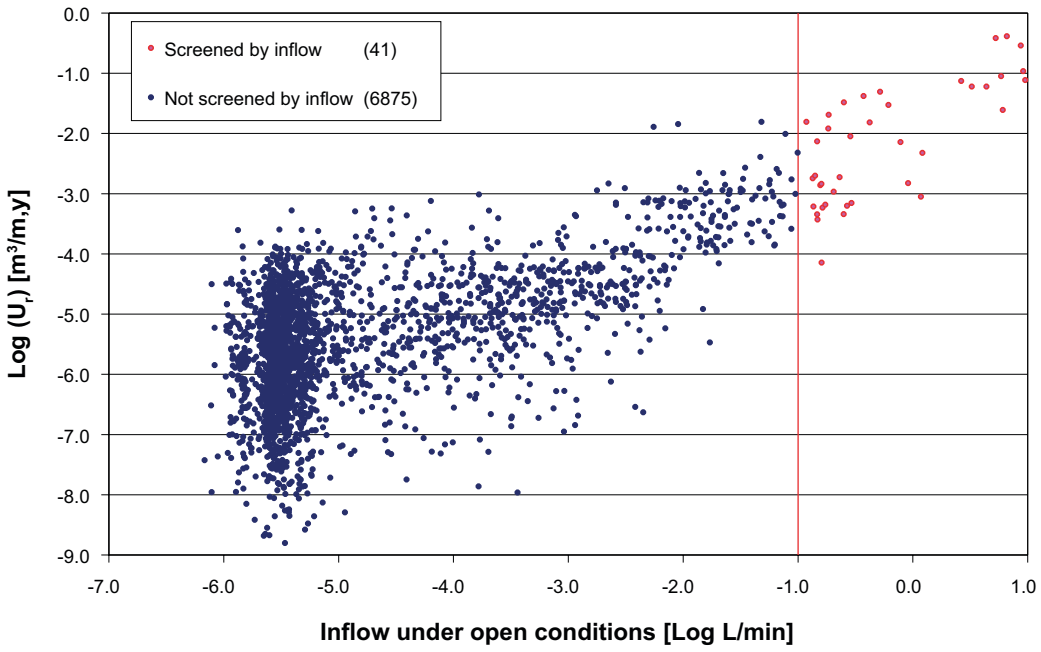

Figure A-17. *Cross plot of inflows to all 6,916 deposition holes under open repository conditions against U_i, the initial equivalent flux into the fractured rock adjacent to the deposition holes under closed repository conditions at 2000 AD, for case r2. Deposition holes with inflows greater than 0.1 L/min are shown in red and those with lesser inflows in blue.*

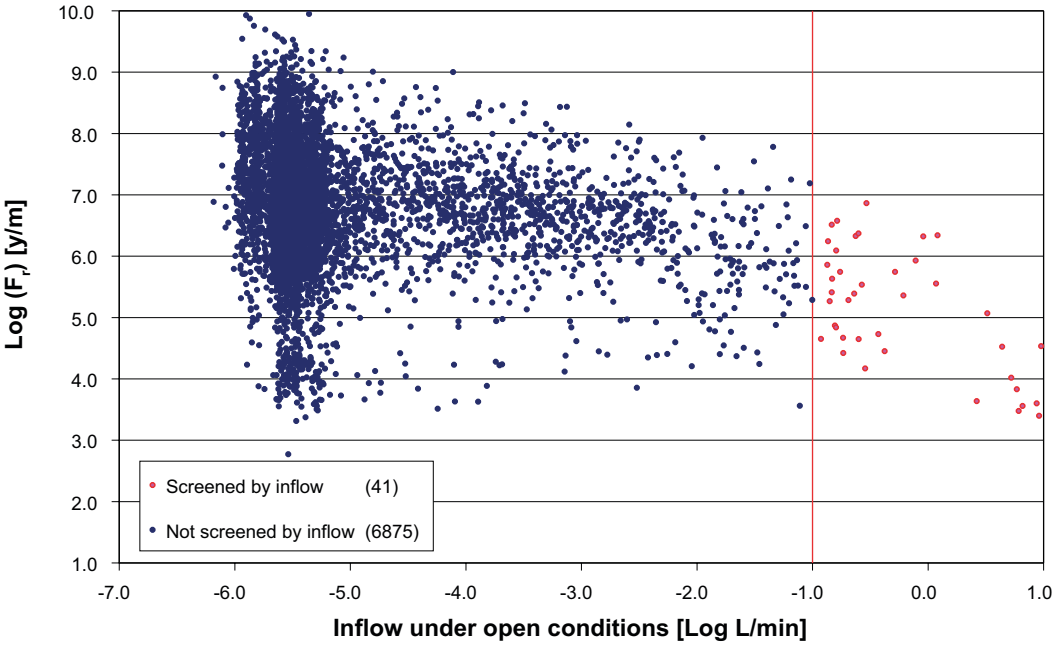

Figure A-18. *Cross plot of inflows to all 6,916 deposition holes under open repository conditions against F_i, the flow-related transport resistance in the rock under closed repository conditions at 2000 AD, for case r2. Deposition holes with inflows greater than 0.1 L/min) are shown in red, while others with lesser inflows in blue.*

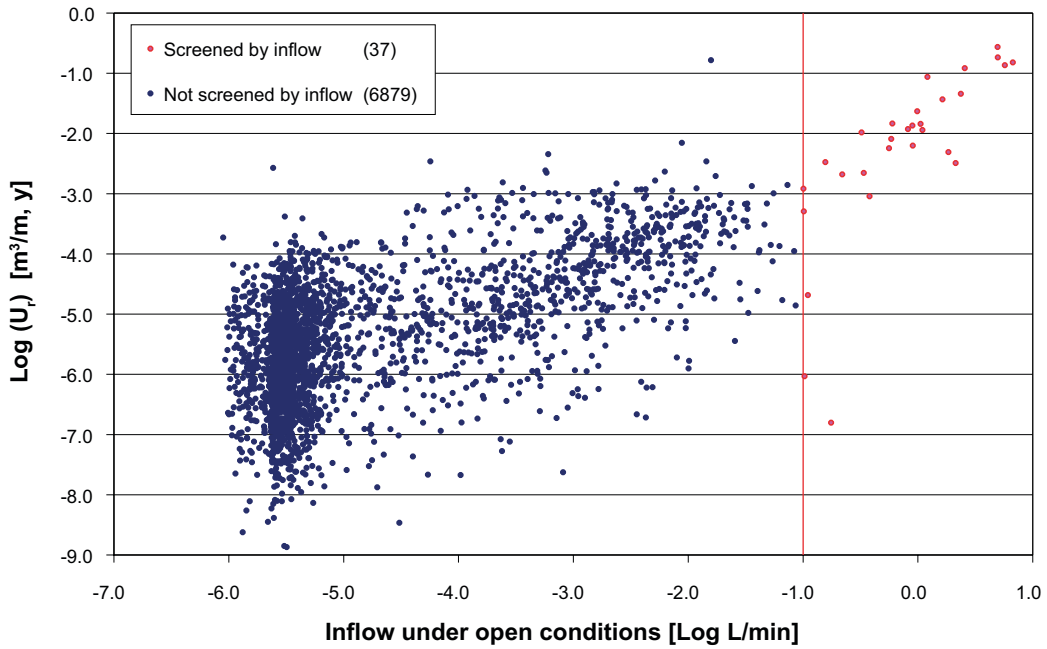

Figure A-19. *Cross plot of inflows to all 6,916 deposition holes under open repository conditions against U_r, the initial equivalent flux into the fractured rock adjacent to the deposition holes under closed repository conditions at 2000 AD, for case r3. Deposition holes with inflows greater than 0.1 L/min are shown in red and those with lesser inflows in blue.*

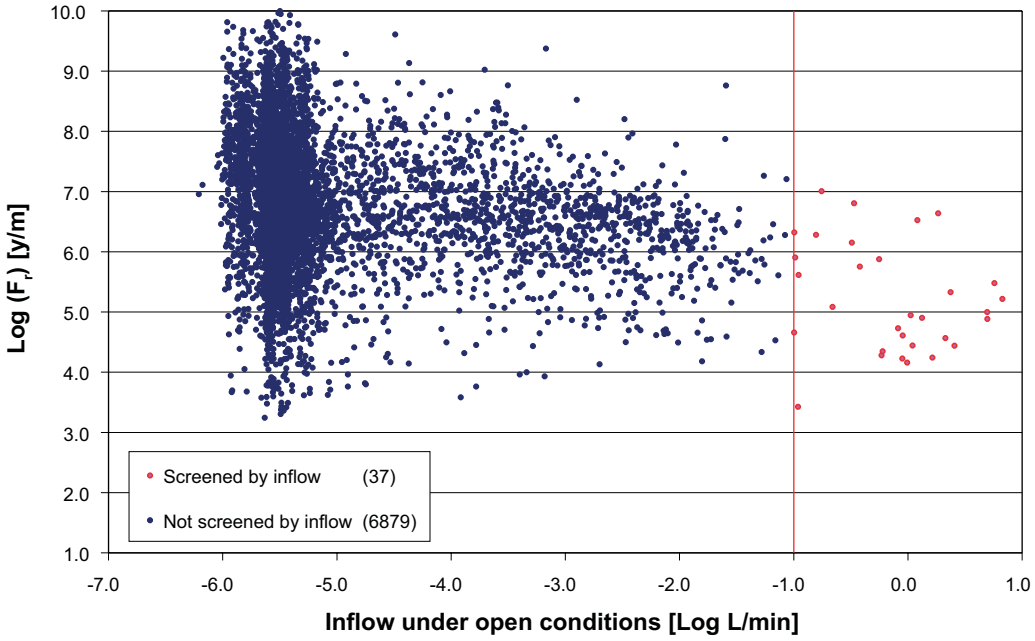

Figure A-20. *Cross plot of inflows to all 6,916 deposition holes under open repository conditions against F_r, the flow-related transport resistance in the rock under closed repository conditions at 2000 AD, for case r3. Deposition holes with inflows greater than 0.1 L/min) are shown in red, while others with lesser inflows in blue.*

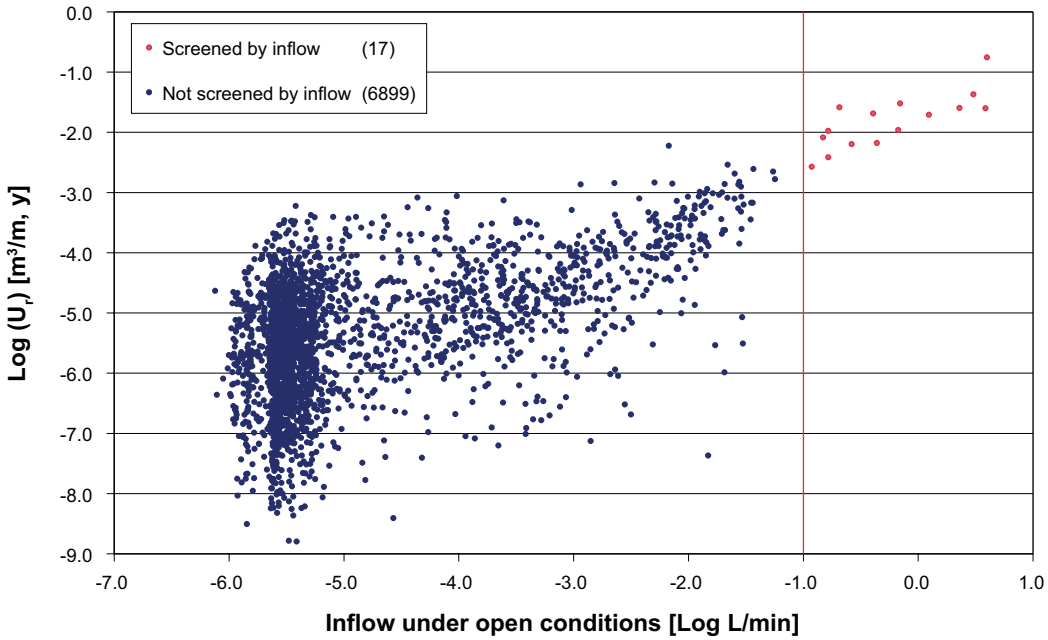

Figure A-21. *Cross plot of inflows to all 6,916 deposition holes under open repository conditions against U_r, the initial equivalent flux into the fractured rock adjacent to the deposition holes under closed repository conditions at 2000 AD, for case r5. Deposition holes with inflows greater than 0.1 L/min are shown in red and those with lesser inflows in blue.*

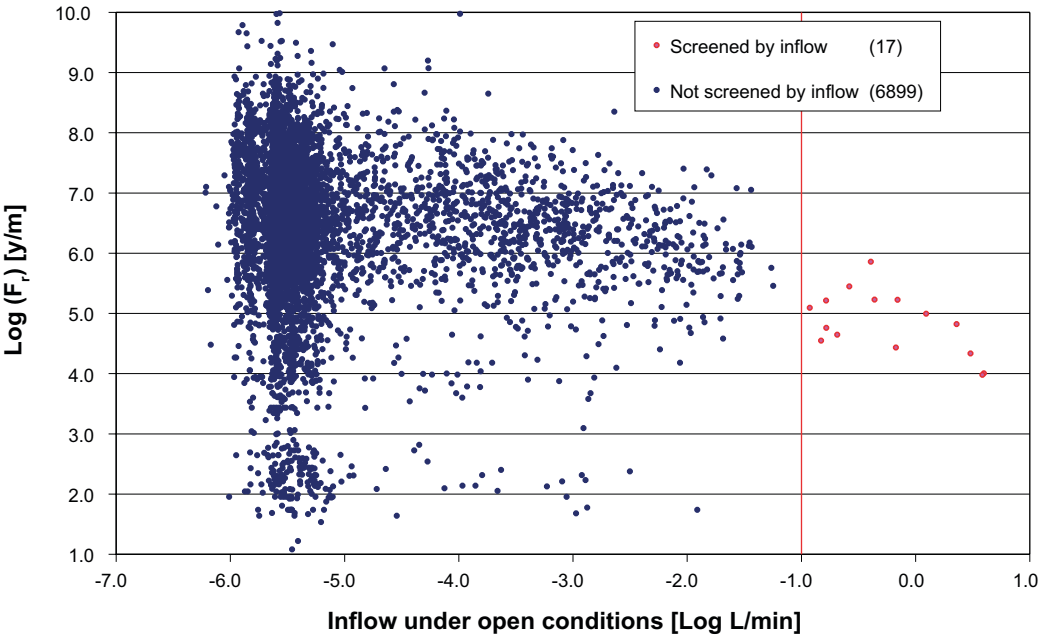

Figure A-22. *Cross plot of inflows to all 6,916 deposition holes under open repository conditions against F_r, the flow-related transport resistance in the rock under closed repository conditions at 2000 AD, for case r5. Deposition holes with inflows greater than 0.1 L/min are shown in red, while others with lesser inflows in blue.*

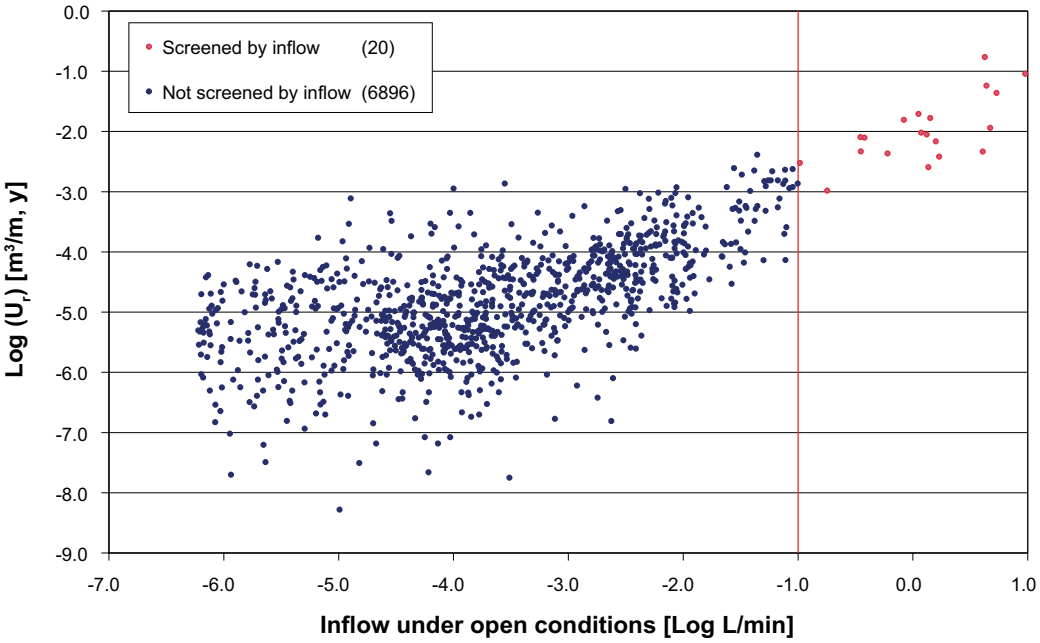

Figure A-23. *Cross plot of inflows to all 6,916 deposition holes under open repository conditions against U_r, the initial equivalent flux into the fractured rock adjacent to the deposition holes under closed repository conditions at 2000 AD, for case r0 with no EDZ. Deposition holes with inflows greater than 0.1 L/min are shown in red and those with lesser inflows in blue.*

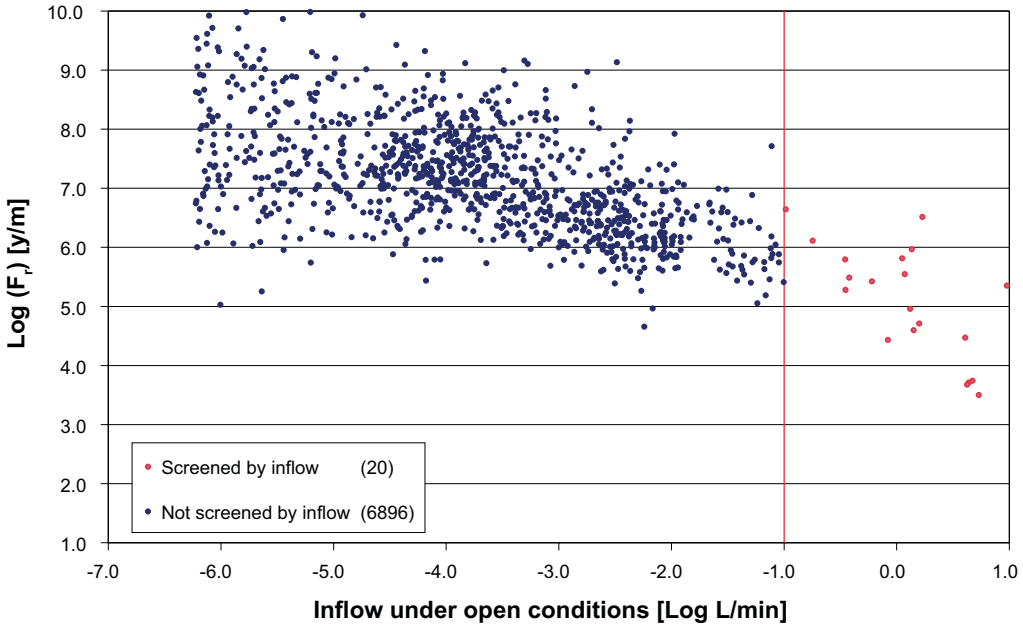

Figure A-24. *Cross plot of inflows to all 6,916 deposition holes under open repository conditions against F_r, the flow-related transport resistance in the rock under closed repository conditions at 2000 AD, for case r0 with no EDZ. Deposition holes with inflows greater than 0.1 L/min are shown in red, while others with lesser inflows in blue.*